Modeling and Verification of Simulation tools for Carburizing and Carbonitriding

by

Lei Zhang

A dissertation submitted to the faculty

of the

WORCESTER POLYTECHNIC INSTITUTE

in partial of fulfillment of the requirement for the

Degree of

Doctor of Philosophy

in

Material Science and Engineering

December 2016

Approved by: _____

Prof. Richard D. Sisson, Jr., Advisor

George F. Fuller Professor

Director of Manufacturing and Material Engineering

Abstract

The CHTE surface hardening simulation tools, CarboNitrideTool© and CarbTool© have been enhanced to improve the accuracy of the simulation and to predict the microstructure and microhardness profiles after the heat treatment process. These tools can be used for the prediction of both gas and low pressure carburizing processes. The steel alloys in the data base include 10XX, 48XX, 51XX, 86XX, 93XX and Pyrowear 53. They have been used by CHTE members to design efficient carburizing cycles to maximum the profit by controlling the cost and time.

In the current software, the model has successfully predicted the carbon concentration profiles for gas carburizing process and many low pressure carburizing processes. In some case, the simulation toll may not work well with the low pressure carburizing process, especially with AISI 9310 alloy. In the previous simulation, a constant carbon flux boundary condition was used. However, it has been experimentally proven that the flux is a function of time. The high carbon potential may cause soot and carbides at the outer edge. The soot and carbides will impede the diffusion of carbon during the low pressure carburizing process. The constant carbon flux cannot be appropriately used as the boundary condition. An improved model for the process is proposed. In the modeling, carbon potential and mass transfer coefficient are calculated and used as the boundary condition.

CarbonitrideTool© has been developed for the prediction of both carbon and nitrogen profiles for carbonitriding process. The microstructure and hardness profile is also needed by the industry. The nitrogen is an austenite stabilizer which result in high amount of retained austenite (RA). RA plays important role in the hardness. The model has been developed to predict the Martensite start temperature (Ms) which can be used for RA prediction. Mixture rule is used then to predict the hardness profiles. Experiments has been conducted to verify the simulation.

The hardness profile is also predicted for tempered carburized alloys. Hollomon-Jaffe

equation was used. A matrix of tempering experiments are conducted to study the Hollomon Jaffe parameter for AISI 8620 and AISI 9310 alloy. Constant C value is calculated with a new mathematical method. With the calculation result, the hardness profile can be predicted with input of tempering time and temperature.

Case depth and surface hardness are important properties for carburized steel that must be well controlled. The traditional testing is usually destructive. Samples are sectioned and measured by either OES or microhardness tester. It is time consuming and can only be applied on sampled parts. The heat treating industry needs a physics based, verified simulation tool for surface hardening processes to accurately predict concentration profiles, microstructure and microhardness profiles. There is also a need for non-destructive measurement tool to accurately determine the surface hardness and case depth. Magnetic Barkhausen Noise (MBN) is one of the promising way to test the case depth and hardness. MBN measures the pulses generating by the interaction between magnetic domain walls in the ferromagnetic material and the pinning sites such as carbides, impurities and dislocation. These signals are analyzed to evaluate the properties of the carburized steel.

Acknowledgement

Firstly, I want to thank my advisor Rick D. Sisson Jr. I am deeply grateful to Prof. Sisson for offering me the opportunity to study at WPI. He has so much knowledge I admire. He understands research profoundly but he can always present to us a way easy to learn. He can always lead me to right direction during all my research at WPI. I can never finish my study without his teaching and encouraging. He is not only a great teacher, but also a close friend. He is humorous and knowledgeable. I always feel positive and delight whenever I talk with him. I will always cherish the memory.

I also want to thank my committee members. They are all important figures during all my PHD study. I want to thank Olly and Emily for their outstanding work. I feel like I am standing right on their shoulders. Their work always inspires me for my research. Prof. Apelian has special vision non only for research but also on philosophy of life. Prof. Shivkumar is one of my favorite teacher at WPI. He knows everything about material science. His wisdom reminds me there is always more than enough knowledge I need to learn.

I would like to express my gratitude to CHTE. It is a new world for me to connect with the industry. The brilliant idea for CHTE has brought us a great view for research. It is not the study restricted in the lab, but the opportunity to solve the real problem in industry. We can talk and learn with experienced engineers. It is not easy to obtain on textbook. I also want to thank all the help from the staff of CHTE and MSE, especially Rita. You really make me feel warm even in cold winter. I will always miss the taste of the coffee you make.

Finally, I want to thank my family and my friend. There is a long distance to my hometown. Because of you, I never feel lonely. Your support means a lot to me.

Table of Contents

Chapter one: Introduction

1.1. The modeling of the carburizing process

The carburizing process is a surface harden technique widely used in industry [1-5]. It is one of the oldest industrial process with carbon provided by gas [5]. The process is usually conducted between 1500°F and 1800°F for a few hours to a day. Both gas carburizing and low pressure carburizing are used by industry. With a typical gas carburizing process as presented in Figure 1 , it may include a boost step which has higher carbon potential at a higher temperature during which, the carbon will diffuse at a high rate. There will also be transition step which help for the diffusion of the carbon further into the bulk. It followed by a diffusion step which decreases the temperature without changing the carbon potential. It is a preparation for the further heat treating process such as quenching.

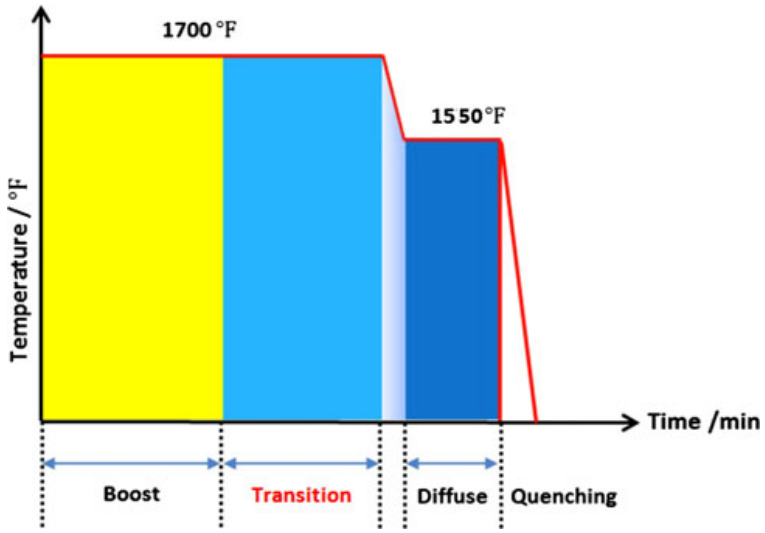

Figure 1: The gas carburizing process [6]

People in industry are in need of reliable tool to simulation the processes. The simulation tool will be helpful for the design of the carburizing processes, to save time and reduce cost. The simulation tool has been investigated by a few research groups [1-11]. Figure 2 presents the process of carburizing [1].

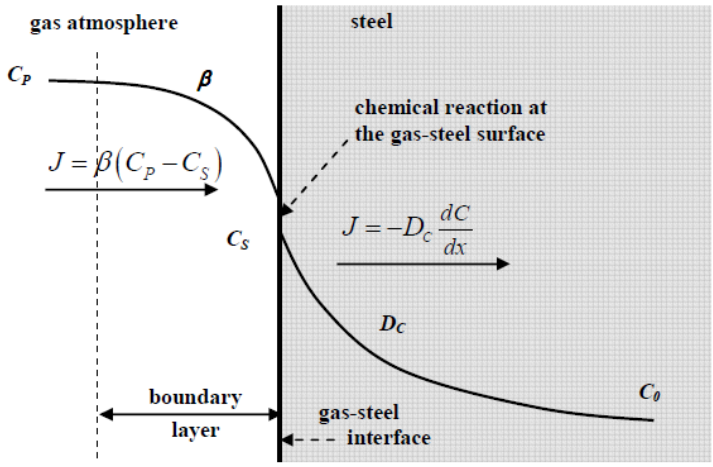

Figure 2: The gas carburizing process [1]

Endothermic carburizing atmosphere consists of CO, H2, and N2 together with CO2, H2O and CH4[2]. The gas provides the sources of carbon atom by thermal chemical reaction. The primary reactions are [2]:

$$2CO \rightarrow C_{(Fe)} + CO_2$$

$$CH_4 \rightarrow C_{(Fe)} + 2H_2$$

$$CO + H_2 \leftrightarrow C_{(Fe)} + H_2O$$

As early as 1978, Goldstein and Moren were the first to simulate processes for gas carburization with Fick's second law [5]. The initial model assumed a constant surface carbon concentration, a constant carbon diffusivity and the semi-infinity boundary condition. The solution to the partial differential equation is the error function.

$$\frac{C_c - C_s}{C_0 - C_s} = erf(x/2\sqrt{Dt}) \quad \textit{Equation 1}$$

Where

Cs=Surface concentration of carbon

C_0=Initial carbon level in Fe

D=Diffusion coefficient in the Austenite phase

C_c=Carbon concentration as a function of distance from surface x and time t

The modeling of the carburizing process has been well studied. Karabelchtchikova and Sisson have investigated the kinetics of carburizing process [1,2]. In the research, mathematical model has been studied as well as the calculation of the mass transfer coefficient and the carbon diffusion coefficient [1,2]. A new software CarbTool© was developed which allows for a variable surface boundary condition and carbon diffusivities.

The carburizing process is controlled by Fick's laws of diffusion:

$$J = -D\frac{\partial C}{\partial x} \qquad \textit{Equation 2}$$

$$\frac{\partial C}{\partial t} = \frac{\partial}{\partial x}\left(D_c \frac{\partial C}{\partial x}\right) + u \cdot \frac{D_c}{r+ux} \cdot \frac{\partial C}{\partial x} \quad \textit{Equation 3}$$

Where

J=Carbon flux Unit:g/cm^2/s

C= Carbon concentration as a function of distance from surface x and time t Unit:wt%

D=Carbon diffusion coefficient Unit:cm^2/s

r, u=Geometry factor of the surface

There are three steps during the diffusion process [1] as Figure 2 presents: In the first step, carbon molecules in the gas are absorbed into the surface of steel. The driving force of the absorption is the higher concentration in the atmosphere than the surface area. The second step is the dissociation of the gas at the surface. The third step is the absorption and diffusion of the carbon atoms to the bulk of steel. A flux balance is used to calculate the carbon flux at the surface. [1].

1.2. The boundary condition of the simulation

To solve the partial differential equation, the boundary condition must be specified. The mass transfer coefficient and the carbon diffusivity were experimentally determined.

$$\beta\left(C_p - C_s\right) = -D_c \frac{\partial C}{\partial x} \quad \textit{Equation 4}$$

Where

β=Mass transfer coefficient Unit:cm/s

C_p=Carbon potential of the atmosphere

C_s=Surface carbon concentration of the steel

X=distance from the surface

The carbon concentration of the surface is calculated from the flux balance. For the modeling, the research has presented two parameters that determine the final profiles, mass transfer coefficient and diffusivity [2].

$$J' = \frac{\partial(\Delta M/A)}{\partial t} = \beta(C_p - C_s^t) \textit{ Equation 5}$$

$$\beta' = \frac{\frac{\partial}{\partial t}\int_{x_\infty}^{x_s} C(x,t)dx}{(C_p - C_s^t)} \quad \textit{Equation 6}$$

Mass transfer coefficient can be calculated experimentally. Weight gain and the carbon concentration difference between atmosphere and the surface carbon will be the input. Range of the mass transfer coefficient is 1.3 to 2.7e-5 cm/s[2].

$$D(x_0) = -\frac{dx}{dC(x_0,t)} \cdot \frac{d}{dt}\int_{x_\infty}^{x_0} C(x,t)dx \quad \textit{Equation 7}$$

To model the process, diffusivities is also calculated with experimental Karabelchtchikova ‘s method[3]. In her paper [1], in order to determine the carbon diffusivity, two separate gas carburizing times are needed. She has used this method to calculate the diffusivities in several alloys [1,2].

1.3. The low pressure carburizing process simulation

In low pressure carburizing, the process is carried at similar temperature as gas carburizing, but at low pressure. It is environmental friendly process with high cost efficiency [4]. The advantage of the process is that there will be less distortion and there will no intergranular oxidation (IGO) along the surface [4]. The gas used for the process can be C_2H_2 C_3H_8 or C_6H_{12}.

Figure 3 presents the carbon concentration change during the low pressure carburizing process [11]. The carbon potential is not well controlled. Cycles are recommended to avoid the formation of the soot on the surface. In the figure, six boost-diffusion cycles are used. The period varies with multiple temperature and carburizing gas pressure.

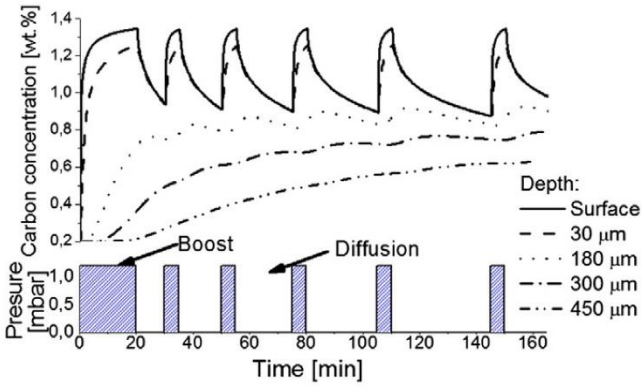

Figure 3: The simulation process for low pressure carburizing process [11]

1.4. Hardness prediction

The thickness of the carburized case is usually controlled 0.5mm-2.5mm. After the carburization heat treatment. The steel is typically quenched in oil or high pressure gas. During quenching, Martensite is found with some retained Austenite. The hardness of the Martensite is a function of the carbon content as seen in Figure 4.

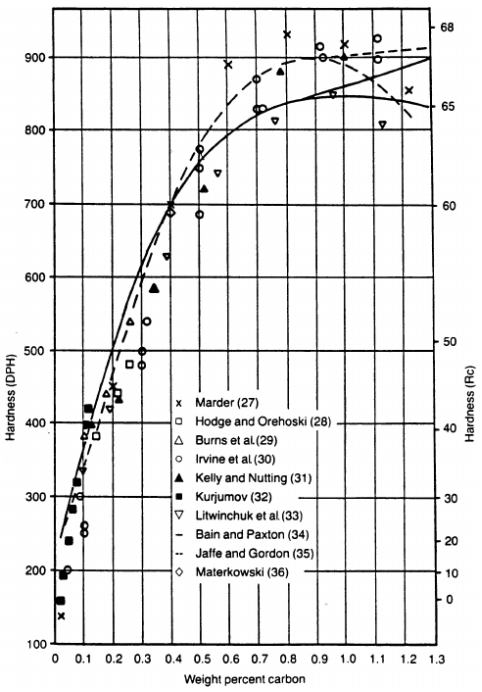

Figure 4: The hardness of martensite change with carbon concentration [16]

Hollomon and Jaffe developed an equation to explain the effects of tempering time and temperature on the hardness as below.

$$P = \frac{T}{1000}(logt + C) \quad Equation\ 8$$

$$Hardness = f(P) \quad Equation\ 9$$

$$Hardness = AP + B\ Equation\ 10$$

Where P is the Hollomon Jaffe Parameter, T is the Temperature in Kevin, t is time in seconds. A and B are constants that shows the linear correlation between the hardness and the Hollomon Jaffe Parameter. The parameter can be used to calculate the hardness of steel after certain tempering process. With carburized steel which has different carbon concentration at different spot closed to surface area, the constant varies.

1.5. Objectives

Objective of the thesis includes:

- Modeling of CarbTool© -Gas carburizing

Simulation include

- The prediction of the surface carbides
- The prediction of the microhardness profiles

- Modify CarbTool© for low pressure carburizing

  Simulation include,

  - Time dependent surface flux boundary condition
  - The prediction of the surface carbides.
  - The prediction of the microhardness profile prediction

- Nondestructive testing development for hardness and case depth evaulation

Chapter Two: Literature Review

2.1. Low Pressure Carburizing simulation

The boundary condition for the low pressure carburizing process is different from the gas carburizing process. In gas carburizing process, the carbon potential can be monitored and well controlled. During low pressure carburizing process, the surface carbon increases dramatically and can reach the maximum solubility [6]. Constant carbon flux was used as the boundary condition in Yingying Wei's work [6].

Figure 5 presents the carbon solubility for Iron and 93XX steel in austenite region [6]. Hydrocarbon molecule will decompose and be absorbed by the surface of the parts in a short time which will result in the formation of carbides [6]. 93XX steel will form carbides when the surface carbon reaches 1.03 wt% at 925℃.

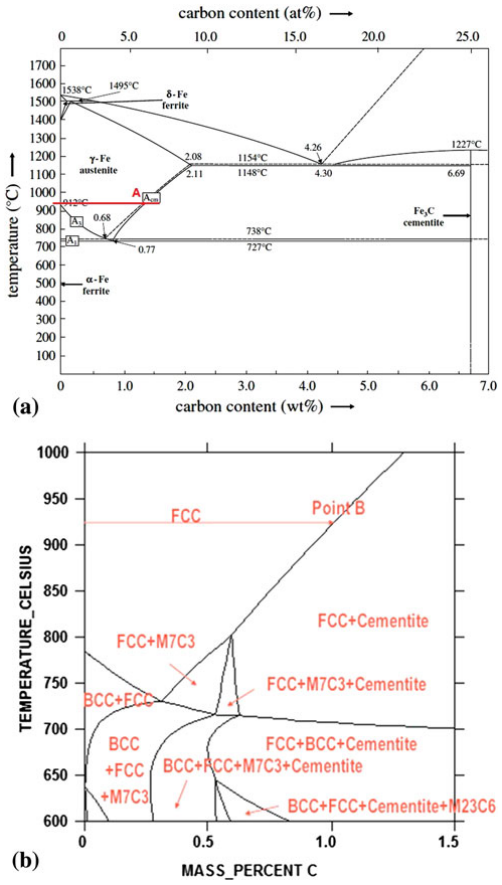

Figure 5: Fe-Fe_3C diagram (a) and 93XX isopleth diagram(b)[6]

Yingying Wei's work has shown that the formation of carbides will affect the low pressure carburizing. The saturation of the carbon will decrease the further diffusion of the carbon. Carbon flux calculated with existing process may not be appropriate for the other. Kula and Woloweiec's research team have found that it forms not only carbides, but also carbon deposit on the surface.

The low pressure carburizing process can form a carbon deposit on the surface of the parts [13][16]. It was studied by R. Gorockiewic.z and A. Lapinski[13]. The It may not be experimentally seen on the final parts with diffusion step [6]. The Figure 6 shows the formation of the carbon deposit after 120 min boost at 950℃ [16]. Low pressure carburizing can process parts with clean surface with less distortion than gas carburizing. But the surface will form carbon deposit layer that will slow down the diffusing rate. To better model the process, the surface condition needs to be well studied.

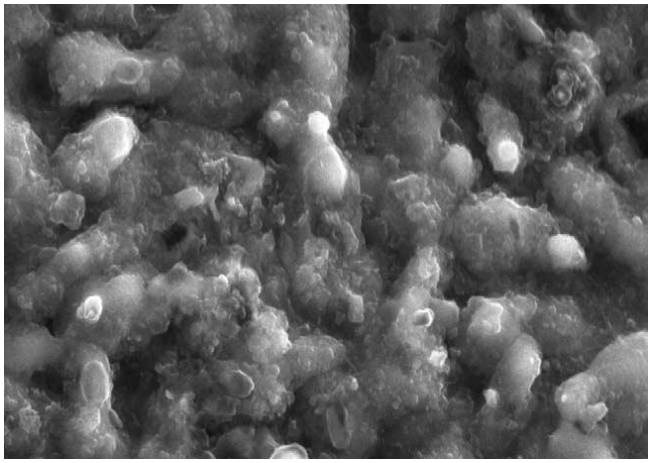

Figure 6: The carbon deposit forms during the low pressure carburizing process [16]

Kula, Woloweiec and Dybowski[4] [8][9]have modeled of the low pressure carburizing process. The factors that have been included in the simulation: the temperature, the composition of the steel, shape and the carburizing procedures. The formation and the decomposition of the carbon deposit layer is studied and include in the simulation.

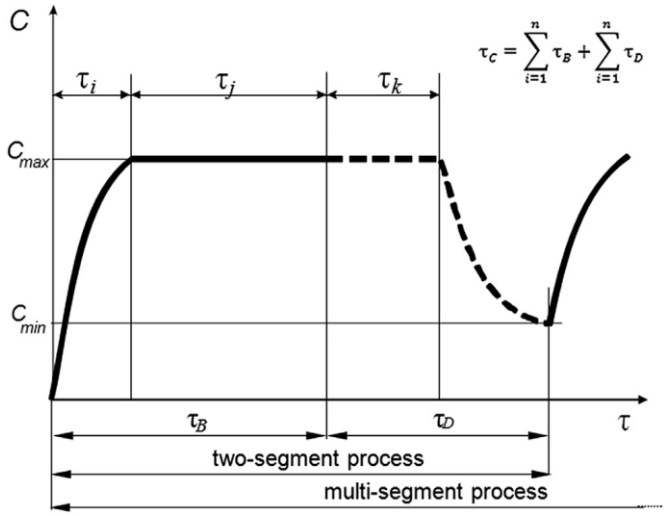

Figure 7: The surface carbon change for low pressure carburizing process [4]

In Kula's simulation process [4], the boost step will also bring a thin layer of graphite on the surface. Kula called it carbon deposit layer [8] as Figure 7 presented. At the beginning of the diffusion step, the carbon deposit layer become the source of carbon. In this way, the actual boost step is longer than the input. Experimental method has been used to estimate the extending of the boost step.

Kula has tested the Armco foil with GD-OES [16]. The results as Figure 8 show that the carbon will reach maximum solubility after a short time which is about 20min in the testing. The carbon content will maintain a constant value after the step. It helps us understand the low pressure carburizing process. Instead of the constant carbon flux input, a nominal carbon potential can be applied for the simulation.

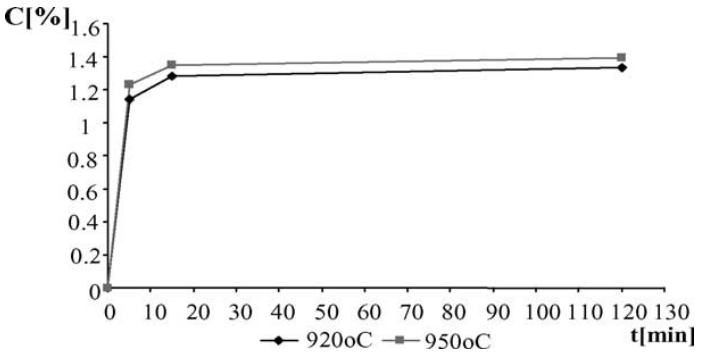

Figure 8: Carbon concentration in the Armco foil as a function of the dwell [16]

M. Zajusz, K. Tkacz-Seiech and M. Danielewsk has also modeled the process. The study shows

instead of a constant mass transfer coefficient, the parameter was redefined as [11]:

$$\beta(t) = Sm_c l_z(t)/\rho_m \qquad \textit{Equation 11}$$

Where,

m_c: mass of carbon per one mole of acetylene

ρ_m: density of the steel Unit:g/cm^3

S: Dimensionless reaction efficiency

Jung from Yongsei University has proposed that the controlled step for the low pressure carburizing process is the diffusion from the surface into the bulk [6]. The carbon concentration will be saturated immediately during the boost step. The boundary condition used for the simulation is the maximum solubility of carbon in austenite. Value of the carbon solubility can be calculated by the ThermalCalc software.

In the paper written by Tsuji and Ishigami[7], the boundary condition is also the saturation carbon of the steel. The time that reach the solubility is measured. The time cost was presented in the paper. The time cost is a function of pressure and the temperature. The time cost to reach surface saturation is function of time and the pressure. In Figure 9, it takes 12ks for CH_4 with 53.3kPa and it takes longer for a lower pressure.

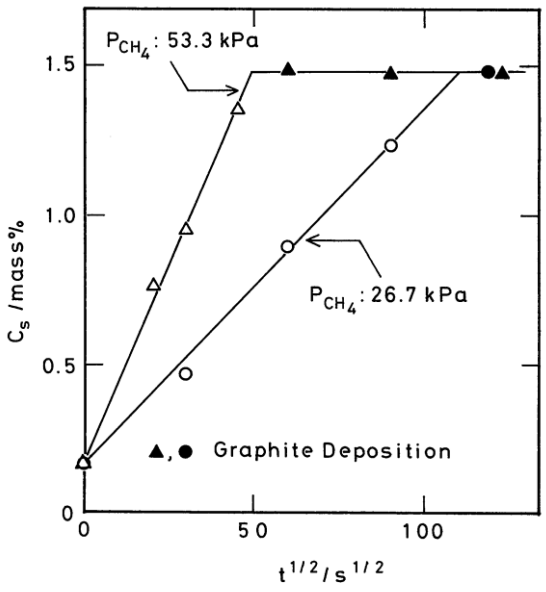

Figure 9 :Variations of the surface carbon conetent with square root of carburizing time

In this thesis, the boundary condition of the low pressure carburizing process will also be studied. The boundary condition is enhanced to have better simulation results.

2.2. The carbonitriding simulation

Carbonitriding has been used for case hardening for decades. Compared to carburizing process, cabonitriding process uses lower temperature and form shallower case [19][20]. Reaction for carbonitriding process can be found in Table 1.

Table 1: The reaction during carbonitriding process

Reaction No.	Reaction
1	$\mathrm{CH_4} \leftrightarrow C + 2H_2$
2	$2\mathrm{CO} \leftrightarrow \mathrm{C} + \mathrm{CO_2}$
3	$\mathrm{CO} + \mathrm{H_2} \leftrightarrow C + H_2O$
4	$\mathrm{HCN} \leftrightarrow \mathrm{C} + \mathrm{N} + \frac{1}{2}H_2$
5	$\mathrm{NH_3} \leftrightarrow N + \frac{3}{2}H_2$
6	$\frac{1}{2}N_2 \leftrightarrow N$
7	$2NH_3 \leftrightarrow N_2 + 3H_2$
8	$CO + H_2O \leftrightarrow CO_2 + H_2$
9	$CO + NH_3 \leftrightarrow HCN + H_2O$

When both carbon and nitrogen are dissolved in austenite, these two interstitials will interact and affect the activity of one another. The diffusion coefficient for carbon in austenite has long been known to be strongly dependent on the carbon content. J. Slyske and T. Ericsson[19] studied the interaction mechanism between carbon and nitrogen in steel carbonitriding process and presented the diffusivity calculation equations. Liang and Sisson have modeled the process [21] as Figure 10 presents.

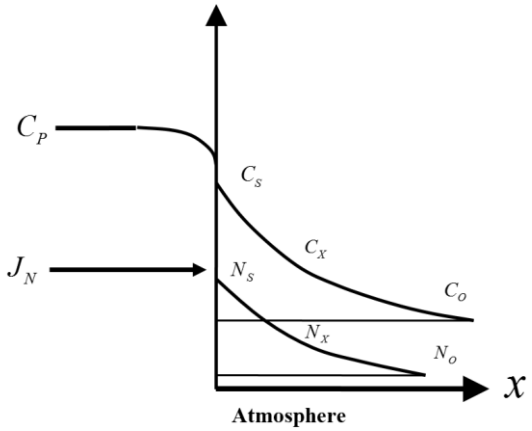

Figure 10: The diagram for carbonitriding process [21]

An approximate value of the diffusion coefficient for carbon in Fe-C-N austenite is obtained by taking the material thermodynamics study into account:

$$D_c^{\gamma} = 4.84 \cdot 10^{-5} \cdot exp\left(-\frac{155000}{RT}\right) \cdot exp\left[\frac{570000-320 \cdot T}{RT} \cdot (x_C + 0.72 \cdot x_N)\right] \cdot \frac{1-5x_N}{1-5(x_C-x_N)} m^2/s \qquad \textit{Equation 12}^{[19]}$$

At higher nitrogen contents and in the presence of high carbon contents this value will be altered. The resulting equation for the diffusion coefficient for nitrogen in austenite as a function of temperature and composition in the (Fe-N-C) system would then become:

$$D_N^{\gamma} = 9.1 \cdot 10^{-5} \cdot exp\left(-\frac{168600}{RT}\right) \cdot exp\left[\frac{570000-320 \cdot T}{RT} \cdot (x_C + 0.72x_N)\right] \cdot \frac{1-5x_C}{1-5(x_C+x_N)} m^2/s \qquad \textit{Equation 13}^{[19]}$$

2.3. The nondestructive testing

Surface hardness and case depth are important properties of carburized steel. Experimental measurement of the properties is time consuming and expensive. It is required by the industry to develop fast, accurate nondestructive testing technique. Barkhausen noise testing is one of the technique that the industry has been used [22][23][24].

The Barkhausen noise phenomenon is found in ferromagnetic materials as seen in Figure 11. The physical principle behind the technology is that microstructural defects including dislocations, small carbides, grain boundaries, etc. which are related with the electric magnetic field [25]. The properties also determine the mechanical properties of the parts. When a ferromagnetic material is subjected to magnetic field, the magnetization is not obtained continuously but made up of discrete jumps which was caused by the movement of domain walls [29]. There is interaction between the domain wall and overcoming barriers in their path [25]. These jumps, due to sudden changes in magnetization, yield electromagnetic and acoustic signals that can be detected by a coil. For carburized and carbonitrided steels, the carbon or nitrogen content increases the number of defects or pinning sites and hence improves hardness. These pinning sites also change the behavior of block walls in magnetic domains and thus the Barkhausen noise level. It is also sensitive to the surface condition and the heat treating processes [30][32][33].

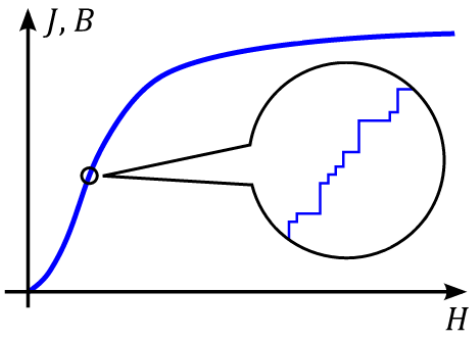

Figure 11: Barkhausen Noise (Wikipedia: Barkhausen noise)

It is now one of the most popular magnetic NDE methods for investigating intrinsic properties of magnetic materials such as grain size heat treatment, strain and other mechanical properties such as hardness.

To produce Barkhausen noise, it is necessary for the specimen to be subjected to varying levels of magnetization to the point of magnetic saturation at a certain rate. This can be achieved by employing a yoke, particularly in surface analysis. To maintain constant induction, the yoke is fed by a bipolar variable source of triangular waveform. The Barkhausen noise sensor consists of an air coil of copper wire with or without a ferrite core. Usually, signals are amplified, filtered, rectified, and integrated to produce a spectrum. The height, half height width, and position with excitation are parameters that provide useful information. Measurements were carried out at different frequencies using electronic filters to distinguish between the signal from the bulk and that from the surface [26][27].

Figure 12: The Barkhausen noise equipment[25]

Figure 12 shows the equipment used for MBN testing. MBN method has showed promising results for stress evaluation [28]. Figure 13 shows the origin MBN signal under different applied stress, left shows MBN signal without applied stress, right shows MBN signal under a tensile stress of 60.44Mpa [31].

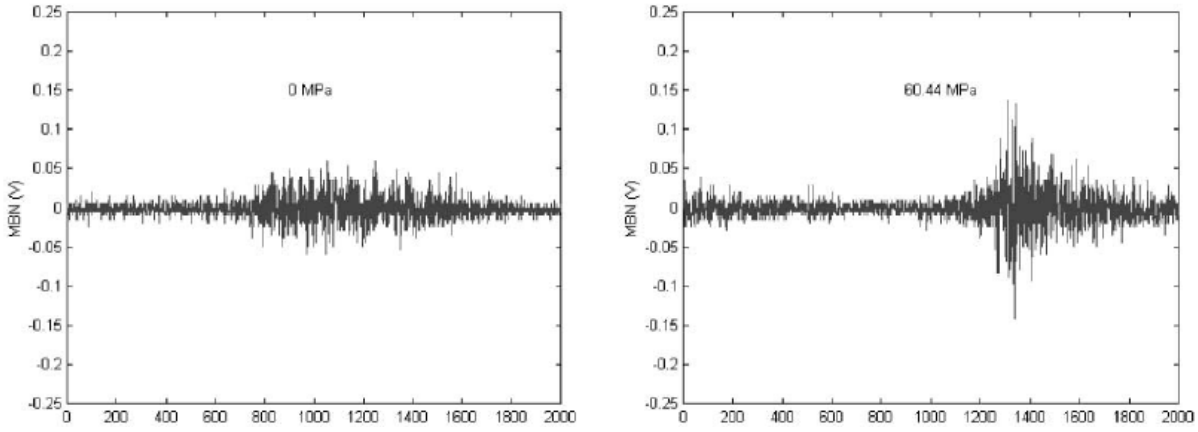

Figure 13: The raw signal of Barkhausen noise measurement[31]

To collect all the information contained in the signal [27], the frequency spectrum of the Barkhausen noise. To do so, the samples were magnetized, as shown schematically in Figure 14, with a yoke at an excitation frequency of 3 Hz. The signals were detected by a coil of copper wire with a ferrite core. These signals were amplified and filtered by a low pass filter at a cut off frequency of 200 kHz. Based on these data, a fast Fourier transform (FFT) was determined. The FFT has been used for the Barkhausen. The spectrum obtained was integrated on ten frequency bands, each 20 kHz wide, from 0 to 200 kHz. These ten values, for each sample, were plotted as a function of the measured case depth of specimens. Based on this, it was possible to determine which range of frequencies is the most appropriate for case depth evaluation[27].

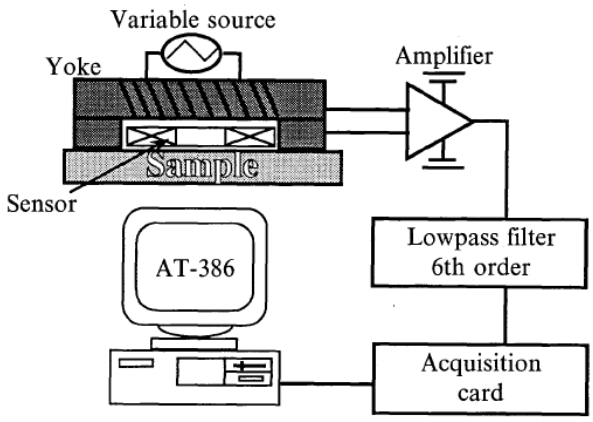

Figure 14: The process of Barkhausen noise measurement[27]

MBN is also sensitive with the carbon concentration. Kameda and Ranjan have studied the effects of carbon concentration tempering condition on the Barkhausen Noise. 1025, 1045 and 1095 steel were tested. Result is presented in Figure 15. Higher carbon concentration leads the MBN signal to a smaller level.

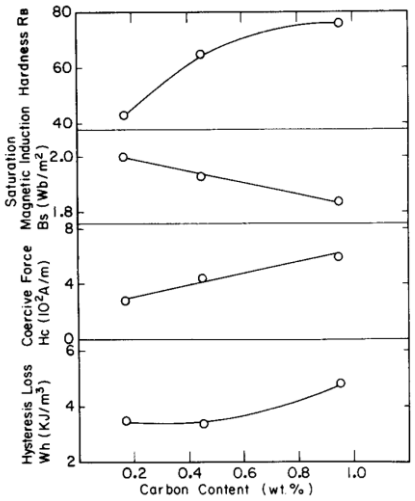

Figure 15: The carbon concentration effects on MBN

Magnetization voltage sweep (MVS) has been used to determine the case depth of the carburized. The approach is still under investigation. M. Dubios and M. Fiset measured the case depth with the integration of the MBN. The Barkhausen noise level decrease with a thicker case [27].

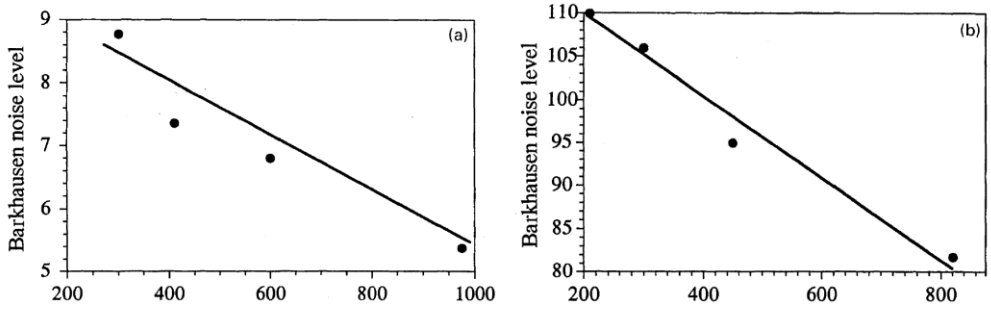

Figure 16: The MBN measurement on the case depth [27]

The measurement of the case depth with case depth can also base on the Barkhausen Noise response from the hard case and the soft core [22][26][34]. The Martensite requires stronger magnetic field to be magnetized than the ferrite because of the high coercively. The dual-peak method is used for the evaluation of case depth by V. Moorth, B.A. Shaw and S. Day. Figure 17 presents the difference in the peak shape for the sample with 0.65mm and 0.95mm case depth.

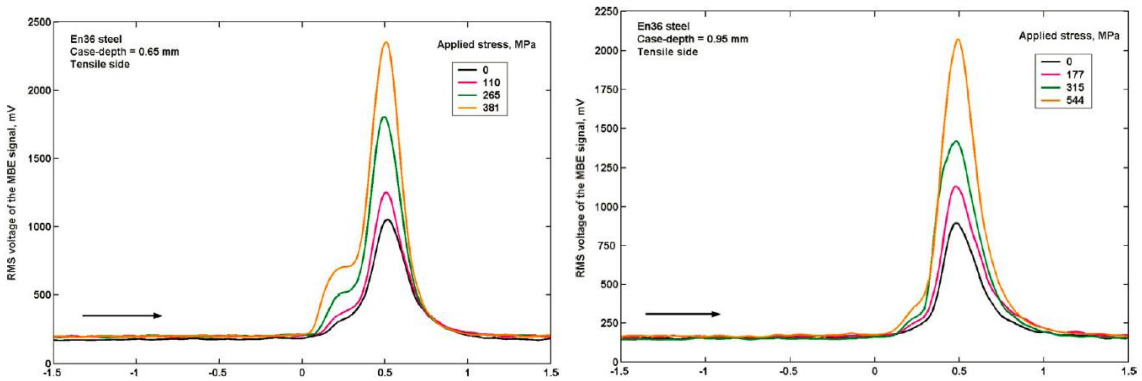

Figure 17: MBN profile, left: case depth=0.65mm, right: case depth=0.95mm [37]

S. Santa-aho has proposed the case depth evaluation by talking the ratio of the magnetic voltage sweep (MVS) curve as Figure 18 presented [24]. The MBN is measured over a range of the voltage at certain frequency. The profile measured shows the response of the MBN to the microstructure of the steel and indirectly evaluate the properties of steel [23][24].

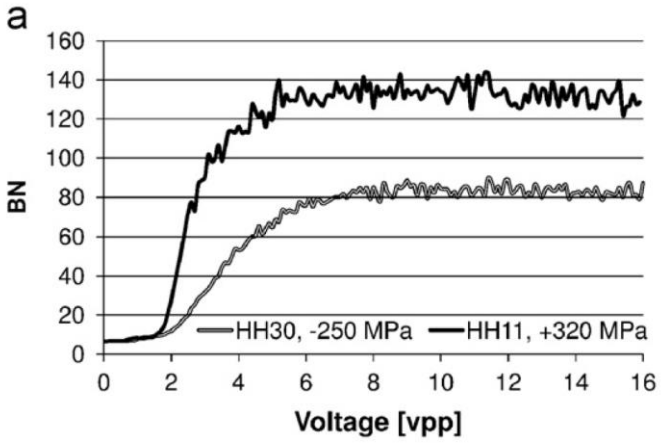

Figure 18: The MVS measurement for two steel grade with different residual stress[24]

The MVS is also used for case depth evaluation [24]. Samples used for the measurement is as presented in Table 2. Samples were induction hardened to different case depth. Set 5 is carburized alloy.

Table 2: The description of the samples used for the MVS case depth measurement

	Set 1	Set 2	Set 3	Set 4	Set 5	Set 6
Hardening method	Induction hardening	Induction hardening	Induction hardening	Induction hardening	Carburizing case-hardening	Induction hardening
Material	34CrNiMo6	34CrNiMo6	34CrNiMo6	42CrMo4	18CrNiMo7-6	34CrNiMo6, 42CrMo4
Hardening layer thickness variations [mm]	Rht 0.65–2.2	Rht 0.825–1.85	Rht 0.65–1.45	Rht 0.35–1.9	CHD 1.2–3.5	Rht 2.8, 2.9 (34CrNiMo6) Rht 3, 4 (42CrMo4)

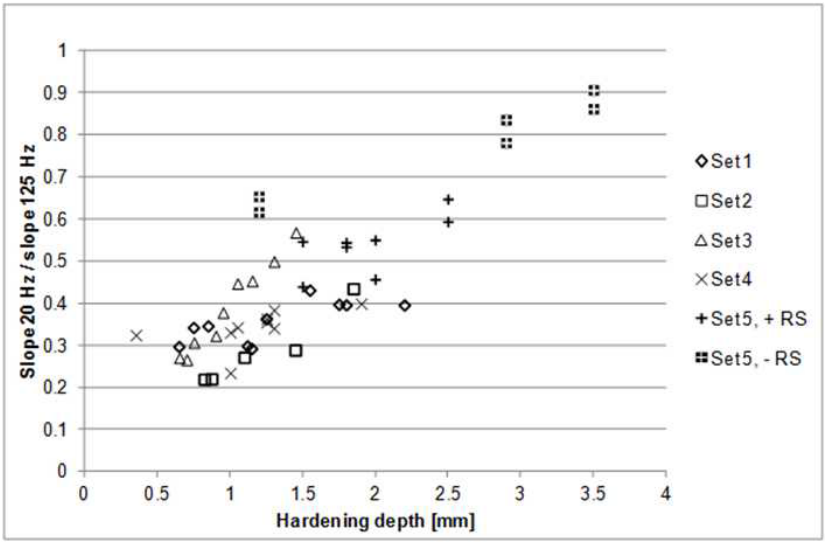

Figure 19: The Barkhausen Noise testing on the case depth [19]

The measurement is presented in Figure 19. The testing results show that for different group of samples. There is always linear correlation between the slope ratio method and the case depth. But the carburized samples have not shown as strong correlation as other groups do.

Reference

[1]. Karabelchtchikova, Olga, and Richard D. Sisson. "Carbon diffusion in steels: a numerical analysis based on direct integration of the flux." Journal of phase equilibria and diffusion 27.6 (2006): 598-604.

[2]. Karabelchtchikova, O., and R. D. Sisson Jr. "Thermodynamic and Kinetic Aspects of Endothermic Carburizing Atmosphere with Natural Gas Enrichment." (2007).

[3]. Kula, Piotr, et al. "FineCarb®–the flexible system for low pressure carburizing. New options and performance." Japan Soc. Heat Treat 49.1 (2009): 133-136.

[4]. Kula, Piotr, et al. "“Boost-diffusion” vacuum carburising–Process optimisation." Vacuum 99 (2014): 175-179.

[5]. Goldstein, J. I., and A. E. Moren. "Diffusion modeling of the carburization process." Metallurgical Transactions A 9.11 (1978): 1515-1525.

[6]. Wei, Y., L. Zhang, and R. D. Sisson Jr. "Modeling of Carbon Concentration Profile Development During Both Atmosphere and Low Pressure Carburizing Processes." Journal of materials engineering and performance 22.7 (2013): 1886-1891.

[7]. Jung, Minsu, Sehoon Oh, and Young-Kook Lee. "Predictive model for the carbon concentration profile of vacuum carburized steels with acetylene."Metals and Materials International 15.6 (2009): 971-975.

[8]. Tsuji, Shinji, Itsuo Ishigami, and Kyuhiko Yamanaka. "Vacuum Carburizing of Low Carbon Steel with Methane." Transactions of the Japan institute of metals 28.1 (1987): 48-56.

[9]. Ryzhov, N. M., A. E. Smirnov, and R. S. Fakhurtdinov. "Control of carbon saturation of the diffusion layer in vacuum carburizing of heat-resistant steels." Metal science and heat treatment 46.7-8 (2004): 340-344.

[10]. Jimenez, H., M. H. Staia, and E. S. Puchi. "Mathematical modeling of a carburizing process of a SAE 8620H steel." Surface and Coatings Technology 120 (1999): 358-365.

[11]. Zajusz, M., K. Tkacz-Smiech, and M. Danielewski. "Modeling of vacuum pulse carburizing of steel." Surface and Coatings Technology 258 (2014): 646-651.

[12]. Khan, R. U., et al. "Pyrolysis of propane under vacuum carburizing conditions: An experimental and modeling study." Journal of Analytical and Applied Pyrolysis 81.2 (2008): 148-156.

[13]. Gorockiewicz, R., and A. Lapinski. "Structure of the carbon layer deposited on the steel surface after low pressure carburizing." Vacuum 85.3 (2010): 429-433.

[14]. Ikehata, Hideaki, et al. "Modeling Growth and Dissolution Kinetics of Grain-Boundary Cementite in Cyclic Carburizing." Metallurgical and Materials Transactions A 44.8 (2013): 3484-3493.

[15]. Ochsner, A., J. Gegner, and G. Mishuris. "Effect of diffusivity as a function of the method of computation of carbon concentration profiles in steel." Metal science and heat treatment 46.3-4 (2004): 148-151.

[16]. Kula, P., R. Pietrasik, and K. Dybowski. "Vacuum carburizing—process optimization." Journal of Materials Processing Technology 164 (2005): 876-881.

[17]. Gorockiewicz, R. "The kinetics of low-pressure carburizing of alloy steels." Vacuum 86.4 (2011): 448-451.

[18]. Tanaka, Kouji, et al. "Calculation of Microstructure in Vacuum Carburizing Incorporating Kinetics Modeling of Grain-boundary Cementite." ISIJ international 52.1 (2012): 134-139.

[19]. Slycke, J., and T. Ericsson. "A study of reactions occurring during the carbonitriding process." Journal of Heat Treating 2.1 (1981): 3-19.

[20]. Slycke, J., and T. Ericsson. "A study of reactions occurring during the carbonitriding process part II." Journal of Heat Treating 2.2 (1981): 97-112.
[21]. He, L., Xu, Y., and Sisson, R. D., "Modeling the Carbonitriding of Steel," Materials Performance and Characterization, Vol. 1, No. 1, 2012, pp. 1-11.
[22]. Blaow, M., J. T. Evans, and B. A. Shaw. "Effect of hardness and composition gradients on Barkhausen emission in case hardened steel." Journal of magnetism and magnetic materials 303.1 (2006): 153-159.
[23]. Sorsa, Aki, et al. "Utilization of frequency-domain information of Barkhausen noise signal in quantitative prediction of material properties." AIP Conference Proceedings. Vol. 1581. 2014.
[24]. Santa-aho, Suvi, et al. "Utilization of Barkhausen noise magnetizing sweeps for case-depth detection from hardened steel." Ndt & E International 52 (2012): 95-102.
[25]. Rollscan 300 Operation instructions Version 1.6b. Nov 2011 by Stresstech
[26]. Vaidyanathan, S., et al. "Evaluation of induction hardened case depth through microstructural characterisation using magnetic Barkhausen emission technique." Materials Science and Technology 16.2 (2000): 202-208.
[27]. Dubois, M., and M. Fiset. "Evaluation of case depth on steels by Barkhausen noise measurement." Materials science and technology 11.3 (1995): 264-267.
[28]. Sorsa, Aki, et al. "Quantitative prediction of residual stress and hardness in case-hardened steel based on the Barkhausen noise measurement." Ndt & E International 46 (2012): 100-106.
[29]. De Campos, M. F., et al. "Magnetic Barkhausen noise in quenched carburized steels." Journal of Physics: Conference Series. Vol. 303. No. 1. IOP Publishing, 2011.
[30]. Kameda, J., and R. Ranjan. "Nondestructive evaluation of steels using acoustic and magnetic Barkhausen signals—I. Effect of carbide precipitation and hardness." Acta Metallurgica 35.7 (1987): 1515-1526.
[31]. Anglada-Rivera, J., L. R. Padovese, and J. Capo-Sanchez. "Magnetic Barkhausen noise and hysteresis loop in commercial carbon steel: influence of applied tensile stress and grain size." Journal of magnetism and magnetic materials 231.2 (2001): 299-306.
[32]. Parakka, Anthony P., et al. "Barkhausen effect in steels and its dependence on surface condition." Journal of applied physics 81.8 (1997): 5085-5086.
[33]. Moorthy, V., et al. "Magnetic Barkhausen emission technique for evaluation of residual stress alteration by grinding in case-carburised En36 steel." Acta Materialia 53.19 (2005): 4997-5006.
[34]. Wilson, John W., et al. "Magneto-acoustic emission and magnetic Barkhausen emission for case depth measurement in En36 gear steel." IEEE Transactions on Magnetics 45.1 (2009): 177-183.
[35]. Moorthy, V., B. A. Shaw, and S. Day. "Evaluation of applied and residual stresses in case-carburised En36 steel subjected to bending using the magnetic Barkhausen emission technique." Acta Materialia 52.7 (2004): 1927-1936.

Chapter Three: Publications

#Paper One:

A new boundary condition for simulation of low pressure carburizing

(To be submitted to Journal of Heat Treatment of Materials)

Lei Zhang, Richard D. Sisson Jr.

Center for Heat Treating Excellence, Worcester Polytechnic Institute,

100 Institute Road, Worcester, Massachusetts, 01609, U.S.A

Abstract

CarbTool© has been an effective tool for the simulation of both gas and low pressure carburizing (LPC) processes. CarbTool© has successfully predicted the carbon concentration profiles which help the development of heat treating process and save cost and time. However, in some cases the LPC model prediction does not agree with the experimental results. It has been found that these disagreements are due to the formation of the carbides and soot on the part surface which reduces the carbon flux. For LPC model, the average carbon flux was initially used as the boundary condition which was calculated from experimental data. The modification of the boundary condition to improve the low pressure carburizing process simulation is presented. The improvement that uses a carbon potential in gas and mass transfer coefficient for the LPC process is presented. Experimental data was used to determine the carbon potential and mass transfer coefficient. Experimental verification is also presented.

1. Introduction

Low pressure carburizing also called vacuum carburizing is gaining interest because the reduced distortion and environmental impact [4][7][20]. In addition, there is no intergranular oxidation (IGO) formed at the surface [6]. High temperature carburizing [27, 28] is also possible with the low pressure atmosphere which will shorter the processing time. A typical low pressure carburizing process will include several boost/diffuse cycles as presented *Figure 20*. Shorter cycles are preferred by a few manufacture to avoid soot formation of the process on the surface [3][4][16].

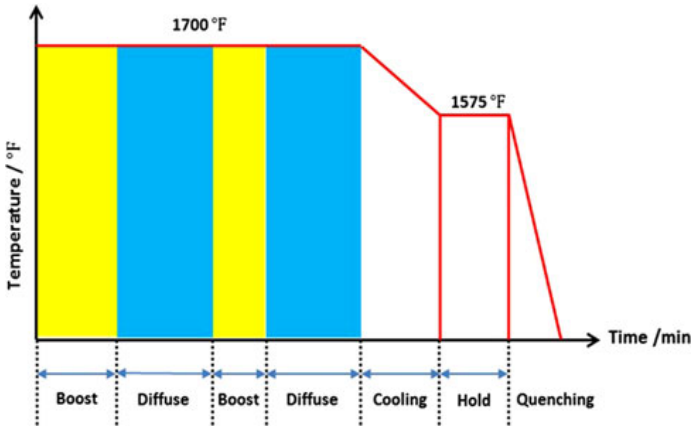

Figure 20: Typical low pressure carburizing process [6]

CarbTool© has been developed by Center of Heat Treatment Excellence to predict the carbon concentration profile in steels [1][2][6]. The software can be used for the prediction of both gas and low pressure carburizing process. The materials in the data base includes 10XX, 48XX, 51XX, 86XX, 93XX, etc. *Figure 21* present the modeling process of carburizing.

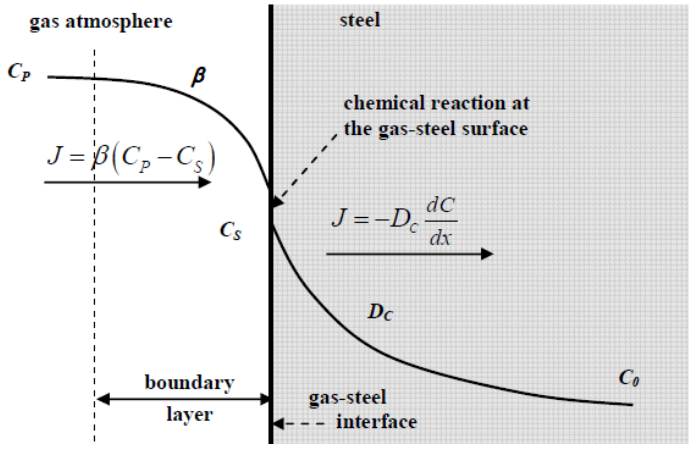

Figure 21: The modeling process for carburizing process [1][2]

Carbon atoms are transferred to the surface from the atmosphere which may be calculated as [1][2][10]:

$$J = \beta(C_p - C_s) \qquad \textit{Equation 14}$$

where J (g/cm^2/s)is the carbon flux, β (cm/s) is the mass transfer coefficient, $C_p$is the carbon potential, $C_S$is the surface carbon concentration (g/cm^3).

Diffusion of the carbon into the bulk is modeled with Fick's First Law [1][2][5]:

$$J = -D_c \frac{dC}{dx} \qquad \textit{Equation 15}$$

where D_c (cm^2/s) is the carbon diffusivity which is a function of temperature and carbon concentration, x (cm) is the distance from the surface.

A mass balance at the surface will be the surface boundary condition [1][2][24].

$$J = \beta(C_p - C_s) = -D_c \frac{dC}{dx} \quad \textit{Equation 16}$$

In the initial model for low pressure carburizing, the carbon flux for the gas was assumed to be constant [6]. Experimental data was used to determined was used to determine the flux.

$$J = J_{cons(}(t) \quad \textit{Equation 17}$$

In most cases, the simulation fits the experimental results well as seen in *Figure 22* [6]. For 5120 and 4320, the experimental constant carbon flux was effective for the simulation of the two alloys.

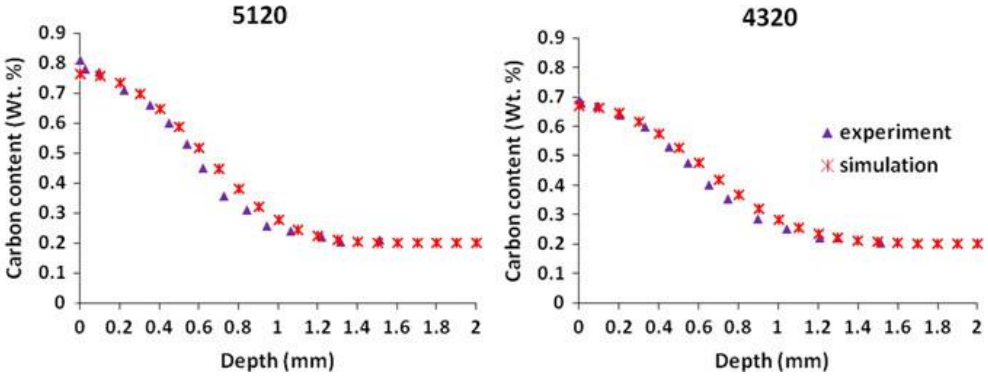

Figure 22: The carbon concentration for low pressure carburizing [6]

However, the prediction does not work well with 9310 steel for low pressure carburizing process. The low pressure carburizing process for 9310 steel was specified and compared with the experimental results. The experiment parameters are presented in *Table 3*. The carbon flux is calculated with previous experimental data. The *Figure 23* presents the concentration profiles.

Table 3: The process parameter for 9310 low pressure carburizing process

Specification:	**Surface carbon: 0.70 ± 0.05**	**case depth: 0.889mm**				
Carbon flux (g/cm2/s)	1st Boost (min)	1st Diffuse (min)	2nd Boost (min)	2nd Diffuse (min)	Cooling (min)	Holding (min)
1.63E-06	27	50	8.5	112	50	32

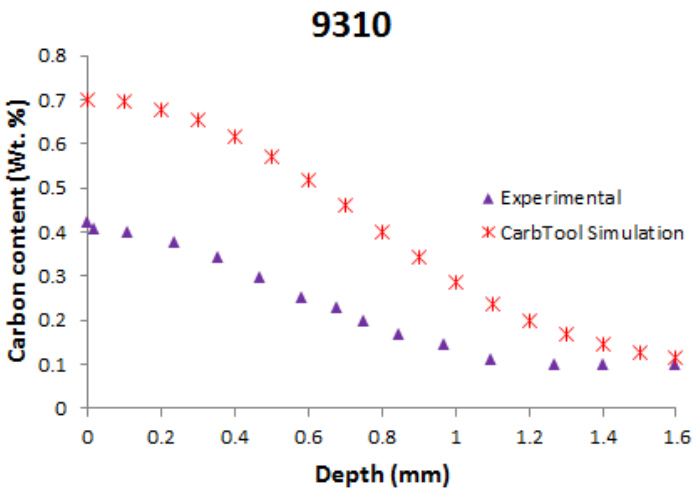

Figure 23: Carbon concentration profile for carburized 9310 with boost and diffusion process

In the simulation process, the carbon flux was calculated from previous experimental results. In *Figure 23*, with the input of carbon flux, 1.63E-06, the concentration profile does not agree with the experimental results. Carbon flux was the boundary condition with CarbTool©. It is sensitive to the gas temperature, pressure and the surface condition. The gas temperature and pressure remains constant. The surface of the steel is well cleaned. The weight gain has been studied by the thermalgravic analysis by Karabelchtchikova in an internal report as *Figure 24* presents. The data can provide us the data for the flux during the first 3 min boost step. The increase of the total carbon flux can be read from the *Figure 25*.

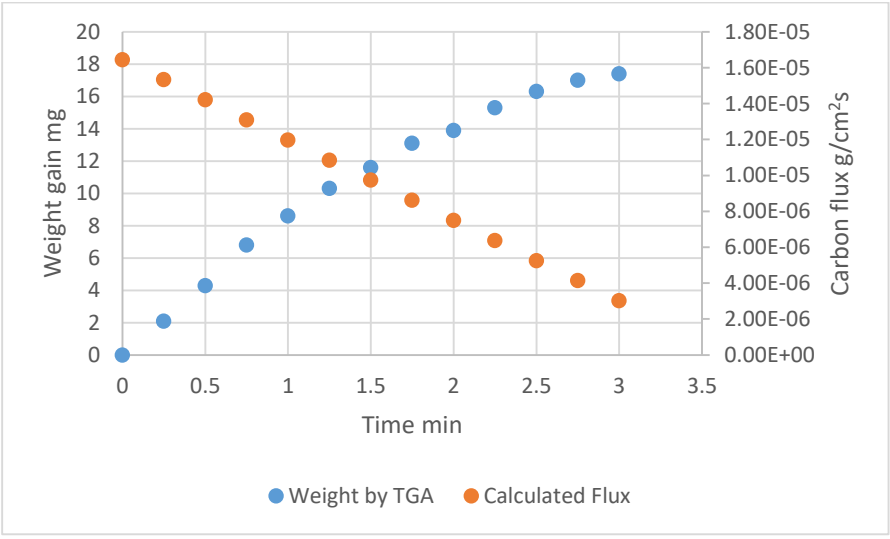

Figure 24: The weight gain during low pressure carburizing process

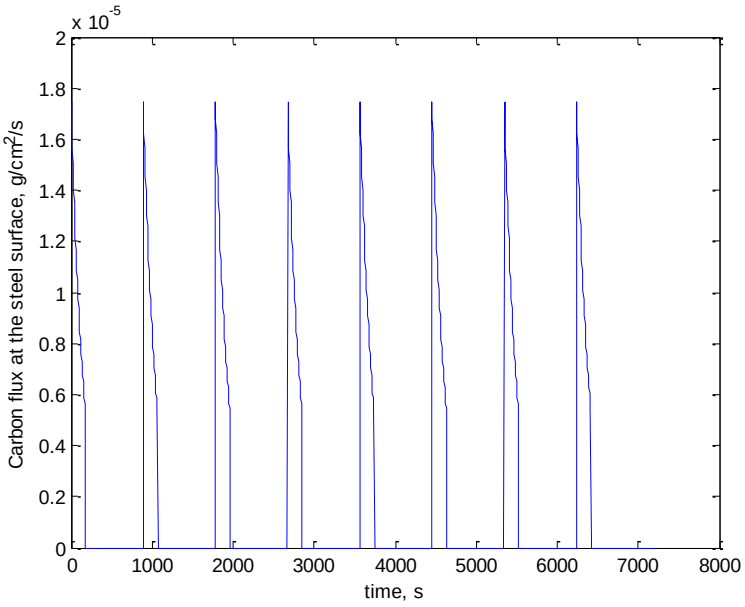

Figure 25: The carbon flux input for existing modeling(Internal report)

The model needs to be improved to better simulate the process. A thin layer of carbon deposit and carbides can form during the boost step of low pressure carburizing [8][16][17][26]. The carbon deposit is made up of hydrocarbons containing radicals [12][22]. Minsu Jung, Sehoon Oh and Young Kook Lee modeled the process with a carbon potential value which equals to the maximum solubility of the carbon in Austenite. [7] P. Kula, R.Pietrasik have developed a boundary condition that use the multicycle boost-diffuse steps for low pressure carburizing process [12]. In this method, constant carbon concentration was used and the boost step was extended because of the carbon deposit [11][16].

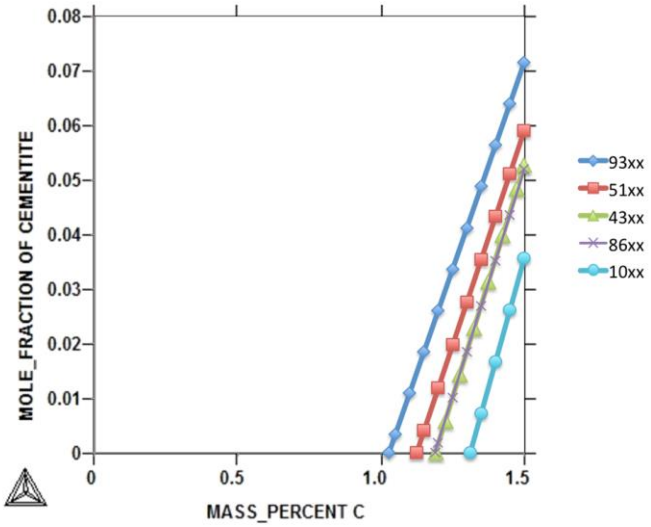

Figure 26: Mole fraction diagram of AISI 93xx, 86xx, 51xx, 43xx and 10xx [6] at 927 ℃

In *Figure 26*, the effects of alloy addition in the solubility of C calculated by ThermoCalc in the steel is presented. It is seen that 9310 has the lowest solubility limit as presented in *Table 4*.

Table 4: The maximum solubility of carbon in austenite for alloys at 927 ℃

	93XX	51XX	43XX	86XXX	10XX
Solubility	1.04 wt%	1.16wt%	1.21wt%	1.21wt%	1.28wt%

As seen with isopleth for 93XX verse carbon, cementite will form on the surface of 9310. Cementite will slow down the absorption of the carbon atoms. The *Figure 27* present the solubility of 9310 at 927℃ approximately 1.04 wt%. Beyond this concentration, carbides are stable.

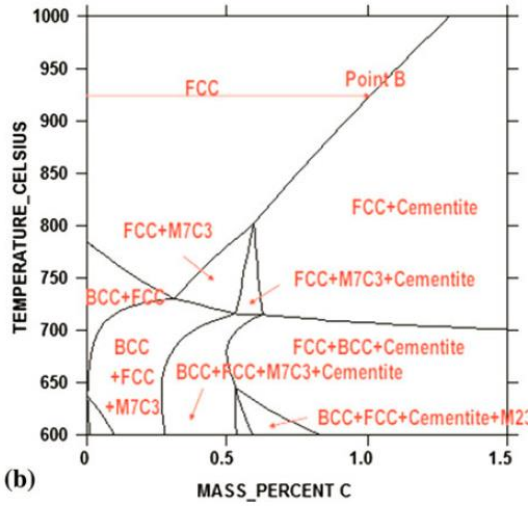

Figure 27: Isopleth for 93XX with carbon. Note: solubility limit at point B [6]

2. Experimental Procedure and Results

To investigate the near surface microstructural developments during low pressure carburizing of 9310. Two cycles were designed with boost steps only with duration of 20min and 60 min at 927℃. There was no carbides found with our previous experiments because the carbides dissolved during the diffusion step. The testing with boost step only will reveal the surface condition after the boost.

In this paper, two separated cycles were conducted with boost step only at 927℃. The boost time are 20 min, 60min. Surface carbon and case depth calculated by CarbTool© are also presented in *Table 5*.

Table 5: The process parameter for low pressure carburizing process

Carbon flux g/cm²s	**Diffusivity at start**	**Boost Time (min)**	**Surface carbon %C**	**Case depth mm**
1.63E-06	1.670e-9	20	1.65	0.25
1.63E-06	1.670e-9	60	2.18	0.56

Figure 28 presents the carbon concentration profile for 9310 after the boost only low pressure carburizing process. For the process with 20min boost, surface carbon concentration is 0.80 wt%. The surface carbon concentration of the 60 min boost process is 1.80 wt%, which indicated carbides precipitation.

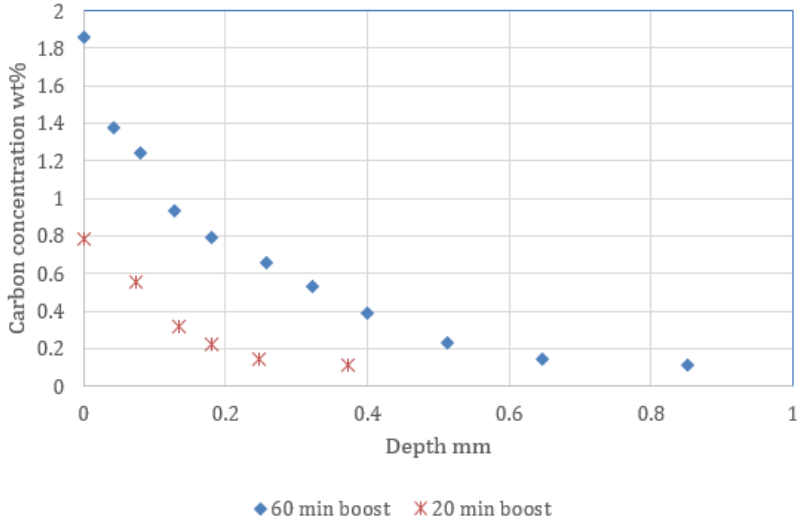

Figure 28: Carbon concentration profile for 20/60 minutes boost only processes at 927℃

X-Ray diffraction and scanning electron microscopy have been conducted to determine the phase development at surface of the parts. The samples with only the boost stages for 20 and 60 minutes were analyzed for surface microstructural development and concentration profiles. The XRD is used for the surface phase identification. The samples were well cleaned before the XRD testing. *Figure 29* and *Figure 30* present the results for both 20min and 60 min processes. At the surface, a strong peak of graphite is found. There is also cementite found at the surface. The 60 min boost step developed more intensity for cementite than the 20 min boost step.

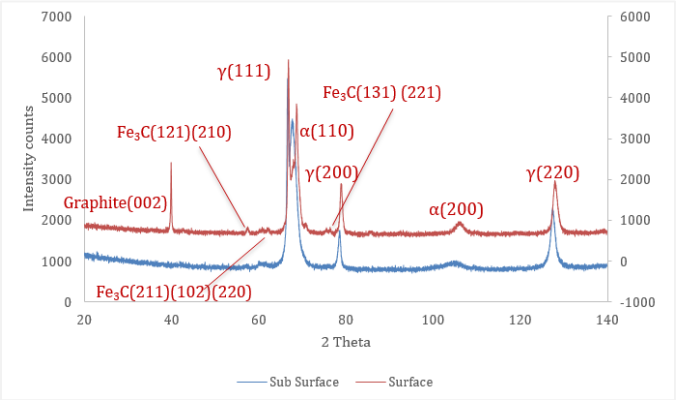

Figure 29: X-Ray Diffraction for 9310 after the 20 minutes boost only process (red), 15µm layer was removed (blue)

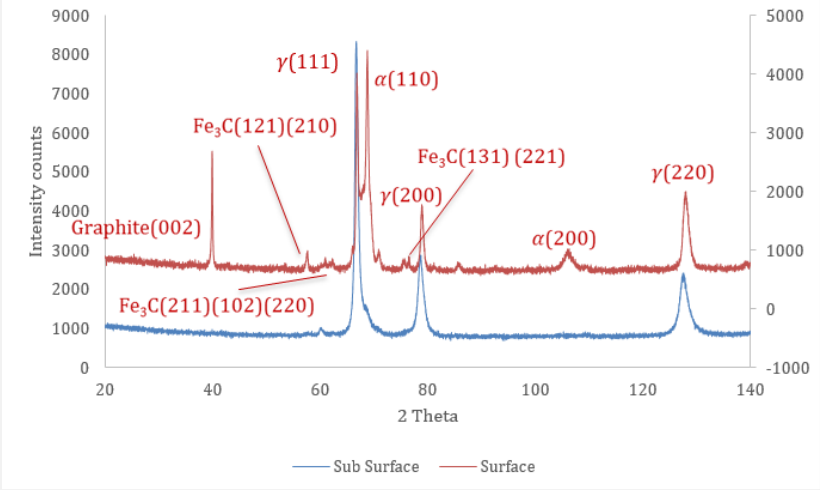

Figure 30: X-Ray Diffraction for 9310 of the 60 minutes boost only process(red), 15µm layer removed was removed (blue)

The X-Ray diffraction of the as-carburized surface reveled graphite and cementite. The graphite and the cementite were not observed after the 15µm layer was removed from the surface by grinding with fine sand paper.

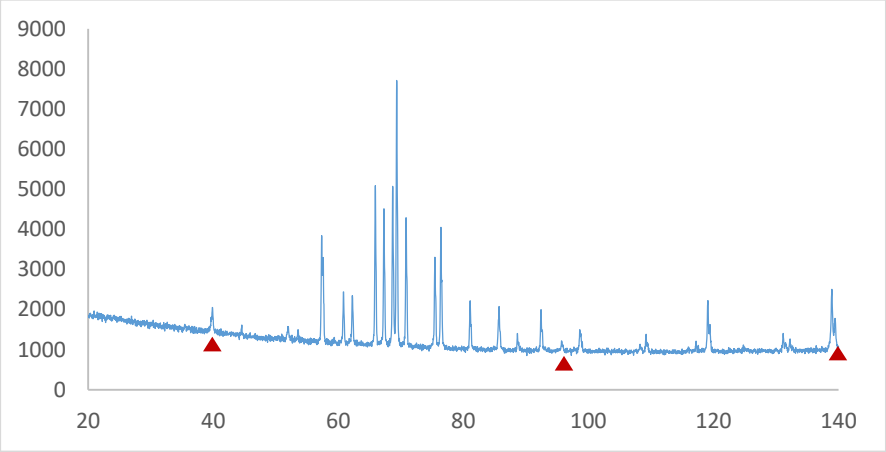

Figure 31: The extracted powder for carburized 9310 alloy with 60 Min boost
Graphite peaks are designated with the red triangle. All the other peaks are cementite.

The SEM has be used for further study the surface of the carburized samples. *Figure 32* presents the cross section of the surface region of the 20min boost only sample. EDS was conducted on the surface cross several regions of the 9310 samples. The carbon centration in the white region is 29.5wt% which indicates the existing of graphite.

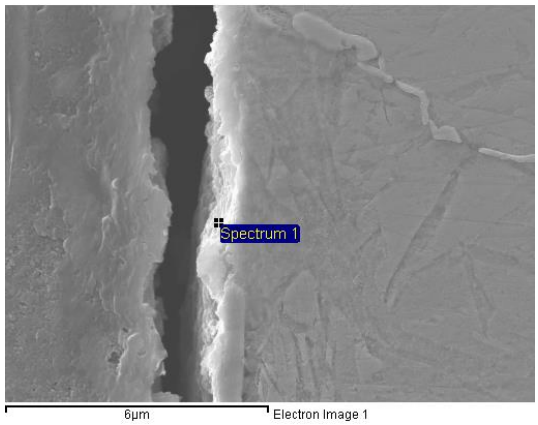

Figure 32: Scanning electron microscopy of cross section of the 20 minute boost at the surface. 20 wt% C austenite was measured by EDS

Figure 33 presents the scanning electron microscopy of a cross section of 9310 after a 60 min boost cycle. The surface carbon concentration is as high as 52.7% as measured with EDS.

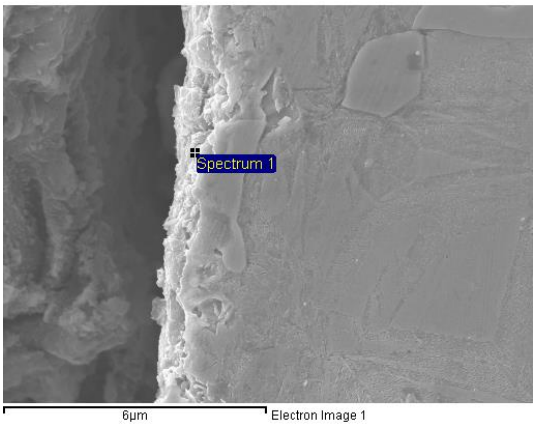

Figure 33: Scanning electron microscopy of cross section of the 60 minute boost at the surface. 52.7 wt% C was measured by EDS

The SEM photomicrograph for carburized surface is presented in *Figure 34*. The graphite can be at the dark region.

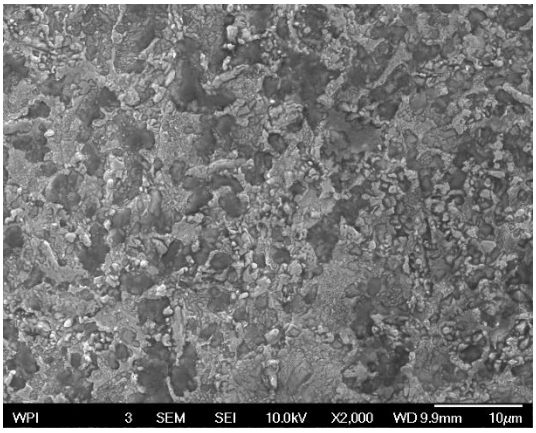

Figure 34: Scanning electric photomicrograph of the surface after 60 minutes boost.

Figure 35 presents the microstructure of cross section of the 60 minute boost carburization just below the surface. Inergranular carbides are clearly seen. As explained previously, due to the high carbon concentration, these carbides form and will be dissolved during the diffusion. The graphite and the carbides form a carbon rich layer that can provide carbon to the low pressure carburizing process. On the other hand, the carbides impede the diffusion process.

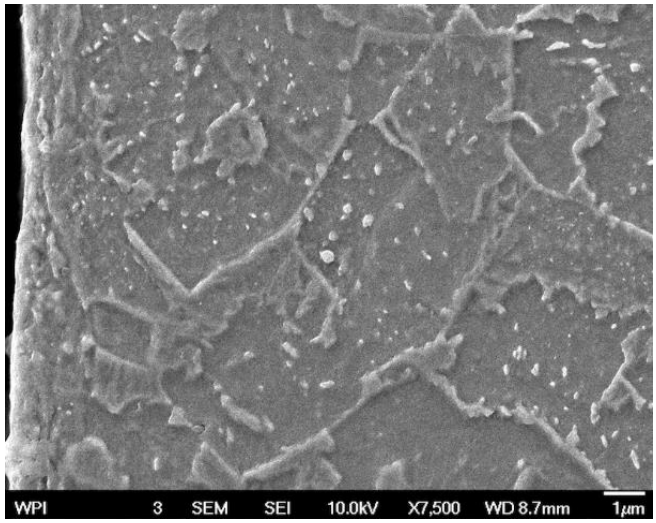

Figure 35: Scanning electric photomicrograph. Cross section of the 60 minute boost. Note: the carbides are found at the surface and at the prior austenite grain boundaries.

TEM result also presents the existing of the carbides at the surface area of the part as *Figure 36* presents.

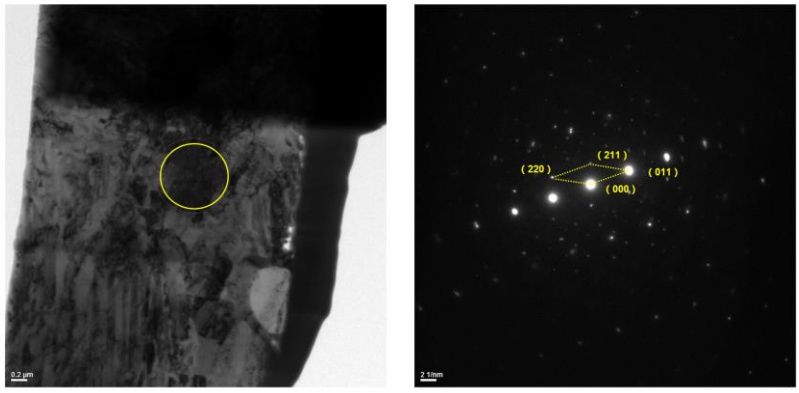

Figure 36: The detection of carbides with TEM for carburized 8620 alloy

The testing results has proved the existing of the carbon deposit on the surface during the boost step which change the diffusion mechanism [16]. The constant carbon flux boundary condition is not applicable in this case. The model needs to be enhanced to better describing the process.

3. Model development

R. Gorockiewicz has studied the kinetics of the low pressure carburizing process [17]. It was observed that carbon deposit formed after 5 min boost process. The carbon deposit is also the carbon source for carburizing during diffuse step [12][17] P. Kula, R. Pietrasik and K. Dybowski

tested the Armco foil testing which is presented in *Figure 37*. The surface carbon concentration of Armco was 1.23 wt% after 5min carburizing at 950℃. It increases to 1.39 wt% after 120min carburizing which is almost the same as the 15min process. The result indicates the maximum carbon concentration that can be achieved in low pressure carburizing is 1.39 wt% at 950℃. The carbon potential is possible to be applied for the simulation.

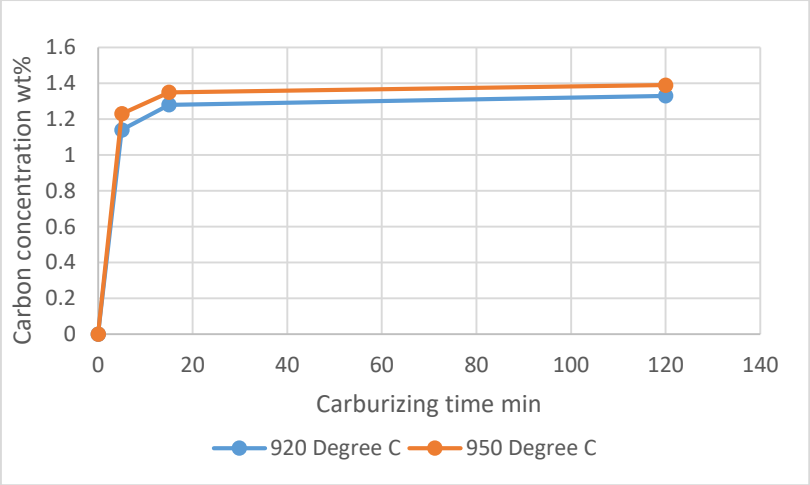

Figure 37: Carbon concentration in Armco foil testing in low pressure carburizing process[16]

Several new assumptions are proposed for the model development. The precipitation and dissolution of the carbides do not influence the carbon diffusivities coefficient. The built-in diffusivity data is used. Carbon deposit layer will form during the low pressure carburizing process. It provides stable carbon source during the carburizing process. *Figure 38* presents the in situ monitor of the resistance of alloy sample during low pressure carburizing studied by M. Bruncko, A. C. Kneissl and I. Anzel. Result presents the carbon deposit layer formed after 5min boost step where there is significant drop of electric resistance. During diffusion step, it takes about 5 min to dissolve the carbon deposit. Another assumption for the simulation is that the boost step is extend about 50% because of the existing of the carbon deposits.

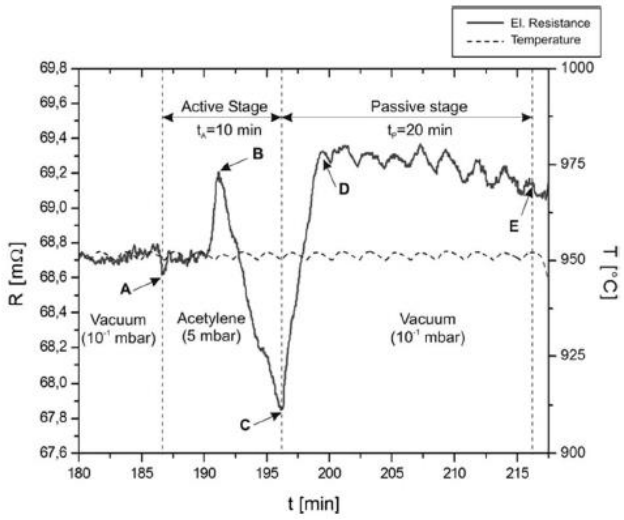

Figure 38: The in situ resistance testing for alloy sample during low pressure carburizing[19]

Assume the carbon deposit is providing carbon atom source for the low pressure carburizing process. The carbon activity is related to the pressure and the temperature of the atmosphere which is constant. When there is a balance at the surface during carburizing process [25]:

$$flux = \beta\left(C_p - C_s\right) = -D\frac{\partial C}{\partial x} \qquad \textit{Equation 18}$$

The mass transfer coefficient can be calculated from weight gain measurements [1][2]. The mass transfer coefficient data used in the model is calculated by the fitting method.

$$\beta^t = \frac{(\Delta m/A)|_{t_0 \to t}}{t(C_p - C_s^t)} \qquad \textit{Equation 19}$$

With the input of the carbon potential, both processes are simulated and presented in *Figure 40* and *Figure 39*. The simulation results agree with the experimental results for the carbon concentration profile. There is more carbon concentration at the surface because of the existing of the carbon deposit. The calculate mass transfer coefficient is 2e-5 cm/s.

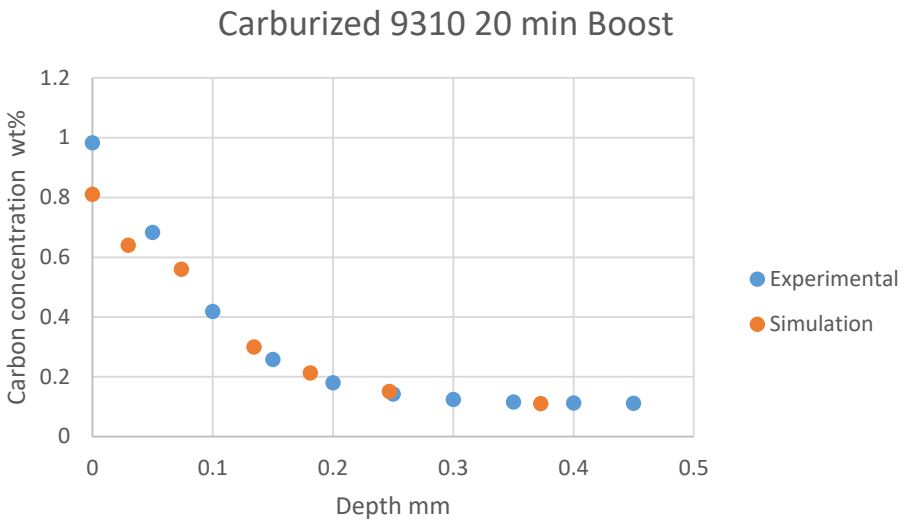

Figure 39: The carbon concentration simulation of carburized 9310 with 20 min boost

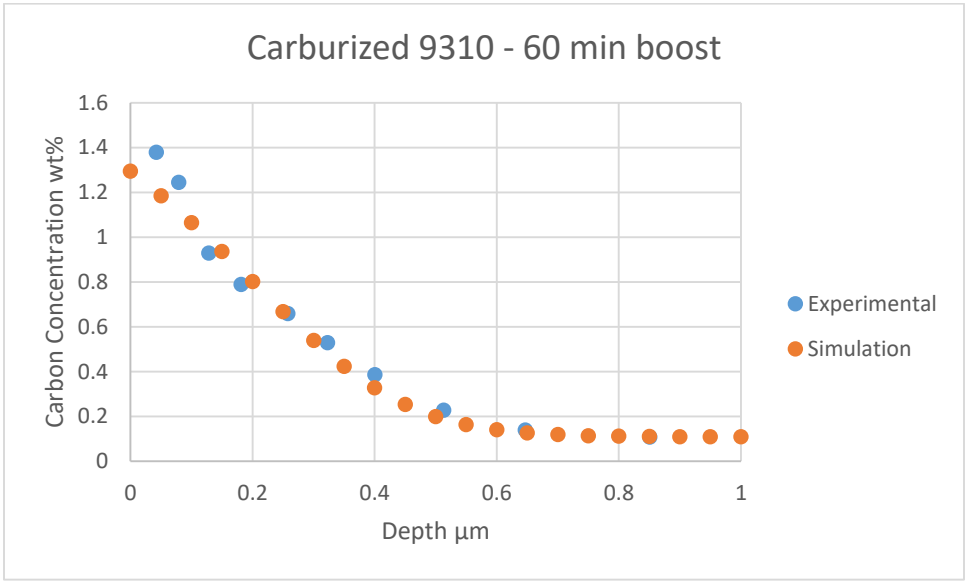

Figure 40: The carbon concentration simulation of carburized 9310 with 60 min boost

The enhanced model has been verified with more alloys with low pressure carburizing process. *Figure 41* shows the simulation of 9310 which was failed to simulate with previous model. It has successfully modeled with the current model. 8620 cycle is also modeled and they can also agree with the experimental results well as presented in *Figure 42*.

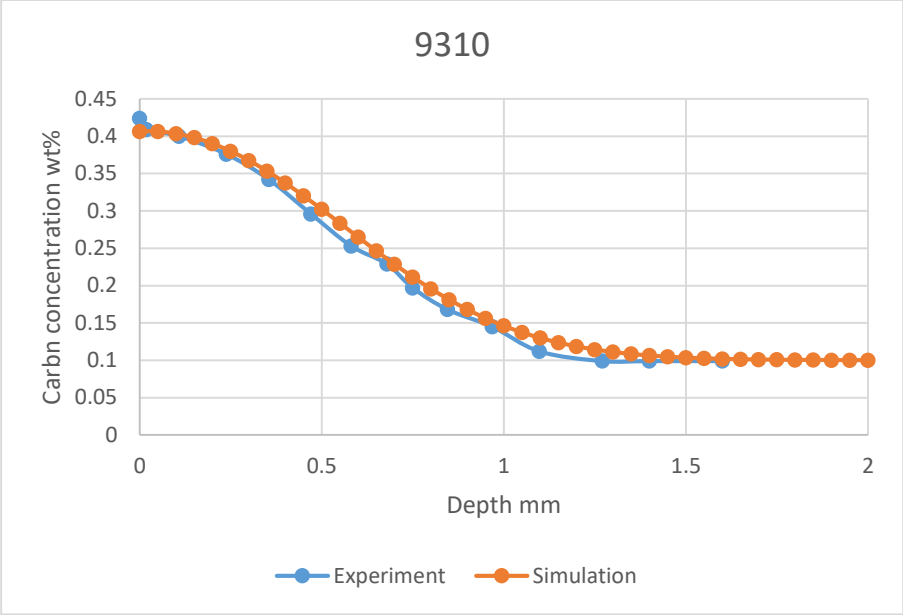

Figure 41: Low pressure carburized 9310

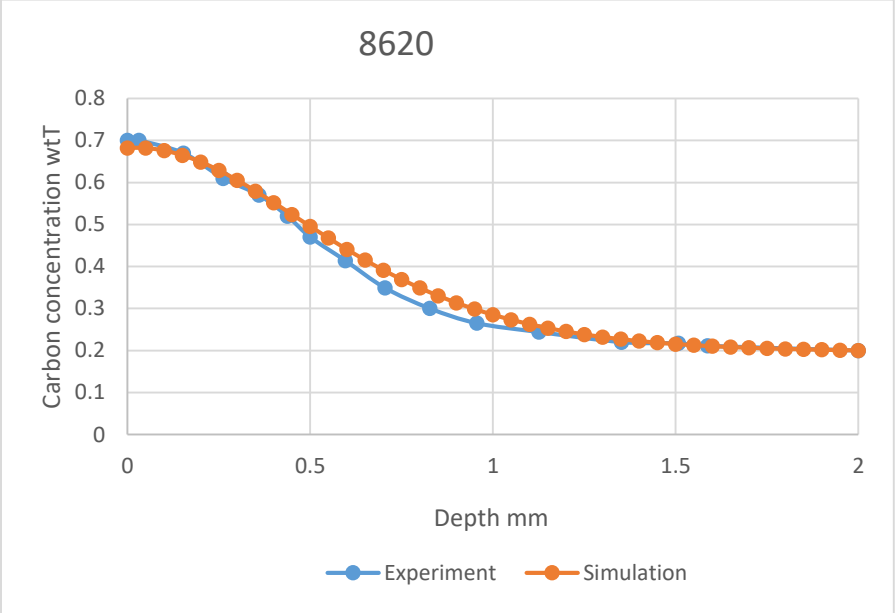

Figure 42: Low pressure carburized 8620

4. Conclusion

- Due to the deposition of graphite and the formation of cementite, CarbTool© does not actually simulate the LPC carburization of 9310.
- The problem is a result of the inaccurate mass balance on the surface of the 9310.
- A new mass balance has been developed that uses a mass balance between the graphite /Cementite deposit and the 9310 steel.
- In the model, the composite of the deposits is used as the carbon potential (I. e. C_p=1.39 wt%).
- Excellent agreement with experimental results was found.

Reference

[1]. Karabelchtchikova, Olga, and Richard D. Sisson. "Carbon diffusion in steels: a numerical analysis based on direct integration of the flux." Journal of phase equilibria and diffusion 27.6 (2006): 598-604.

[2]. Karabelchtchikova, O., and R. D. Sisson Jr. "Thermodynamic and Kinetic Aspects of Endothermic Carburizing Atmosphere with Natural Gas Enrichment." (2007).

[3]. Kula, Piotr, et al. "FineCarb®–the flexible system for low pressure carburizing. New options and performance." Japan Soc. Heat Treat 49.1 (2009): 133-136.

[4]. Kula, Piotr, et al. "“Boost-diffusion” vacuum carburising–Process optimisation." Vacuum 99 (2014): 175-179.

[5]. Goldstein, J. I., and A. E. Moren. "Diffusion modeling of the carburization process." Metallurgical Transactions A 9.11 (1978): 1515-1525.

[6]. Wei, Y., L. Zhang, and R. D. Sisson Jr. "Modeling of Carbon Concentration Profile Development During Both Atmosphere and Low Pressure Carburizing Processes." Journal of materials engineering and performance 22.7 (2013): 1886-1891.

[7]. Jung, Minsu, Sehoon Oh, and Young-Kook Lee. "Predictive model for the carbon concentration profile of vacuum carburized steels with acetylene."Metals and Materials International 15.6 (2009): 971-975.

[8]. Tsuji, Shinji, Itsuo Ishigami, and Kyuhiko Yamanaka. "Vacuum Carburizing of Low Carbon Steel with Methane." Transactions of the Japan institute of metals 28.1 (1987): 48-56.

[9]. Ryzhov, N. M., A. E. Smirnov, and R. S. Fakhurtdinov. "Control of carbon saturation of the diffusion layer in vacuum carburizing of heat-resistant steels." Metal science and heat treatment 46.7-8 (2004): 340-344.

[10]. Jimenez, H., M. H. Staia, and E. S. Puchi. "Mathematical modeling of a carburizing process of a SAE 8620H steel." Surface and Coatings Technology 120 (1999): 358-365.

[11]. Zajusz, M., K. Tkacz-Smiech, and M. Danielewski. "Modeling of vacuum pulse carburizing of steel." Surface and Coatings Technology 258 (2014): 646-651.

[12]. Khan, R. U., et al. "Pyrolysis of propane under vacuum carburizing conditions: An experimental and modeling study." Journal of Analytical and Applied Pyrolysis 81.2 (2008): 148-156.

[13]. Gorockiewicz, R., and A. Lapinski. "Structure of the carbon layer deposited on the steel surface after low pressure carburizing." Vacuum 85.3 (2010): 429-433.

[14]. Ikehata, Hideaki, et al. "Modeling Growth and Dissolution Kinetics of Grain-Boundary Cementite in Cyclic Carburizing." Metallurgical and Materials Transactions A 44.8 (2013): 3484-3493.

[15]. Ochsner, A., J. Gegner, and G. Mishuris. "Effect of diffusivity as a function of the method of computation of carbon concentration profiles in steel." Metal science and heat treatment 46.3-4 (2004): 148-151.

[16]. Kula, P., R. Pietrasik, and K. Dybowski. "Vacuum carburizing—process optimization." Journal of Materials Processing Technology 164 (2005): 876-881.

[17]. Gorockiewicz, R. "The kinetics of low-pressure carburizing of alloy steels." Vacuum 86.4 (2011): 448-451.

[18]. Tanaka, Kouji, et al. "Calculation of Microstructure in Vacuum Carburizing Incorporating Kinetics Modeling of Grain-boundary Cementite." ISIJ international 52.1 (2012): 134-139.

[19]. Bruncko, M., A. C. Kneissl, and I. Anzel. "In Situ Monitoring of Vacuum Carburizing." Materials and Manufacturing Processes 24.7-8 (2009): 809-813.

[20]. Gräfen, Winfried, and Bernd Edenhofer. "New developments in thermo-chemical diffusion processes." Surface and Coatings Technology 200.5 (2005): 1830-1836.

[21]. Şimşir, Caner, and Cemil Hakan Gür. "A FEM based framework for simulation of thermal treatments: Application to steel quenching." Computational Materials Science 44.2 (2008): 588-600.

[22]. Khan, R. U., et al. "Modeling of acetylene pyrolysis under vacuum carburizing conditions of steel in a tubular flow reactor." Proc. 10th Int. Electronic Conf. on 'Synthetic organic chemistry', Basel, Switzerland. 2006.

[23]. Sugianto, Arif, et al. "Numerical simulation and experimental verification of carburizing-quenching process of SCr420H steel helical gear." journal of materials processing technology 209.7 (2009): 3597-3609.

[24]. Kim, Dong-Wan, et al. "A numerical model for vacuum carburization of an automotive gear ring." Metals and Materials International 17.6 (2011): 885-890.

[25]. Wołowiec, Emilia, et al. "Mathematical Modelling of the Vacuum Carburizing Process." Thermal

Process Modeling 2014:: Proceedings from the Fifth International Conference on Thermal Process Modeling and Computer Simulation. ASM International, 2014.

[26]. Kula, Piotr, et al. "The precipitation and dissolution of alloy iron carbides in vacuum carburization processes for automotive and aircraft applications-Part I." Advanced Materials Research. Vol. 486. Trans Tech Publications, 2012.

[27]. Stratton, P. F., S. Bruce, and V. Cheetham. "Low-pressure carburizing systems: A review of current technology." BHM Berg-und Hüttenmännische Monatshefte 151.11 (2006): 451-456.

[28]. Kula, Piotr, et al. "High Temperature Low Pressure Carburizing with Prenitriding Process− The Economic Option for Vacuum Carburizing." CHIANG MAI JOURNAL OF SCIENCE 40.5 (2013): 865-873.

#Paper Two:

Enhancement of CarbonitrideTool©- The determination of Retained Austenite and Microhardness Profile

(To be submitted to Journal of Heat Treatment of Materials)

Lei Zhang, Liang He, R. D. Sisson Jr.

Center for Heat Treating Excellence; Worcester Polytechnic Institute;

100 Institute Rd; Worcester, MA 01609, USA

Abstract

A software simulation tool, CarbonitrideTool©, has been developed by Center for Heat Treatment Excellence (CHTE) to predict the Nitrogen and Carbon concentration profiles in selected steels during the carbonitriding process. In this paper, an introduction of the software will be presented. The software uses a finite difference analysis for the simulation of absorption and diffusion of carbon and nitrogen into the steel. The surface boundary condition will be discussed as well as the composition dependent diffusivities of the carbon and nitrogen. Addition to the software, the prediction of the microstructure, as well as the Retained austenite and microhardness profiles will be presented. The experimental verification of the simulation is also presented and discussed.

1. Introduction

CarboNitrideTool© [1] was developed by CHTE predict the carbon and nitrogen concentration profiles during the carbonitriding process. This tool provides heat treaters with new opportunities to develop the process parameters and control strategies to minimize cycle times and cost while enhancing the quality of the heat treated products.

During the carbonitriding process, both carbon and nitrogen atoms are absorbed by the steel from the atmosphere while the steel is heated into the Austenite phase region [1] [2]. The steel is quenched after the process to form the hardened case. The fraction of retained austenite (RA) increases with the concentration of nitrogen and carbon. The faction of the retained austenite must be calculated to predict the microhardness of carbonitrided steel. Nitrogen content is an important factor for the

Martensite start (Ms) temperature [1]. However, the current empirical method [3] of calculating the Ms temperature does not consider the effects of the nitrogen. In this paper, the method will be modified to predict the RA fraction in the carbonitrided samples. The microhardness will be calculated as well as RA fraction.

The user interface for the CarbonitrideTool© software is presented in Figure 43. The carbon and nitrogen concentration profiles can be calculated based on the user-defined initial conditions and the process parameters [4,5]. The carbon boundary condition will be the flux balance at the interface with a surface-limited mass transfer coefficient. The boundary condition for the calculation of nitrogen diffusion is an experimentally determined constant nitrogen flux [4,5].

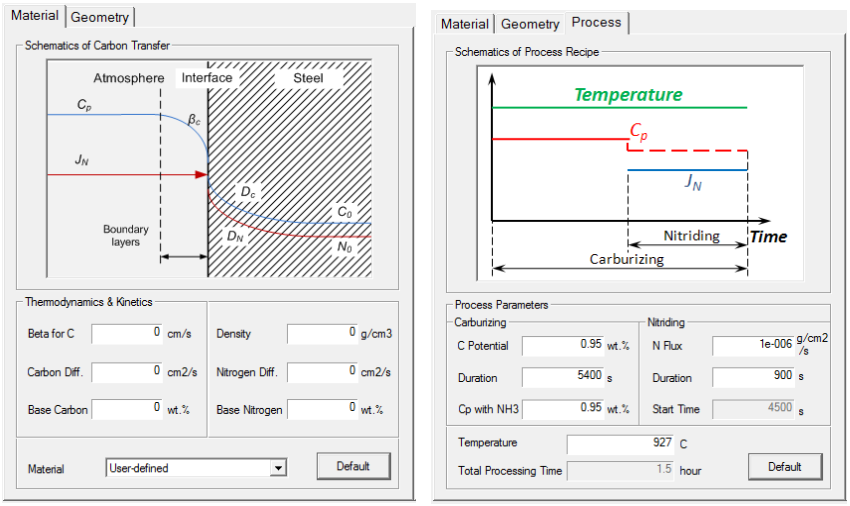

Figure 43: The interface of CarbonitrideTool©

When both carbon and nitrogen are dissolved in Austenite, these two interstitials affect the activity of one another. The diffusion coefficient for carbon in Austenite has long been known to be strongly dependent on the carbon content. It is also well know that carbon and nitrogen concentration affect their diffusivities. J. Slyske and T. Ericsson [2] studied the interaction between carbon and nitrogen in steel and presented the effects of the %C and %N on the diffusivities of C and N. Their diffusivity equations were used in this software.

Figure 44 presents the comparison between experiment and simulation results for AISI 1018 at 850℃ with 5% and 10% ammonia addition for 45 min. The prediction results agree with the experimental concentration profiles very well.

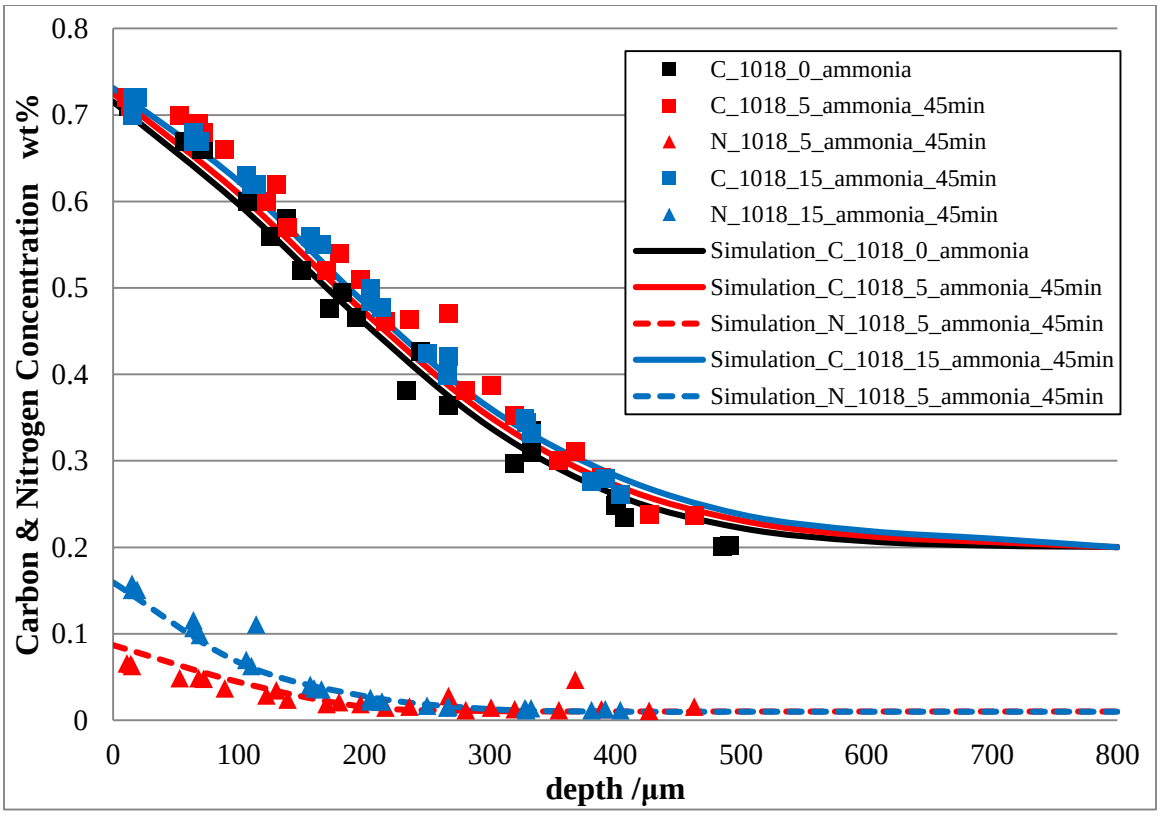

Figure 44: Comparison between experiment results and simulation result

2. Modeling of Retained austenite fraction (%RA)

%RA plays an important role in the performance of the carbonitrided steel [7]. Large amounts of RA will decrease the wear resistance and the strength of the material. The existing methods of the RA prediction have successfully predicted the fraction of %RA after carburizing process [3]. Currently there is not an applicable model to include nitrogen concentration. In the paper, the effects of nitrogen concentration on the %RA will be discussed. Figure 45 presents the carbonitriding process. In the experiments, the ammonia is added followed the carburizing process. The carburizing atmosphere is also modified to maintain a constant carbon potential.

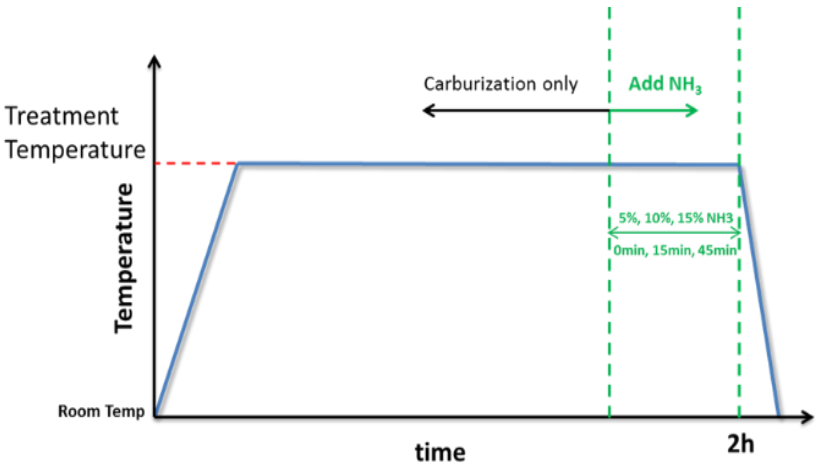

Figure 45: The carbonitriding process

In this paper, the X-ray diffraction method is used to measure the %RA. To study the correlation between the carbon and nitrogen concentration and %RA, samples are ground layer by layer to obtain the depth profile. Figure 46 presents the X-ray diffraction pattern of the carburized and carbonitrided AISI 1018 steel.

The $\gamma(220)$, and $\alpha(200)$ peaks are used for the %RA calculation [6].

$$\frac{I_\gamma}{I_\alpha} = \frac{e^{-2M_\gamma} * P_\gamma * |F_\gamma|^2 * Lp * V_\gamma * v_\alpha^2}{e^{-2M_\alpha} * P_\alpha * |F_\alpha|^2 * Lp * V_\alpha * v_\gamma^2} \qquad \textit{Equation 20}$$

Where I is the intensity, M is the Debye-Waller temperature factor, P is multiplicity factor, F is the atomic scattering factor, Lp is the Lorentz-polarization factor, V is the volume fraction, v is the cell volume.

The integrated intensity ratio is used to calculate the fraction. With the all the parameters input. The fraction of RA is calculated as below.

$$\frac{I_\gamma}{I_\alpha} = 2.588 * \frac{V_\gamma}{V_\alpha} \qquad \textit{Equation 21}$$

$$V_\gamma = \frac{\frac{I_\gamma}{I_\alpha}}{\frac{I_\gamma}{I_\alpha} + 2.588} \qquad \textit{Equation 22}$$

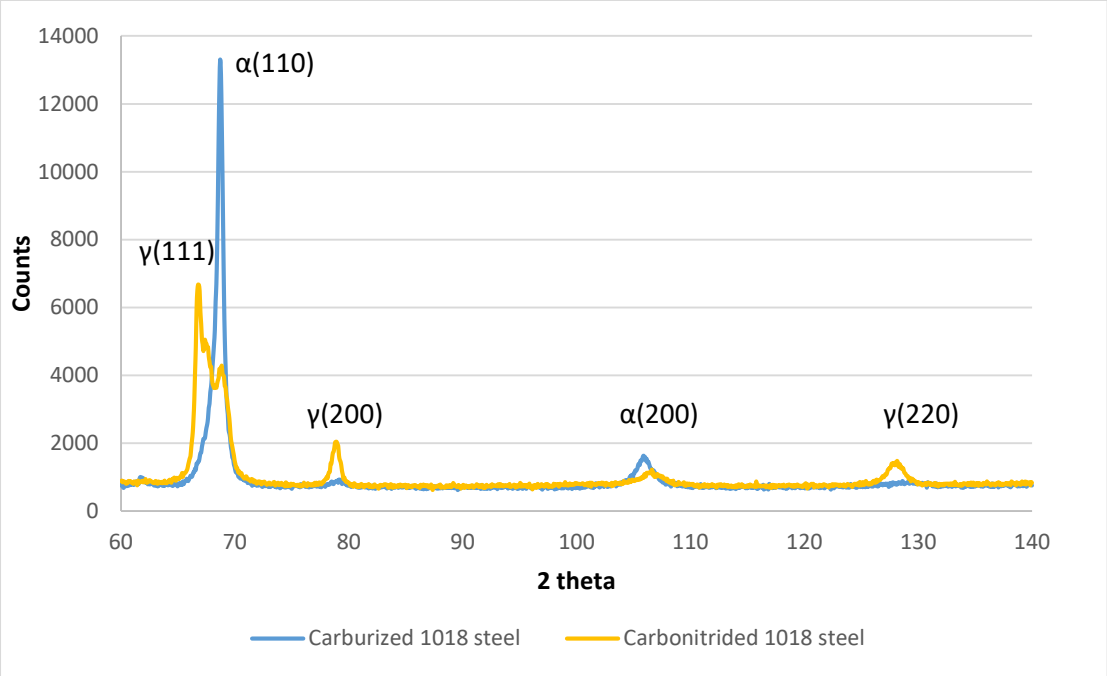

Figure 46: The X-Ray diffraction results of carburized and carbonitrided AISI 1018 steels

Based on experimental results, Koistinen and Marburger have developed an empirical equation to predict the volume fraction of RA [3]. The RA was obtained by the X-Ray diffraction results and was suitable for the prediction of RA fraction in steel with 0.37% to 1.1% carbon centration.

$$\%RA = exp(-0.011 * (M_s - T_{Quench})) \qquad \textit{Equation 23}$$

Ms is the Martensite start temperature, T_{quench} is the quenchant temperature below the Ms. With this equation, the %RA can be calculated as a function of temperature.

The Martensite start temperature may be calculated as below.

Ms (degree C)=539-423(%C)-30.4(%Mn)-12.3(%Cr)-17.7(%Ni)-7.5(%Mo) Equation 24

Figure 47 presents the prediction of % RA. It seems that the simulation results do not match the experimental results. The calculation does not include the nitrogen concentration for Ms prediction.

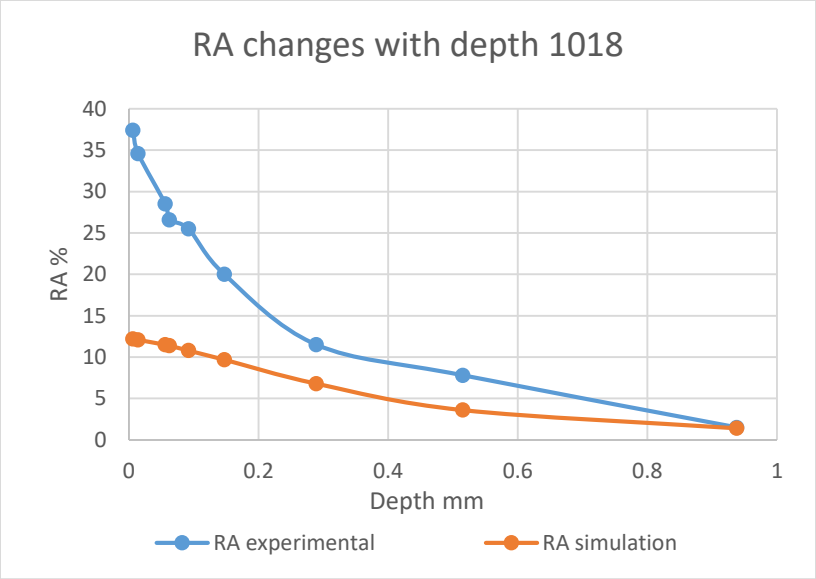

Figure 47: The %RA profile for AISI 1018 steel without %N included

To modify the equation, both of the carbon and nitrogen profiles are required. The chemical compositions of each steel are measured by Optical Emission Spectrometry (OES). Depth profile is obtained by measurements layer by layer as Figure 48 presents.

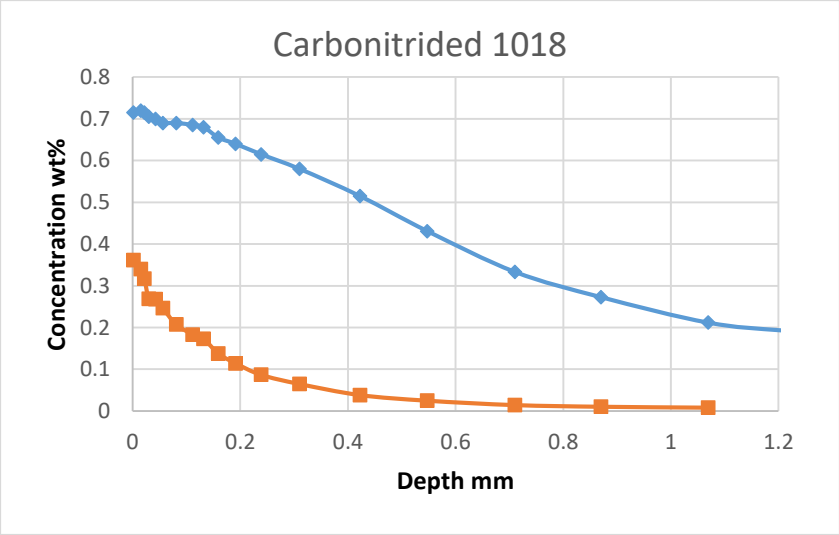

Figure 48: The carbon and nitrogen concentration profile

The effect of nitrogen is analyzed using a regression method. The equation is modified with the addition of %N. The fitted value of 298 with nitrogen in equation below when the %RA profile can meet the experimental results well as Figure 48 presented.

$$Ms(\text{degree C}) = 539 - 423(\%C) - 30.4(\%Mn) - 12.3(\%Cr) - 17.7(\%Ni) - 7.5(\%Mo) \mathbf{-298(N\%)}$$

Equation 25

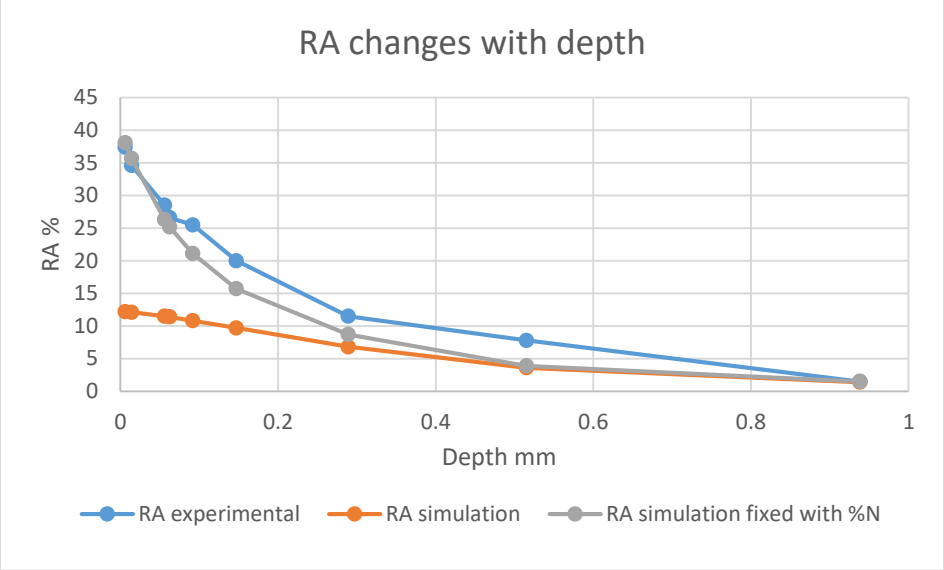

Figure 49: The comparison of experimental and calculated %RA with %N included

The modified Ms temperature as a function of depth is presented in Figure 50. With higher nitrogen concentration at the surface, Ms decreases from 200 ℃ to 100 ℃ because of the nitrogen concentration. The nitrogen causes the RA increasing from 12wt% to 38wt% as presented in Figure 49.

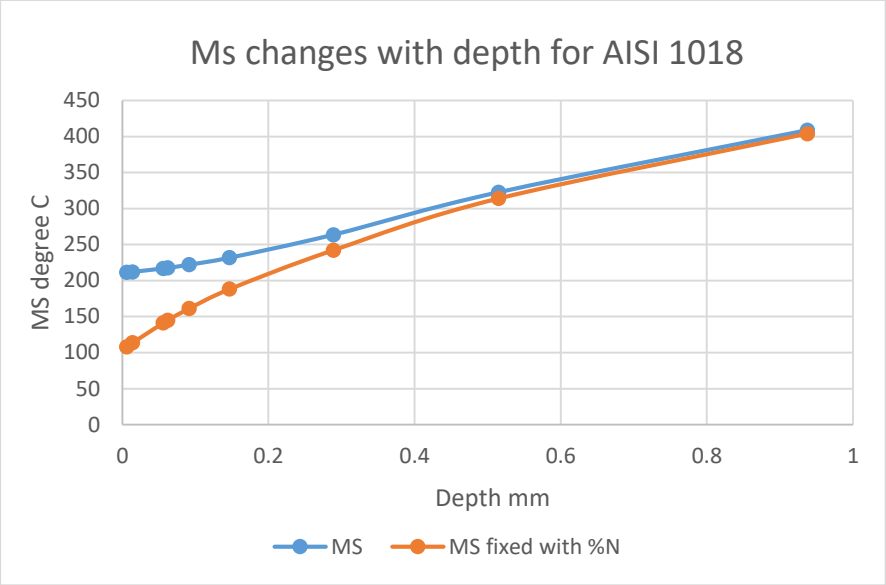

Figure 50: The Ms changes with depth for carbonitrided AISI 1018 steel

3. The hardness profile prediction of the carbonitrided steel

The hardness of carbonitrided samples may be determined with the fraction of the Martensite and RA [8]. In the Figure 51, the SEM micrograph with surface region is presents. The microstructure of carbonitrided AISI 1018 is composed of Martensite and RA in the case. The rule of mixture is used to calculate the microhardness as below.

$$Microhardness = (RA\%*HV_{RA} + Martensite\%*HV_{M})\ ^{[8]} \qquad Equation\ 26$$

HV_{RA} is the Vickers hardness where the microstructure is 100% RA. HV_M is the microstructure where the microstructure is 100% Martensite.

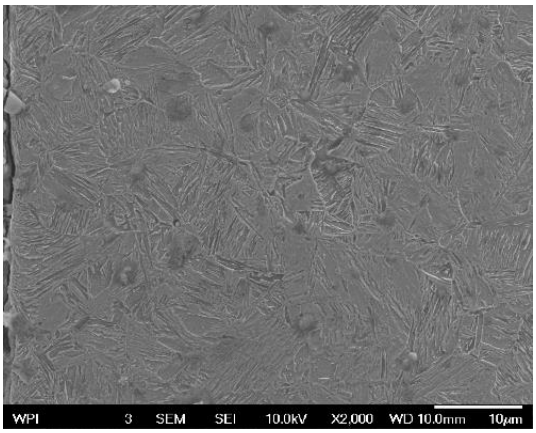

Figure 51: The microstructure of carbonitrided AISI 1018 steel

The Martensite hardness is a function of the carbon concentration [9]. The correlation between the microhardness of Martensite and the carbon concentration is measured for AISI 1018 steel with only a carburizing process. There is no RA found in the steel as the X-Ray diffraction result presents in *Figure 4*. The correlation between the carbon concentration and the microhardness is found experimentally as seen in Figure 52. The correlation is used to calculate the microhardness of Martensite changing with carbon concentration.

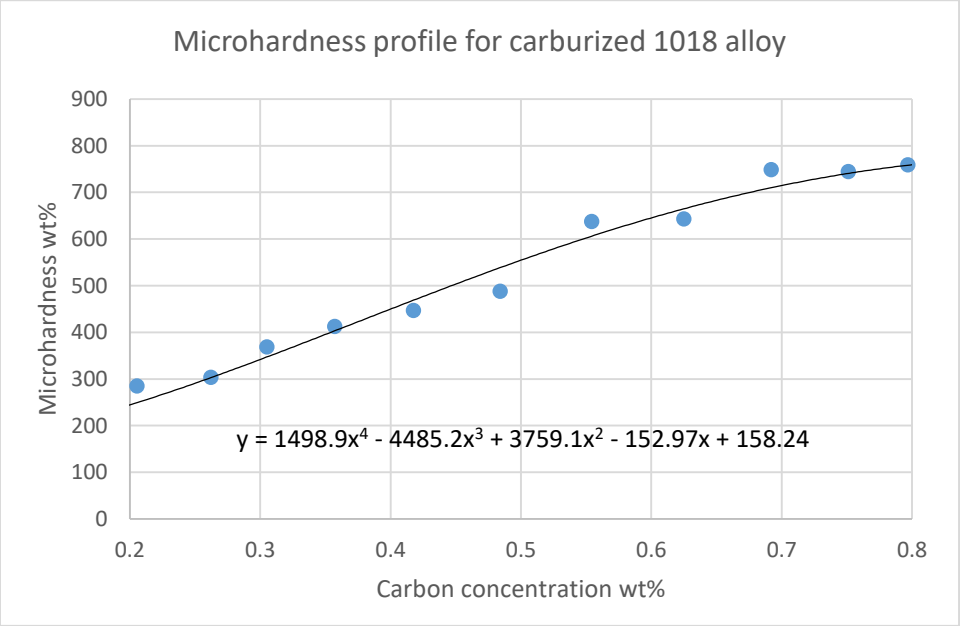

Figure 52: Microhardness changes with carbon concentration

The equation is used for the hardness calculation based on the data in Figure 52, as

$$Hardness\ of\ Martensite = 1498.9(\%C)^4 - 4485.2(\%C)^3 + 3759.1(\%C)^2 - 152.97(\%C) + 158.24$$

Equation 27

(%C) is carbon concentration in weight percent. In carbonitriding process, the diffusion of the nitrogen atoms increases the hardness of the steel.

For the carbonitrided AISI 1018 steel, as Figure 7 presents, the RA is formed primarily in the case with depth less than 0.3mm. In this region, the equivalent carbon concentration is higher than 0.8wt%. In this case we can assume the hardness of the RA is constant. A depth is selected where

the fraction of RA is 19.5%, and the equivalent carbon concentration is 0.87 wt%. The microhardness is 726 Hv measured by microhardness tester. The hardness of RA is calculated to be 550Hv.

$$726=(19.5*HV_{RA}+80.5*HV_{M}(\%C+N\%=0.87)) \quad \text{Equation 28}$$

The empirical equation for the microhardness is calculated.

$$Microhardness= RA\%*550+Martensite\%*HV_{M} \quad \text{Equation 29}$$

This equation is able to predict the hardness of carbonitrided AISI 1018. Figure 53 compares the experimental and simulation results for the as quenched carbonitried steel.

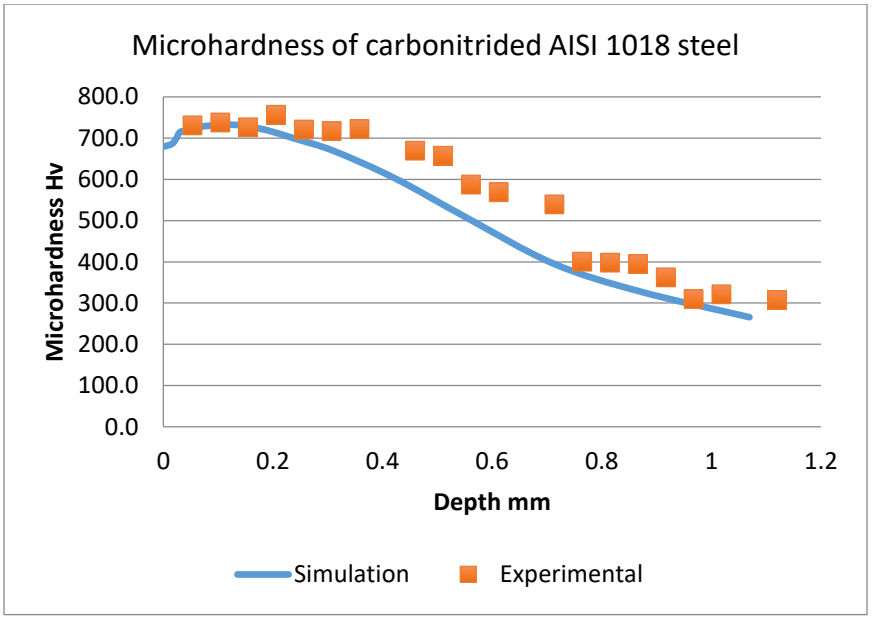

Figure 53: The comparison of the experimental and calculated hardness for AISI 1018

4. Experimental Verification

Microhardness= RA%*550+Martensite%*HV_M Equation 29 is an empirical equation for the hardness prediction after the carbonitriding process. The data was calculated and fitted with the experimental data measured with carbonitrided AISI 1018 steel. To verify the simulation, carbonitrided AISI 8620 steel was tested. Table 6 presents the data used and the results of the hardness profile calculation. Carbon and nitrogen concentration is predicted with

CarbonitrideTool© which was verified by the experimental result. To calculate the microhardness, the sample with carburizing process only for AISI 8620 is also used. The correlation between the Martensite hardness and the equivalent carbon concentration is calculated based on the experimental results. This correlation can also be calculated in CarbTool©. The carbon concentration profile determines the Martensite hardness. Then the hardness profile is calculated as listed in the last column of the table.

Table 6: The hardness profile calculation for carbonitrided 8620 steel

(M:Martensite hardness, Cal:Calculated hardness)

Depth mm	**C% Wt%**	**N% Wt%**	**RA%**	**M Hv**	**Cal Hv**
0	0.7	0.253	14.6	769.5	733.7
0.113	0.61	0.09	9.7	759.2	736.4
0.163	0.54	0.037	7.0	730.0	715.5
0.267	0.422	0.015	3.8	662.3	657.0
0.33	0.333	0.011	2.5	590.9	589.3
0.465	0.242	0.012	2.2	497.7	498.3
0.575	0.226	0.01	2.0	475.9	476.8
0.661	0.206	0.01	1.8	450.3	451.6

The Figure 54 presents the comparison of the experimental and calculated microhardness profile. They match each other well. The prediction method developed based on the AISI 1018 steel experimental data can also be used for carbonitrided AISI 8620 steel. The prediction process will be integrated into the CarbonitrideTool©.

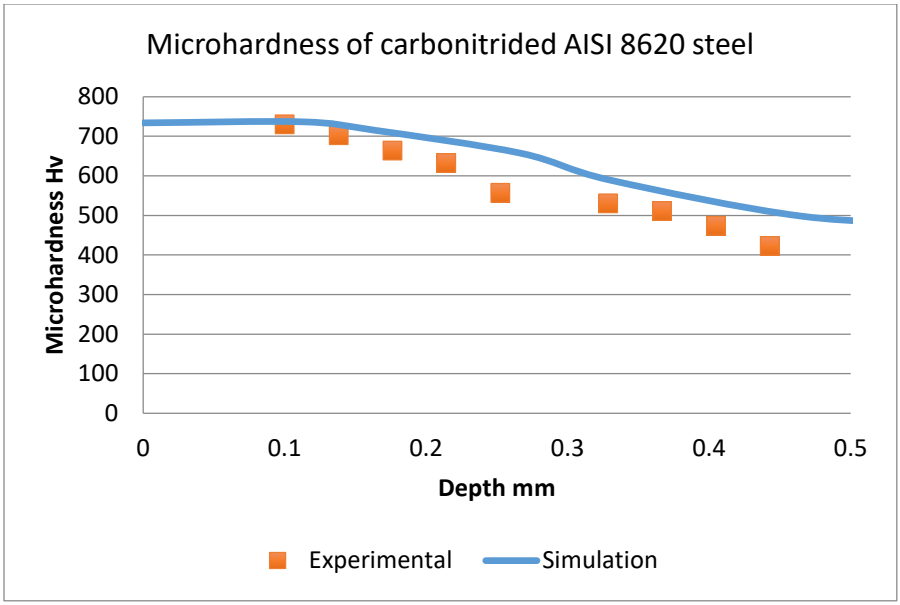

Figure 54: The comparison of the experimental and calculated hardness for AISI 8620

5. Conclusion

The CarbonitrideTool© can successfully predict the carbon and nitrogen concentration profiles.

The traditional method predicting the Ms was modified based on the effects of nitrogen. The %RA calculation is modified as well. The prediction results agree with the experimental results well.

The microhardness prediction was also developed in this paper. It is used to predict microhardness profile of AISI 1018 and 8620 steels. The calculation results agree with the experimental results well. The RA fraction and the microhardness profiles calculation have been added to CarbonitrideTool©

References

[1]. Slycke, J., and T. Ericsson. "A study of reactions occurring during the carbonitriding process." *Journal of Heat Treating* 2.1 (1981): 3-19.

[2]. Slycke, J., and T. Ericsson. "A study of reactions occurring during the carbonitriding process part II." *Journal of Heat Treating* 2.2 (1981): 97-112.

[3]. Wilson, B. M., and W. N. Weins. "Retained Austenite and tooling failure case studies." *20 th ASM Heat Treating Society Conference*. 2000.

[4]. Karabelchtchikova, Olga, and Richard D. Sisson. "Calculation of gas carburizing kinetics from carbon concentration profiles based on direct flux integration." *Defect and Diffusion Forum*. Vol. 266. 2007.

[5]. Karabelchtchikova, Olga, and Richard D. Sisson. "Carbon diffusion in steels: A numerical analysis based on direct integration of the flux." *Journal of phase equilibria and diffusion* 27.6 (2006): 598-604.

[6]. ASTM International, West Conshohocken, PA (2003) http://dx.doi.org/10.1520/E0975-13

[7]. J. Dossett, Carbonitriding of Steels, ASM Handbook, Volume 4A, Steel Heat treating Fundamentals and Processes. 2013, pp 599-615

[8]. Smoljan, Božo, Dario Iljkić, and Furio Traven. "Predictions of mechanical properties of quenched and tempered steel." *Strojniški vestnik-Journal of Mechanical Engineering* 56.2 (2011): 115-120.

[9]. Krauss, George. "Martensitic transformation, structure and properties in hardenable steels." *Metallurgical Society AIME,* (1978): 229-248

#Paper Three:

Prediction of Microhardness Profile in Carburized Steel after Tempering

Lei Zhang, Nichole Holman, Karen Paklin, Shikha Shrestha, Richard D. Sisson Jr.

(To be submitted to Journal of Heat Treatment of Materials)

Center for Heat Treating Excellence, Worcester Polytechnic Institute,
100 Institute Road, Worcester, Massachusetts, 01609, U.S.A

Abstract:

CarbTool© has been developed by Center for Heat Treatment Excellent (CHTE). With this software, carbon concentration profile has been well predicted for both gas carburizing and low pressure carburizing processes. Hardness profile prediction is also needed by industry which is studied in this paper for both as quenched and tempered condition. The Hollomon Jaffe equation was used for the prediction. A series of tempering experiments were used to calculate the Hollomon Jaffe parameter. The transformation of Retained Austenite (RA) during the tempering process is also discussed. The modeling result is verified experimentally.

1. Introduction

Carburizing simulation has been successfully developed by Center for Heat Treating Excellent(CHTE). In industry, the hardness profile prediction is also needed for process optimization. The tempering process is always used to relieve the residual stress and improve the toughness of the steel parts.

Hollomon and Jaffe developed an equation to explain the effects of tempering time and temperature on the hardness [1]. The correlation is further employed by Larson and Miller on the rupture and creep stresses [2]. It is an effective method to model the tempering heat treatment process in industry [3][4].

$$P = \frac{T}{1000}(logt + C) \quad \textit{Equation 30}$$

$$Hardness = f(P) \quad \textit{Equation 31}$$

$$Hardness = AP + B \quad \textit{Equation 32}$$

Where P is the Hollomon Jaffe Parameter, T is the Temperature in Kevin, t is time in seconds. A and B are constants in the linear correlation between the hardness and the Hollomon Jaffe Parameter. The Constant C in the equation will vary with the %C in the case. The parameter can be used to calculate the hardness of steel after tempering. In carburized steel, a carbon concentration profile is developed in the case. The objective of the study is to calculate the correlation between the C and the carbon concentration. A few constant C values were studied by Hollomon and Jaffe as *Table 7* presents. High alloy steels have the larger C value which can be as high as 30. Low alloy steels have a value closed to 20. For plain steel, higher carbon leads to a value of 15, while lower carbon leads to 19.5.

Table 7: Constant Value C for varying concentrations of Carbon in Steel in Hollomon-Jaffe [1]

Constant Value, C	15	19.5	20	30
Carbon Content in Steels (%)	0.90-1.20	0.15-0.45	C-Mn and low alloy steels	High alloy steels

The constant *C*, as determined by Hollomon and Jaffe in the paper varies with the alloy content and the carbon content. It can be calculated with equivalent condition which lead to the same hardness with different combination of time and temperature. The method have been widely used for the determination of the constant [3].

$$T_1(logt_1 + C) = T_2(logt_2 + C) \quad \textit{Equation 33}$$

2. Experiment

AISI 8620 and AISI 9310 alloys were used for this testing. The compositions measured by OES are presented in *Table 8*. AISI8620 alloy has fewer alloy content than AISI 9310 alloy which has 3.18% nickel. Nickel is austenite stabilize element that will develop more retained austenite during quenching [5]. Discs samples are used with diameter of 1 inch, thickness of 0.4 inch.

Table 8 The composition for 8620 and 9310 alloy

	C	Si	Mn	Cr	Ni	Mo
8620	0.180	0.249	0.82	0.54	0.452	0.156
9310	0.110	0.259	0.59	1.12	3.18	0.073

2.1. The carburizing of the alloys

Samples were carburized with endo gas atmosphere. The carburizing parameters are presented in *Table 9*. There are three major process for the carburizing. Within boost process, there is high carbon potential 0.95 ± 0.05 at $1700°F$, while in diffuse step, the carbon potential is 0.80 ± 0.5 at $1700°F$. The austenizing step help to cool the part down to $1550°F$ followed by oil quench.

Table 9: The carburizing process for both 8620 and 9310 alloy

	Preheat 1	**Boost**	**Diffuse**	**Austenize**
Atmosphere		Endo	Endo	Endo
%C Set Point		0.95	0.8	0.8
Tolerance (+/-)		0.05	0.05	0.05
Temperature SP(°F)	1250	1700	1700	1550
Soak Time (hrs)	3	10	4	3
Tolerance (+/- min)	15	15	15	15

2.2. Tempering experiments

The samples are in as-quenched condition after carburizing process. To study the Hollomon Jaffe equation, different combinations of tempering conditions are used. The tempering process matrix is presented in *Table 10*. For both alloys, four temperatures and four times are used. There are 16 samples heat treated for each alloy. Time is recorded when the temperature reaches the set temperature. After tempering, samples are cooled in air.

Table 10：Experiment plan for tempering of AISI 8620 and 9310 alloy

205℃	**1h**	**4h**	**9h**	**16h**
315℃	1h	4h	9h	16h
425℃	1h	4h	9h	16h
595℃	1h	4h	9h	16h

The carbon concentration profile is measured with optical emission spectroscope (OES). Sample layers were removed and measured to determine the profile. Vickers hardness is measured on the cross section on the well-polished surface, with the unit of Hv. The hardness profile is measured for every sample.

3. Experimental results

3.1. The carbon concentration and microhardness profiles

The measured carbon concentration and microhardness profiles for carburized AISI 8620 alloy was presented in *Figure 55*. Surface carbon concentration is as high as 0.7 wt%. The case depth is 1.25mm which is defined as the depth where carbon concentration equals to 0.35wt%.

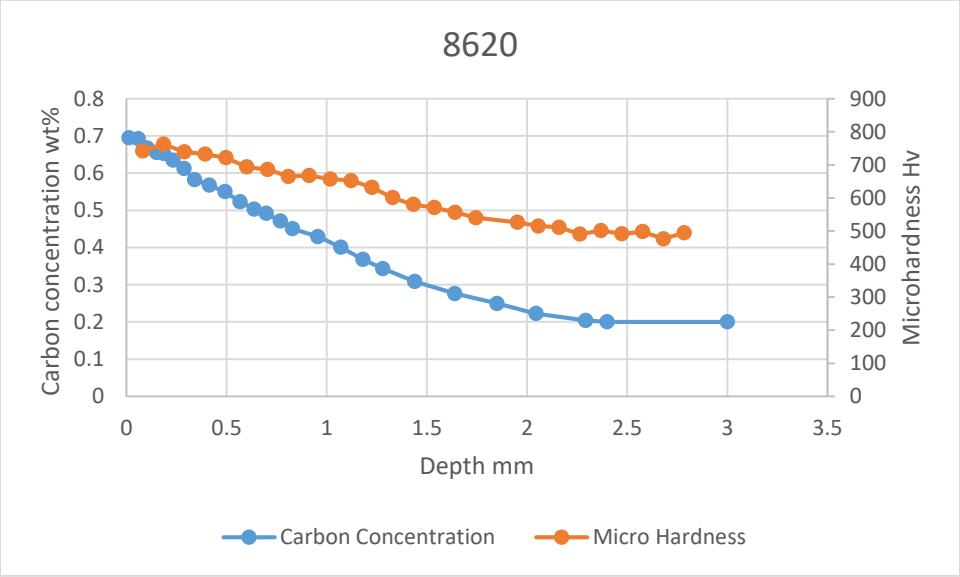

Figure 55: The carbon concentration and hardness profile verse depth for AISI 8620

The correlation between the carbon concentration and the microhardness is presented in *Figure 56*. It has linear correlation except the data point at the surface. Lower hardness at the surface is caused by the retained austenite. The wear resistant properties can also be affected by the existing of the Retained Austenite (RA) [6][7]. In this paper, we will focus on the study of the Hollomon Jaffe equation application on the carburized alloys. The RA phase transformation during the tempering process will also be discussed.

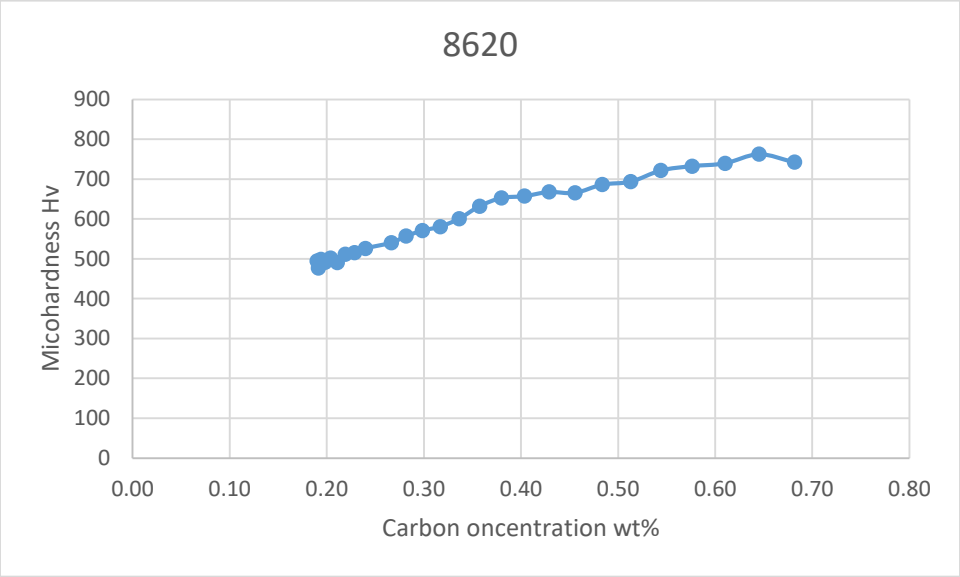

Figure 56: The correlation between the microhardness and the carbon concentration for AISI 8620

The carbon concentration and microhardness profiles for AISI9310 alloys are presented in *Figure 57*. The surface carbon concentration is 0.68 wt%. The surface hardness is 580Hv, while the maximum hardness is reached at 0.4mm depth with a value of 660Hv. The RA formation decrease the hardness.

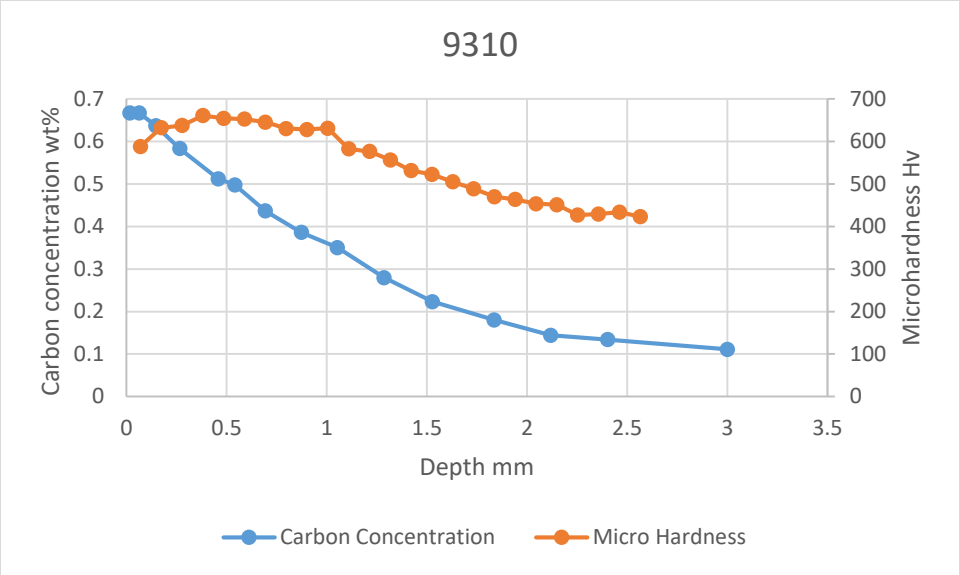

Figure 57: The carbon concentration and hardness profile against depth for AISI 9310

The correlation between the microhardness and the carbon concentration for carburized AISI 9310 is presented in *Figure 58*. There is linear correlation when the carbon concentration is less than 0.55wt%. At the region where the carbon concentration is larger than 0.55%, the microhardness decreases due to the existing of the RA.

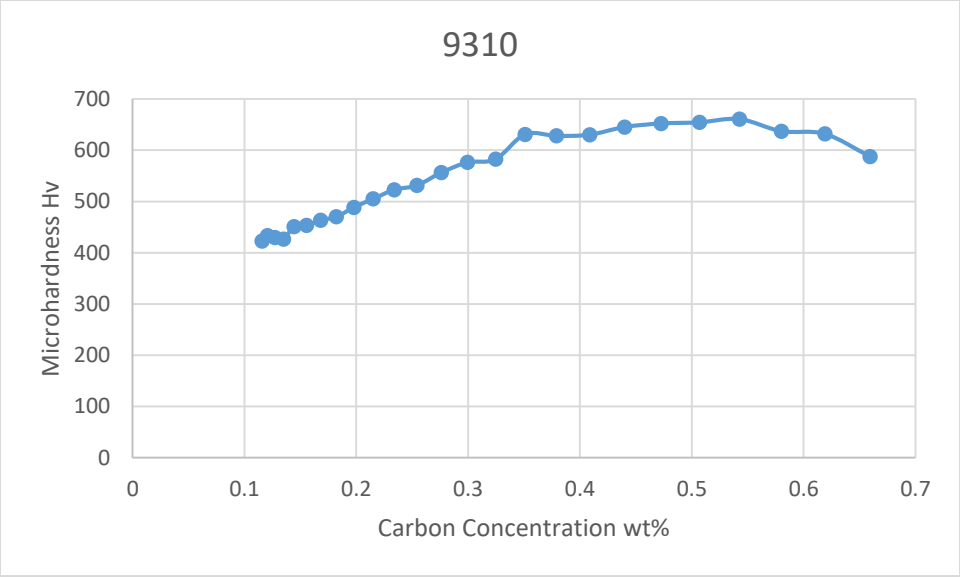

Figure 58: The correlation between the microhardness and the carbon concentration for AISI 9310

3.2. The measurements of the microhardness after tempering process

The hardness data is smoothed and fitted with polynomial fitting. *Figure 59* presents the hardness profile of carburized 8620 tempered for 1h at 205/315/425/595 ℃. Hardness is sensitive to the tempering temperature, for hardness at the surface, it decreases to 370 Hv after 1h tempering at 595℃ compare to 670Hv which was tempered at 205℃ for 1h.

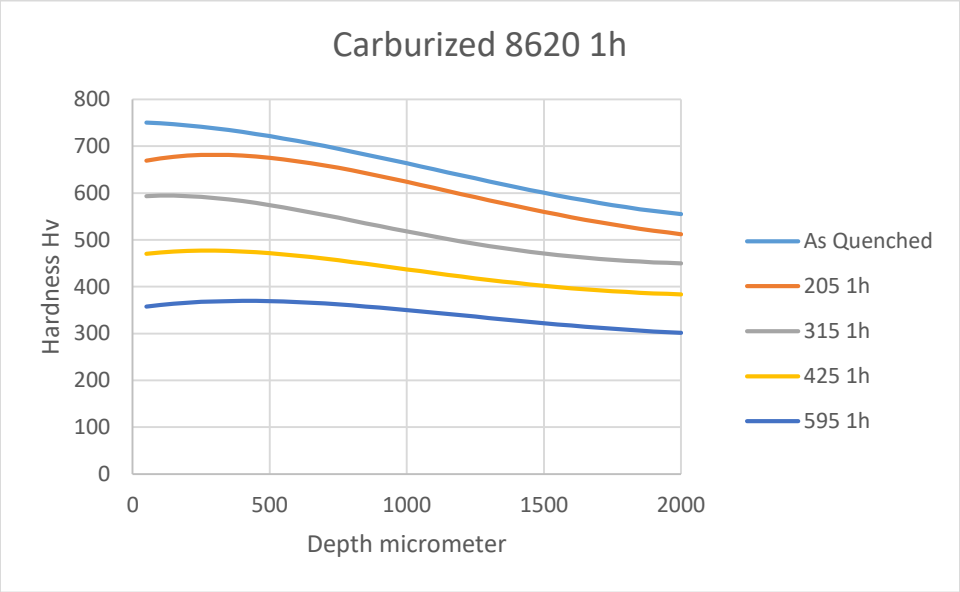

Figure 59: The hardness profile for AISI 8620 with 1h tempering at different temperature

For tempering at 205℃ for 1h/4h/9h/16h, there is not big variation in hardness for different spots. As quenched and 1h tempering process has smaller hardness at the surface. 4h/9h/16h tempering process has reached the maximum hardness at the surface. The 16h tempering leads to smallest hardness compare to the others.

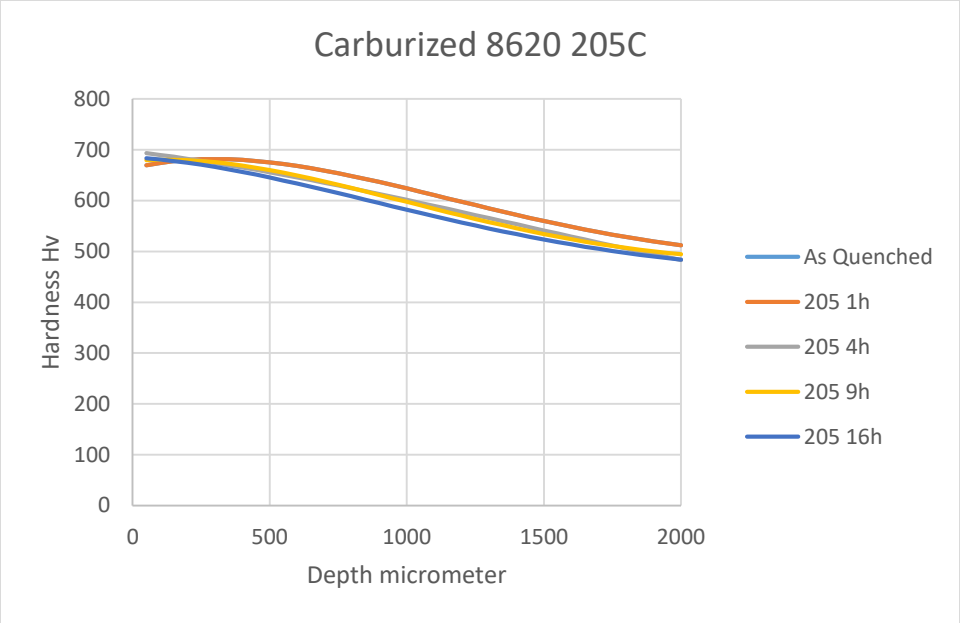

Figure 60 : The hardness profile for AISI 8620 tempered at 205℃ *for different time*

At 595℃, there is significant hardness decreasing compare to the as quenched condition. The hardness decrease slightly with the tempering time.

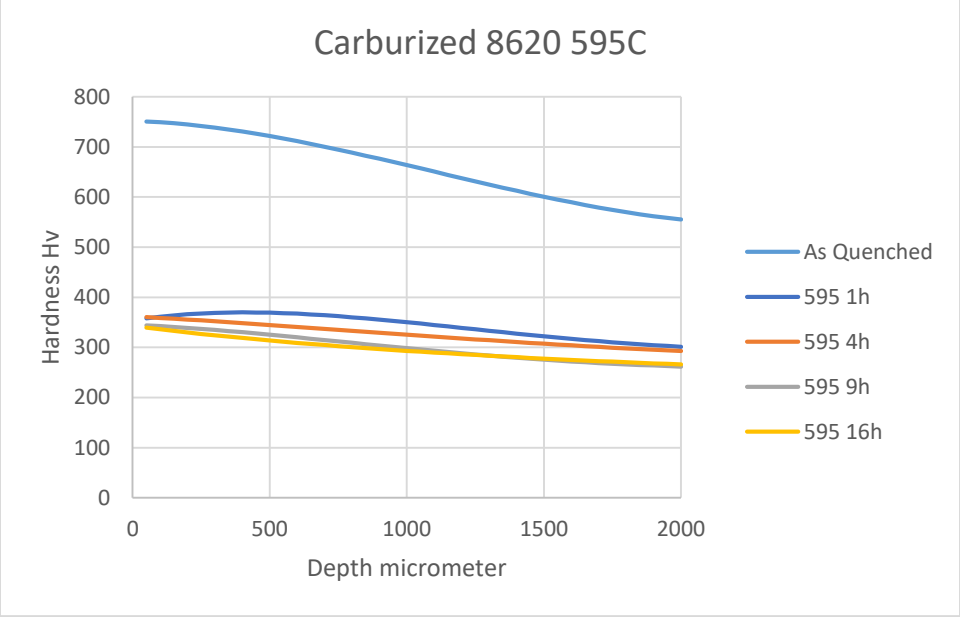

Figure 61: The hardness profile for AISI 8620 tempered at 595℃ *for different time*

For tempering of carburized AISI 9310 alloy, the as quenched and the 1h tempering at 205℃ has similar shape in curve. The maximum hardness is at the depth about 0.5mm. Surface hardness is smaller due to the existing of RA. As the temperature increases to 315℃, the hardness at the surface is the maximum spot which indicating the effects of RA is not effective any more. The 595℃ tempering will decrease the surface hardness to be less than 400 Hv.

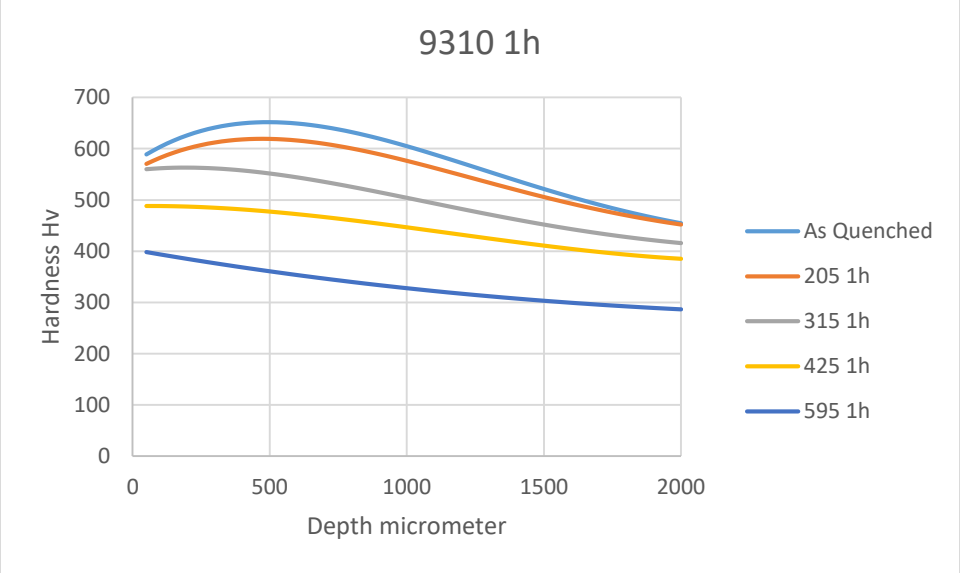

Figure 62: The hardness profile for AISI 8620 with 1h tempering at different temperature

Figure 63 presents the hardness profile for tempered 9310 at 205℃ for 1h/4h/9h/16h. 1h/4h/9h process has similar hardness profile, while after 16h tempering, there is obvious hardness decreasing. Surface hardness is 550Hv compare to 580Hv as quenched condition. The maximum hardness for 16h tempered sample is 560Hv at 0.4mm compare to the as quenched sample with the hardness of 650Hv at 0.5mm depth.

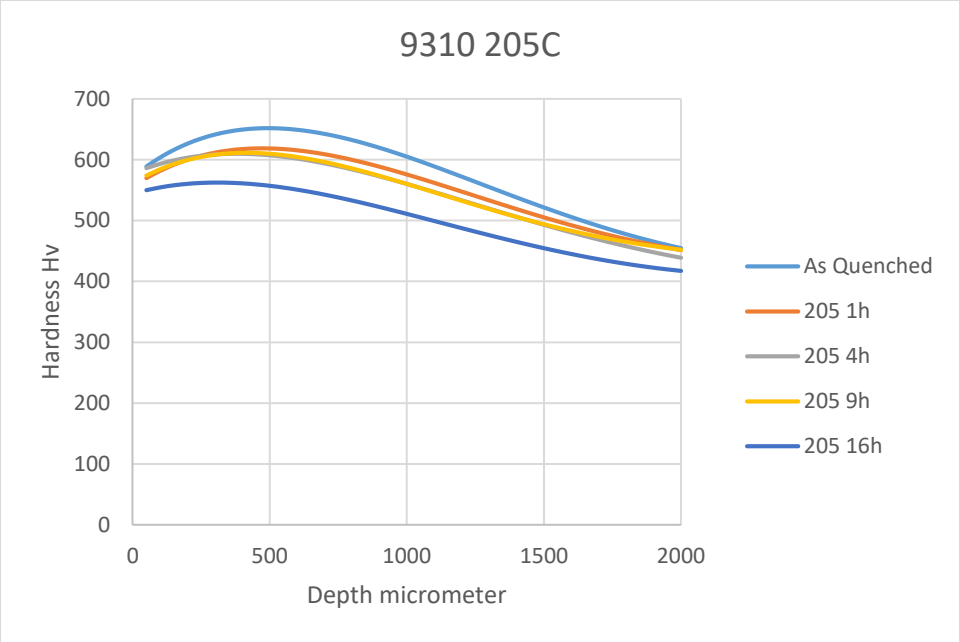

Figure 63 : The hardness profile for AISI 9310 tempered at 205℃ *for different time*

Figure 64 presents the hardness profile for tempered AISI 9310 alloys at 595℃. The tempering time are 1h/4h/9h/16h. Similar with AISI 8620 alloy, there is significant change in hardness compare to the as quenched sample.

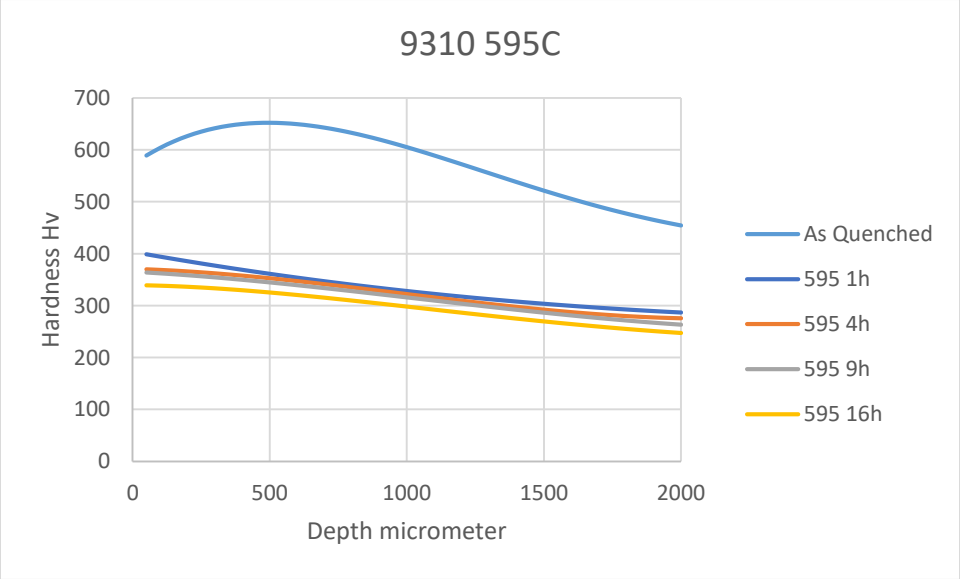

Figure 64: The hardness profile for AISI 9310 tempered at 595℃ *for different time*

4. The calculation of the C constant

The typical calculation of C constant method is as $T1logt1{+}C{=}T_2(logt_2 + C)$ *Equation 33* presented. In some case, there may not be equivalent condition available for the calculation. Shlyakman, Yampolskii and Ratushev have done mathematical calculation to include all the experimental combinations and calculated a best fit constant value for C calculation [4]. The C calculation result is presented as below.

$$C = \frac{\alpha\varepsilon - \beta\delta}{\beta\gamma - \alpha\delta} \qquad \textit{Equation 34}$$

Where,

$$\alpha = n\sum Ty - \sum T \sum y \qquad \textit{Equation 35}$$

$$\beta = n\sum Tlog\tau * y - \sum Tlog\tau \sum y \qquad \textit{Equation 36}$$

$$\gamma = n\sum T^2 - (\sum T)^2 \qquad \textit{Equation 37}$$

$$\delta = n\sum T^2 log\tau - \sum Tlog\tau \sum T \qquad \textit{Equation 38}$$

$$\varepsilon = n\sum T^2 log^2\tau - (\sum Tlog\tau)^2 \qquad \textit{Equation 39}$$

$$\mu = \sqrt{n\sum y^2 - (\sum y)^2} \qquad \textit{Equation 40}$$

The method is used for the calculation of C at different depth which has specific carbon concentration. In this way, the correlation between the C constant with the carbon concentration will be determined.

For each hardness profile, the value has been obtained for eight separate carbon concentration. With each carbon concentration, a set of data is obtained and can be used for calculation.

Table 11: The hardness selection for each carbon concentration value

C wt%	0.3	0.35	0.4	0.45	0.5	0.55	0.6	0.65
Hardness Hv	H1	H2	H3	H4	H5	H6	H7	H8

The *Table 12* presents the hardness calculation of each tempering condition for AISI 8620 with carbon concentration of 0.65. Each value will be calculated for each carbon concentration value.

Table 12:The hardness for carburized AISI8620 with carbon concentration of 0.65%

Hv	**1h**	**4h**	**16h**
205℃	678	681	673
315℃	594	570	567
425℃	476	485	465
595℃	365	357	332

With the calculation of the C value at different carbon concentration spot. The correlation between the C constant and the carbon concentration is finally obtained as presented in *Figure 65*. The C value is increasing with carbon concentration ranges from 13 to 30. With carbon less than 0.5 wt%, the C constant does not change much. It maintains 13-15. Higher carbon leads the value as high as 30.

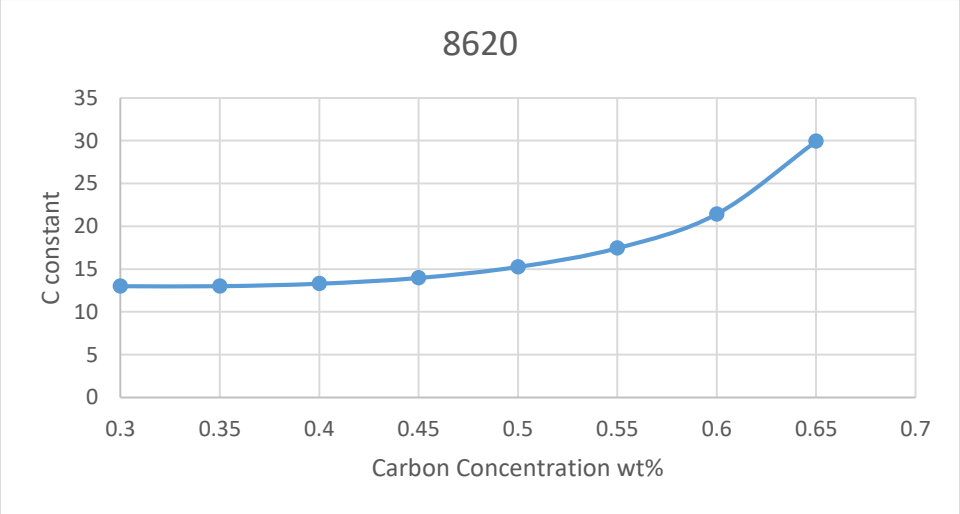

Figure 65： The C calculation for 8620 against the carbon concentration

The Hollomon Jaffe parameter can be calculated when C constant is known. The hardness can be obtained at by fitting the Hollmon Jaffe parameters with hardness. It has been studied in the original paper that the correlation between the Hollomon Jafee Parameter and the hardness is

linear. *Figure 66* presents the fitting of the two values for carbon concentration of 0.65 wt%. A set of data can be found. A is -0.0404 and B is 43.431 corresponding to C value of 29.92.

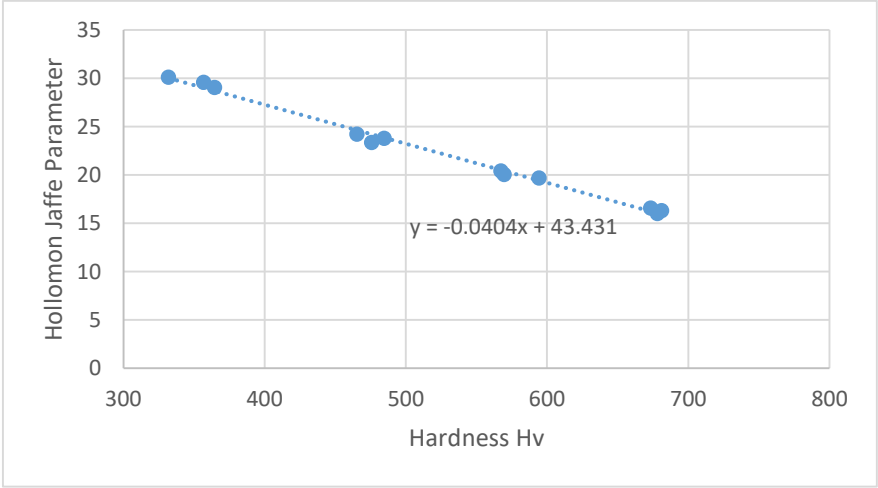

Figure 66: The correlation between Hollomon Jaffe Parameter and hardness

In this method, A and B value can be obtained for all the carbon concentration as presented in *Figure 67* and *Figure 68*.

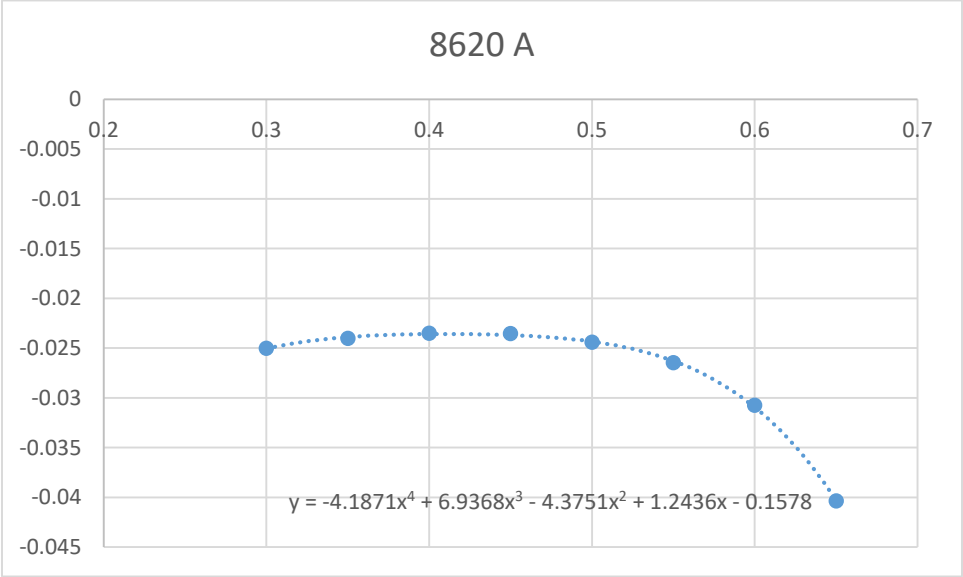

Figure 67: The A calculation for 8620 against the carbon concentration corresponding to C

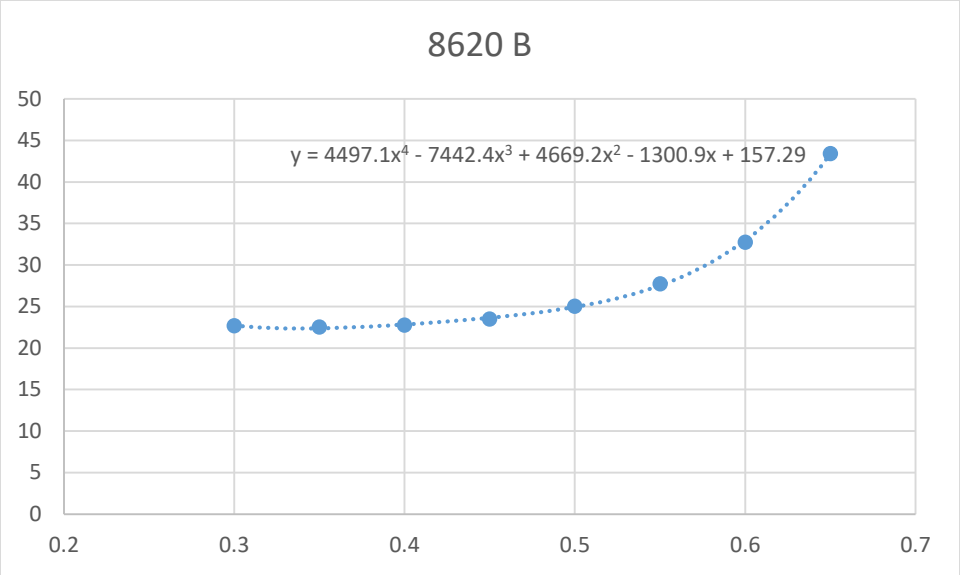

Figure 68: : The B calculation for 8620 against the carbon concentration corresponding to C

In the same way, the C constant is calculated for carburized AISI 9310 alloy. The C constant increases from 11 to 13.5 when carbon increases to 0.5 wt%. The C constant decreases to 11.5 when the carbon increases to 0.65. It has different trend compares to carburized AISI 8620 due to the phase transformation of RA.

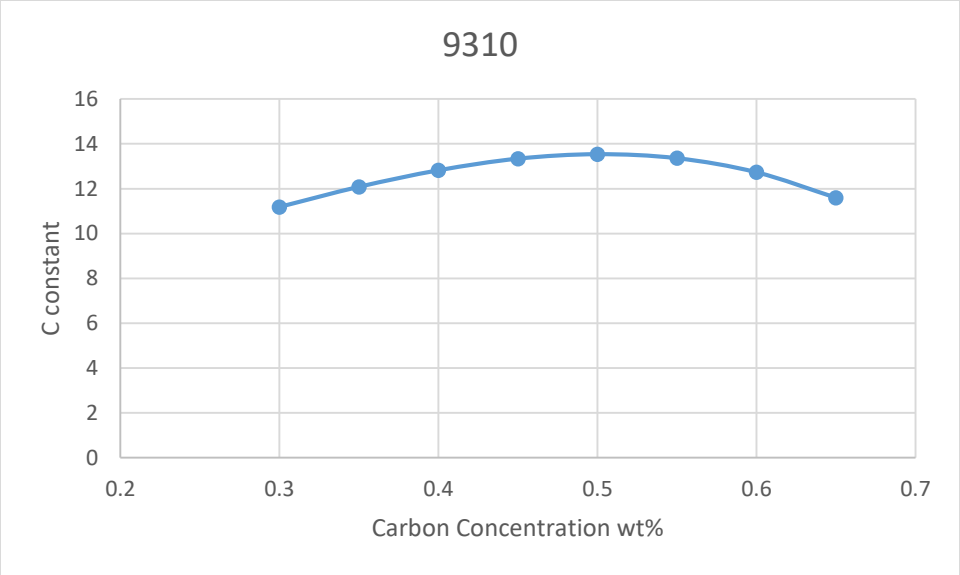

Figure 69 ： The C calculation for 9310 against the carbon concentration

A and B calculation is presented in *Figure 70* and *Figure 71*.

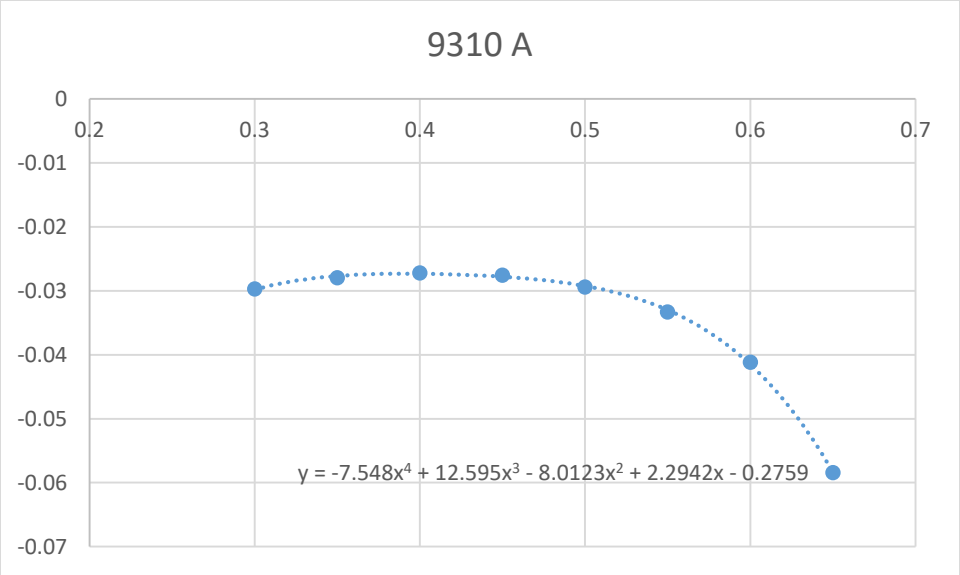

Figure 70: The A calculation for 9310 against the carbon concentration corresponding to C

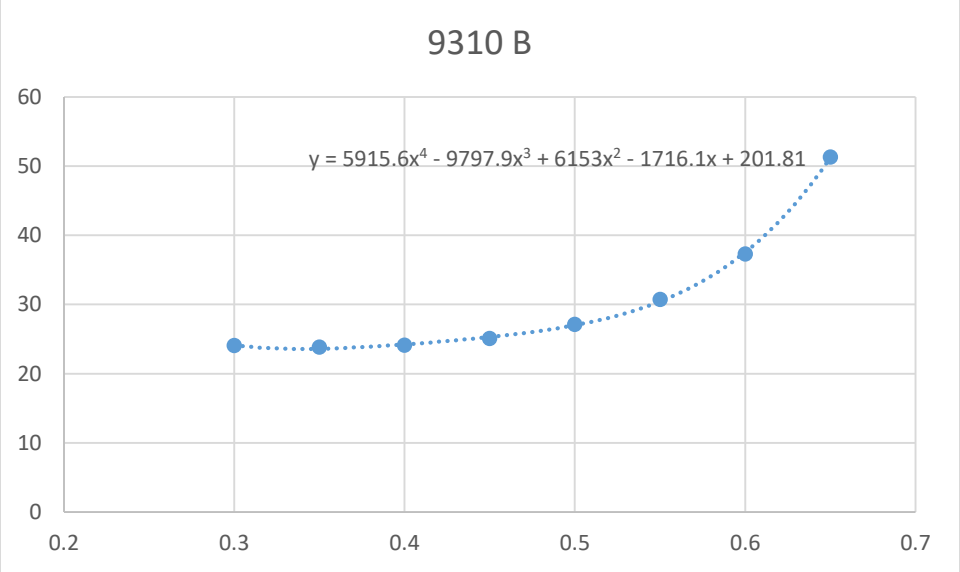

Figure 71: The B calculation for 9310 against the carbon concentration corresponding to C

5. Retained Austenite effects

AISI 9310 alloy has higher nickel content which is an Austenite stabilizer. X-ray Diffraction has been used for the identification of the RA. The RA is measured for as quenched samples and tempered at 205℃ and 425℃ for 1h. It was found that the as quenched AISI 9310 has about 27% RA with surface carbon concentration of 0.78 wt%. After the tempering for 1h at 205℃, there is

slight change in RA content which decreases to 24%. When the temperature increases to 425℃, the RA was transformed to ferrite and carbides. The RA measured is less than 3%.

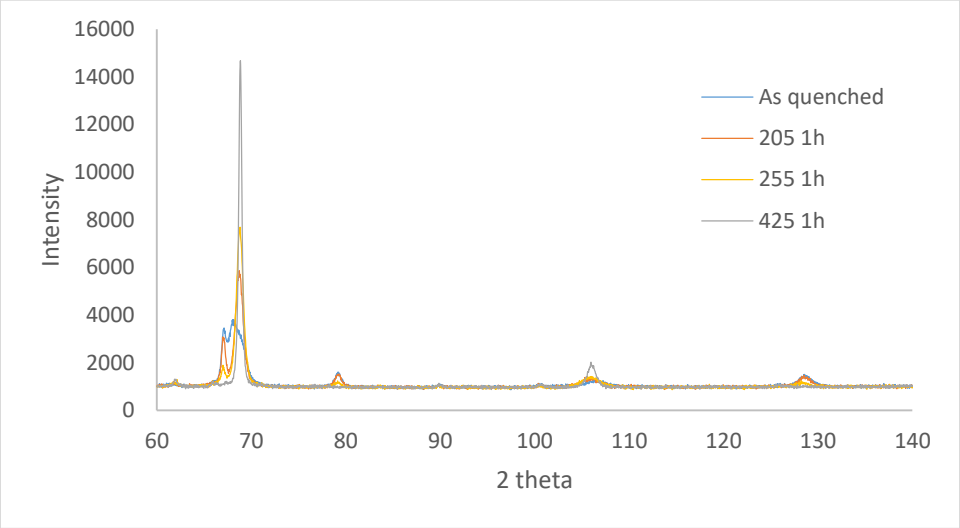

Figure 72: The XRD testing for as quenched and tempered AISIS 9310 at 205℃/425℃

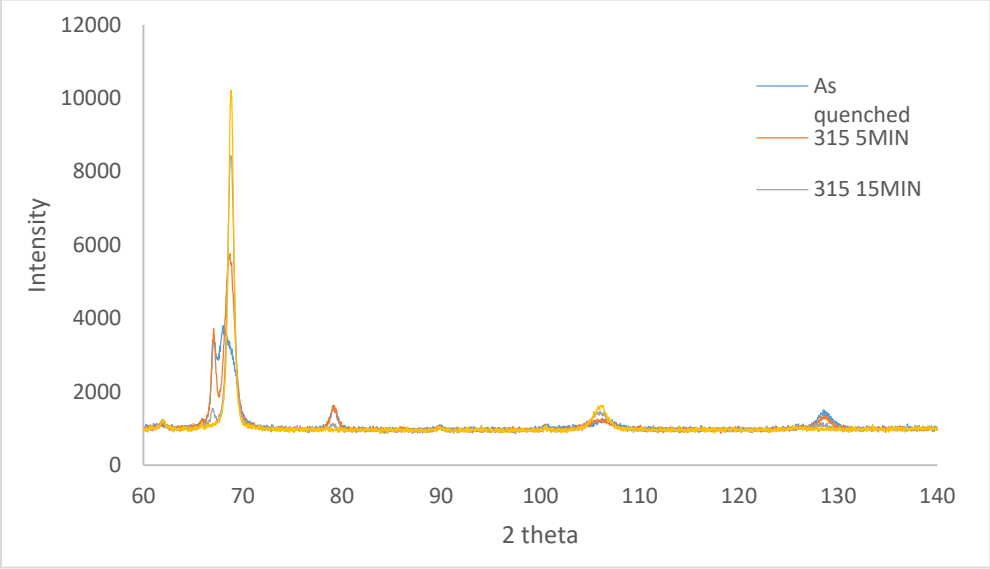

Figure 73:The XRD testing for as quenched and tempered AISIS 9310 at 315℃

Microstructure has been studied for the three samples. At surface region, the as quenched sample shows martensitic microstructure and a small amount of RA. There is also intergranular oxidation found as expected for gas carburized steels. For tempered sample at 205℃, there is no obvious change in microstructure. RA is still existing, while at 425℃, there is nearly no RA can be found by microstructure. During tempering, the austenite may decompose to form Banite.

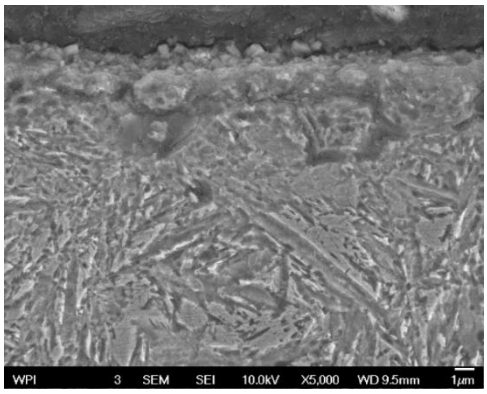

As quenched

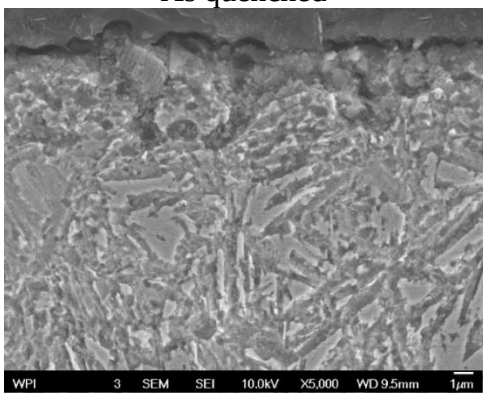

Tempered at 205℃ for 1h

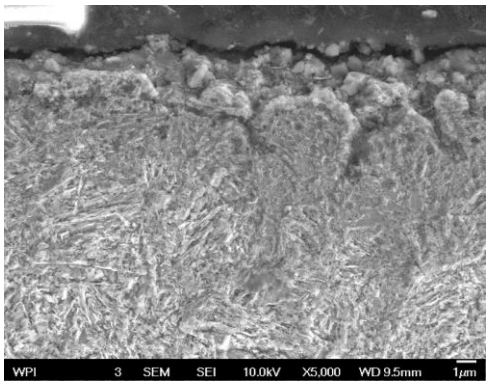

Tempered at 425℃ for 1h

Figure 74: The microsturcture of as quenched and tempered AISI 9310

6. Conclusion

The Hollomon Jaffe equation is studied in this paper. A set of tempering testing are conducted to calculate the constant C for both AISI 8260 and 9310 alloy. The values for A and B which shows the linear correlation between the Hollomon Jaffe parameter and hardness are also calculated. The existing and the phase transformation of RA during the tempering process is also studied.

Reference:

[1] Hollomon, J. H., and L. D. Jaffe. "Time-temperature relations in tempering steel." Trans. AIME 162 (1945): 223-249.

[2] Larson, Frank R., and James Miller. A time-temperature relationship for rupture and creep stresses. publisher not identified, 1952.

[3] Janjuševic, Zoran, et al. "The investigation of applicability of the Hollomon-Jaffe equation on tempering the HSLA steel." Chemical Industry and Chemical Engineering Quarterly/CICEQ 15.3 (2009): 131-136.

[4] Shlyakman, B. M., O. N. Yampolskii, and D. V. Ratushev. "A method for determining constant C in the Hollomon parameter." Metal Science and Heat Treatment 52.9 (2011): 451-453.

[5] Wang, Jiajun, Pieter J. van der Wolk, and Sybrand van der Zwaag. "Determination of martensite start temperature in engineering steels part I. Empirical relations describing the effect of steel chemistry." Materials transactions, JIM 41.7 (2000): 761-768.

[6] Preciado, M., P. M. Bravo, and J. M. Alegre. "Effect of low temperature tempering prior cryogenic treatment on carburized steels." Journal of Materials Processing Technology 176.1 (2006): 41-44.

[7] Bensely, A., et al. "Enhancing the wear resistance of case carburized steel (En 353) by cryogenic treatment." Cryogenics 45.12 (2005): 747-754.

#Paper Four:

A Study of Magnetic Barkhausen Noise for Evaluation of Case Depth and Surface Hardness in Carburized Steel

（To be submitted to ND&T International）

Lei Zhang, Richard D. Sisson Jr.

Center for Heat Treating Excellence, Worcester Polytechnic Institute,

100 Institute Road, Worcester, Massachusetts, 01609, U.S.A

Abstract

Carburizing is traditional technique widely used for harden the surface of steel. Surface hardness and case depth is critical for the performance of parts. Magnetic Barkhausen Noise (MBN) measurement have been evaluated as an effective method for hardness and case depth evaluation. MBN measures the pulses generating by the interaction between the alternating current magnetization and the magnetic domain walls in the ferromagnetic material. In carburized steel, carbon atoms change the structure of magnetic domain walls by interacting with vacancies, impurities and grain boundaries. These interactions may be used to evaluate the surface hardness and case depth of the carburized steel. For this study, samples of 1018 and 8620 were gas carburized to selected surface hardness and case depths. MBN was determined to be an effective method to evaluate the surface hardness and the case depth. In this paper, results of this investigation are presented and discussed.

1. Introduction to Barkhausen Noise

Barkhausen noise phenomena is found in ferromagnetic materials [1]. When a ferromagnetic material is placed in an excited alternating current field, the magnetic domain will move and interact with the microstructural defects, including the grain boundary, dislocation and carbides. As *Figure 75* presents, the hysteresis curve is not smooth but with a considerable amount of noise. The noise is collected and filtered.

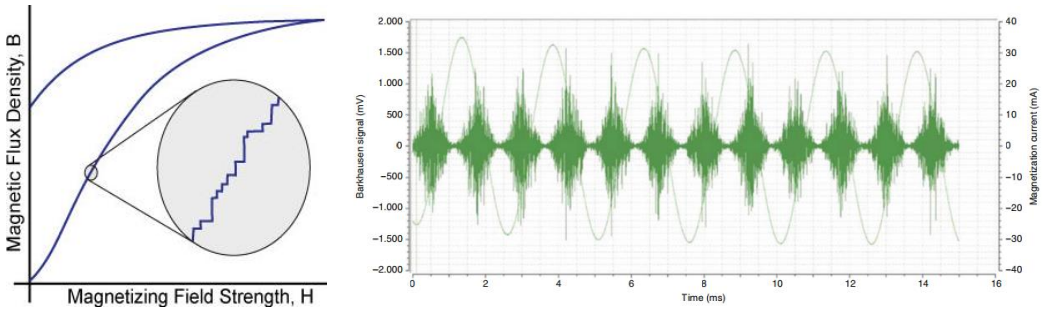

Figure 75: The generation of original Barkhausen Noise[1]

The device was developed by a few laboratories. M. Blaow, J. T. Evans and B.A. Shaw has used the device as Figure 76 presents [12]. Sample was placed in an alternating electromagnetic filed. Sensor was used for capture the signal. Amplifier and band pass filter were used to filter the signal. ADC converts the signal to be useful data analysis.

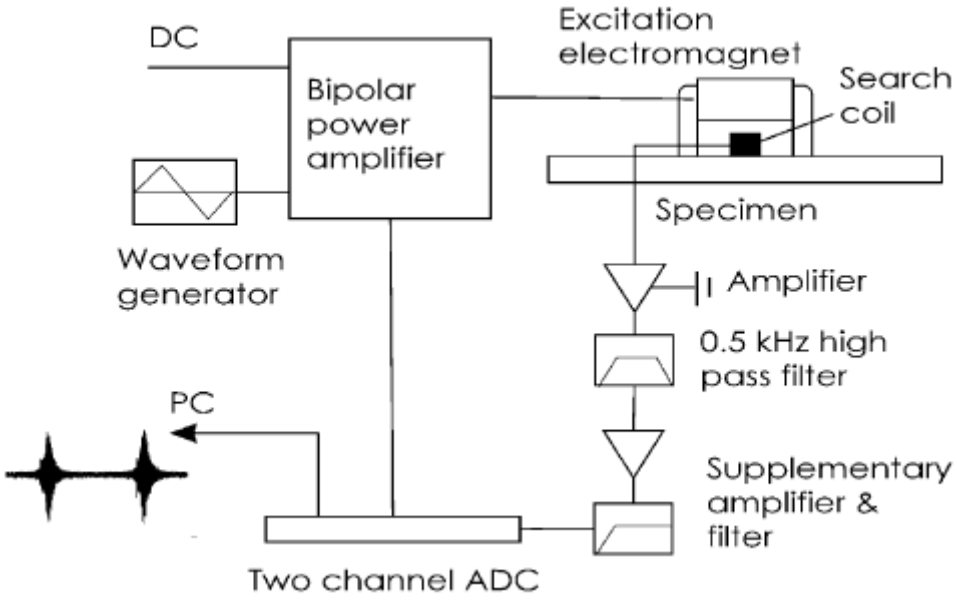

Figure 76: The Schematic of MBN apparatus [12]

The Rollscan 300 by American Stress Technology has been used for the testing as *Figure 77* presented. There are three measuring mode available. The magnetic parameter (MP) takes the root mean square of ten peak value. Magnetizing voltage sweep (MVS) provides the MP changes with magnetizing voltage at an input frequency. Magnetizing frequency sweep (MFS) provides MP changes with frequency at an input voltage. The Figure 111 show the original data from the unit with MVS mode. 8Hz and 250Hz are used. The magnetizing voltage peak to peak ranges from 0-16Vpp. There are three band pass filters available, 10-70kHz, 70-200kHz and 200-450kHz.

Figure 77: The Rollscan 300 Device by AST

With Rollscan 300 or Rollscan 350, the Microscan software can be used for measurements. Figure 75 shows the capability of the software. It can not only directly measure the magnetic parameter, but also the detects of the hysteresis loop. Magnetic permeability can also be read from the software direction as well as the coercively.

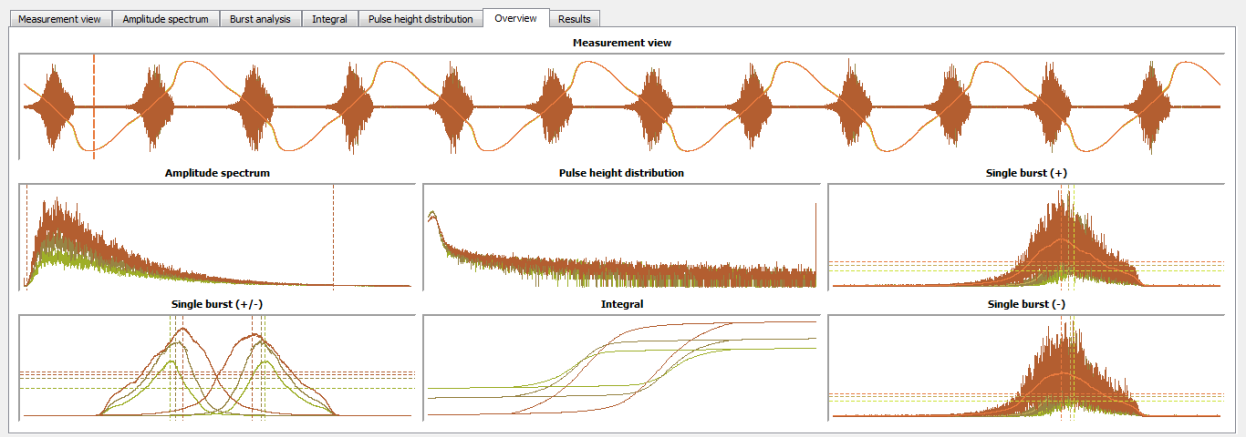

Figure 78: The interface of Microscan software

The penetration depth of the magnetic field is determined by both magnetizing frequency and the band pass filter. The penetration depth which is also called skin depth can be estimated as:

$$\delta = 1/\sqrt{\pi\mu\sigma f} \quad \textit{Equation 41}^{[3]}$$

μ is the permeability, σ is the electric conductivity, f is the frequency. With This equation, the skin can be calculated as *Table 13* presents. The conductivity is 1e7 S/m and the relative permeability is 30 in the calculation.

Table 13: The penetration depth of alloy change with frequency

Frequency Hz	Skin depth mm
25	5.81
100	2.91
300	1.68
500	1.30

The measurement depth is not determined by the skin depth. The noise was generated by the electromagnetic field. But the noise will be damped during the transmission through the steel. The damping of the noise can be calculated with the following equation. The input will be the frequencies of band pass filer, conductivity and the permeability.

$$D(x) = \frac{\int_{f1}^{f2} g(f) exp[-AX_n\sqrt{f}]df}{\int_{f1}^{f2} g(f)df} \qquad \textit{Equation 42}\ ^{[1]}$$

Where:$A = \sqrt{\pi\mu\sigma}$, μ is the permeability (H/m), σ is the conductivity (S/m), x is the distance from the surface. g(x) is the form of the amplitude variation ranges from 0.1 to 1. For band pass of 20kHz to 70kHz, the depth of measurement can be found in *Figure 79*. The band pass filter is built in the device and can be selected in the setting. With Rollscan 300 unit, there are three options for frequency, 10kHz-70kHz, 70kHz to 200kHz and 200kHz to 450kHz [1].

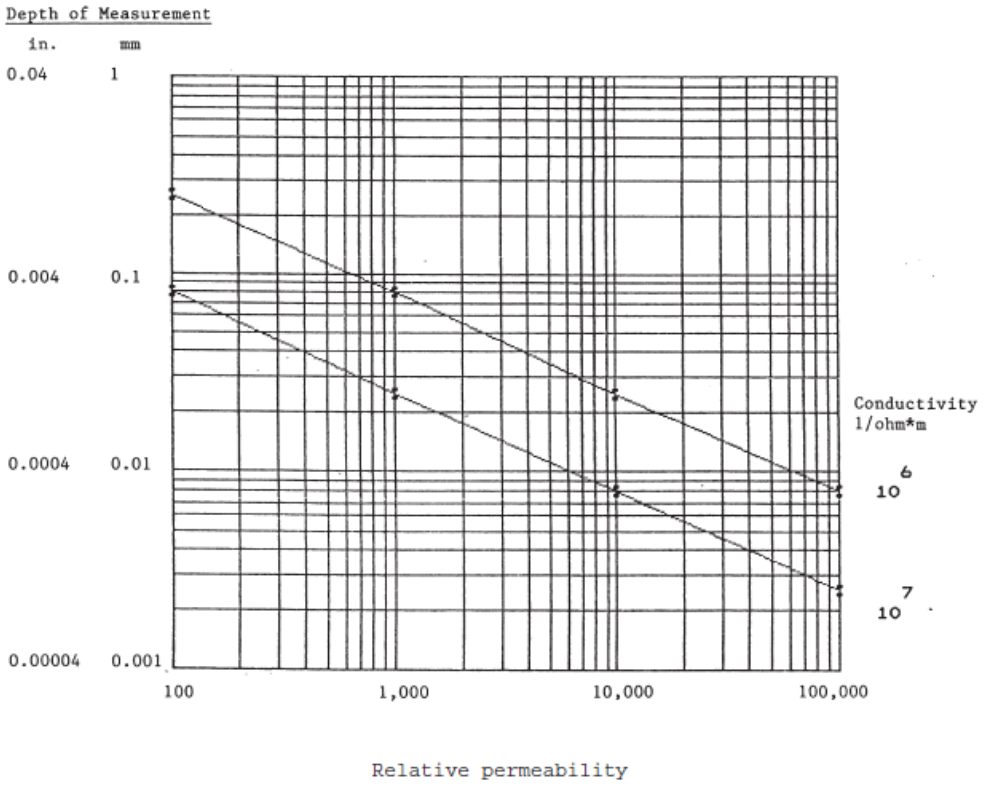

Figure 79: The depth of measurement for band pass of 20kHz-70kHz [2]

The measurement of carburized case depth requires a larger measurement depth. 10kHz-70kHz band pass will be the choice. Frequency combination is provided with experimental method.

2. Approach

The objective of the project is to measure the surface hardness and case depth of the carburized steel nondestructively. The carburizing process diffuses carbon atoms into steel. At temperature in the austenite phase region, the carbon will form a solid solution. The carburizing process is followed by a quenching and tempering processes. Quenching will lead to Martensite microstructure and a large amount of dislocations. Tempering process will lead to the decreasing of the hardness by the precipitation of carbides and reduce the carbon concentration in the Martensite.

The change in the microstructure will also change electoral magnetic properties as *Figure 80* presents. The size and geometry of the magnetic domains are also determined by the microstructure. By correlating the mechanical properties with the magnetic parameter, Barkhausen Noise testing presents the potential for the hardness and case depth measurement.

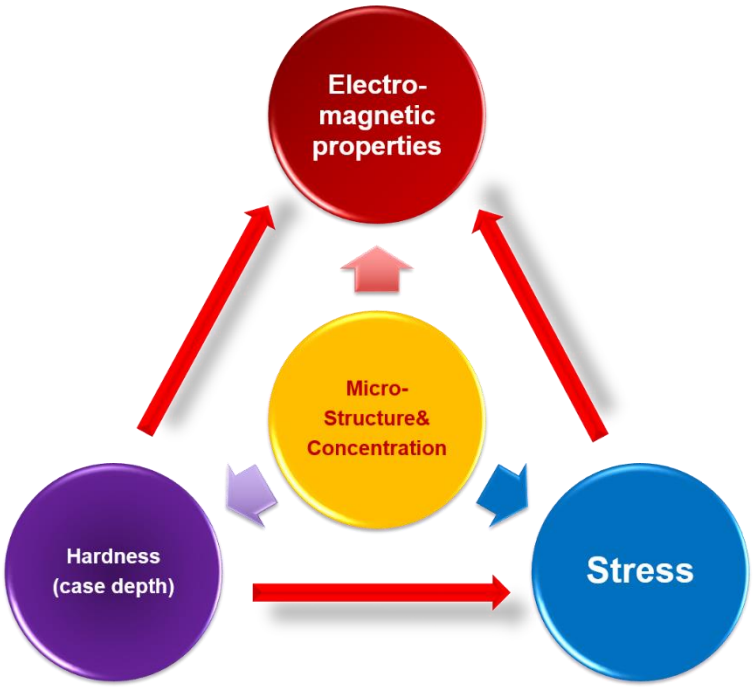

Figure 80: The correlation between the microstructure and the electromagnetic properties.

AISI 1018 and 8620 alloys are used in this project. The chemical composition are presented in Table 14. The alloys were gas carburized to selected case depths and surface hardness. The carbon

concentration and the microhardness profile are presented in Figure 81. The carburized AISI 1018 steel has a case depth of 0.8mm. Case depth is defined by the depth where carbon concentration equals to 0.35wt%.

Table 14: The composition of the 1018 and 8620 steel measured with OES

	C	Cr	Fe	Mn	Mo	Ni	P	S	Si
1018	0.184	0.120	Bal.	0.745	0.0225	0.0810	0.0044	0.014	0.2150
8620	0.214	0.560	Bal.	0.805	0.1535	0.4525	0.0065	0.014	0.2355

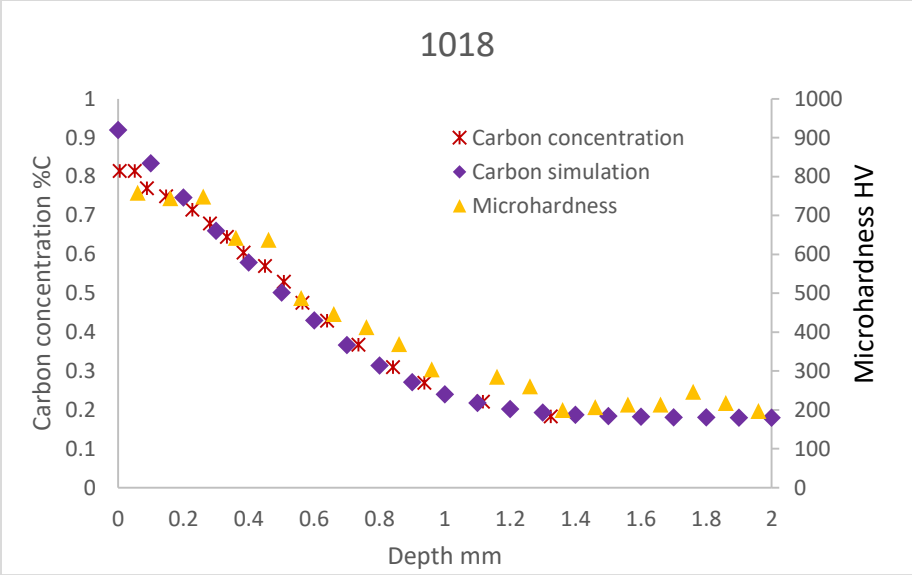

Figure 81: The carbon concentration and microhardness profile for as-quenched carburized 1018 alloy

The geometry of the samples is presented in *Figure 82*. AISI 4140 alloy is also used for this study. The samples were quenched and tempered to vary the microstructure and hardness.

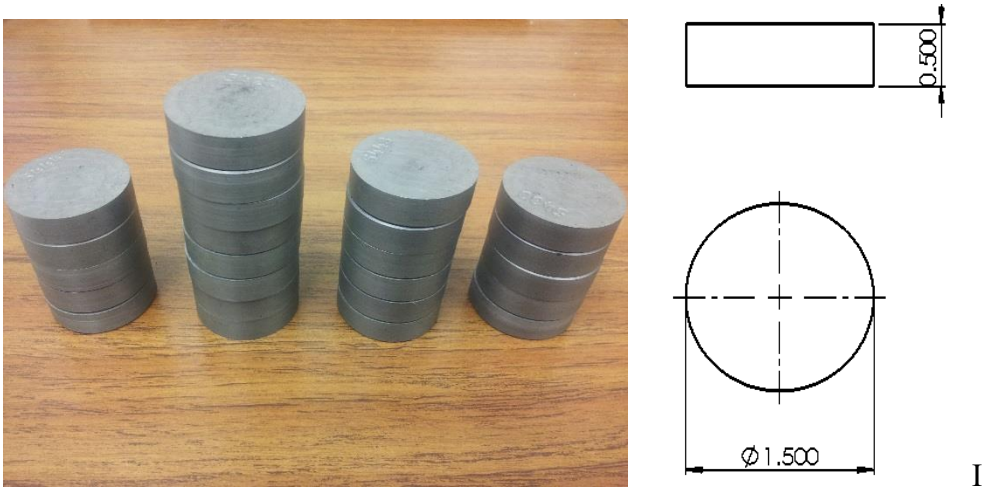

Figure 82: The geometry of the disc sample for carburized 1018, 8620 alloy and 4140 alloy

Barkhausen noise testing was used for the evaluation of surface hardness and case depth. The measured MP is determined by the microstructure. The Barkhausen noise is caused by the interaction between the motion of domain walls and the microstructure. Stress also plays important role for the MP because the strain will also interact with the domains. Data needs to be analyzed and correlated with the hardness.

To evaluate the case depth, Magnetic Voltage Sweep (MVS) method is used which employ two frequencies [7]. Low frequency will give the information of the thicker layer, while the higher frequency will provide the thinner one. A slope ratio method based on the MVS data is used for the measurement. Figure 83 presents the factors that will affect the MP including hardness surface finish and residual stress.

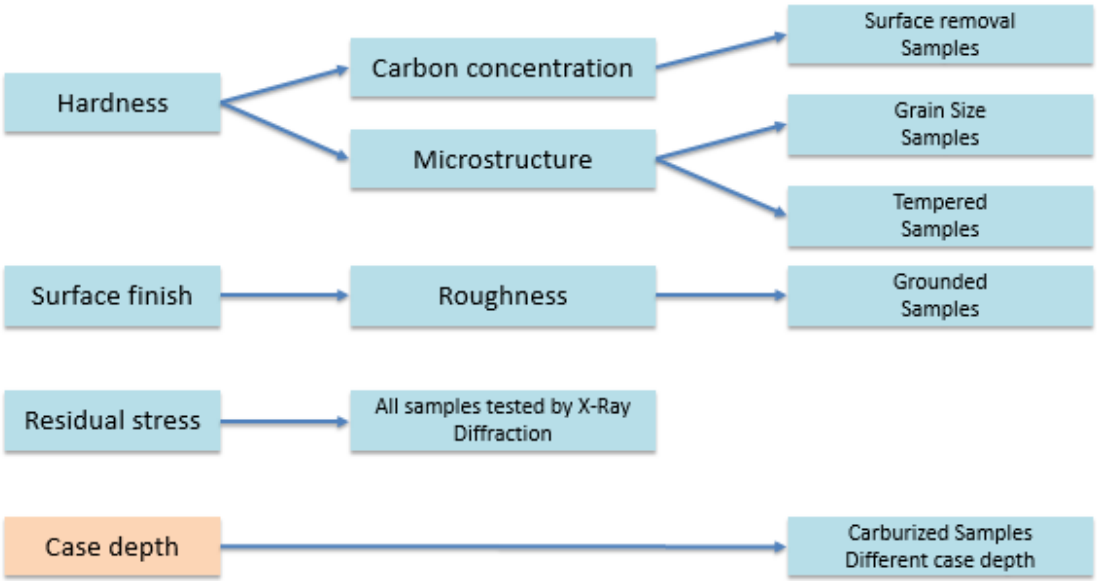

Figure 83: The factors that affect the Barkhausen Noise measurement

Table 15 presents the preparation procedure for all the samples. They were designed to meet certain surface condition. All test samples are metallurgically ground and polished. The surface carbon and the case depth were experimentally measured. The residual stress was also measured by X-Ray diffraction.

Table 15: The samples list for MBN study

	Dimension	Heat treat condition	Case depth
8620/1018	1.5inch(d)*0.4inch	Carburized/As quenched	0.8mm/1.2mm/2.5mm
8620/1018 Machined	1.5inch(d)*0.4inch	Carburized/As quenched	0.8mm/1.2mm/2.5mm
4140	1.5inch(d)*0.4inch	Quenched	
4140	1.5inch(d)*0.4inch	Quenched Tempered	
1018/1045/1080	1.25inch(d)*0.4inch	Quenched	
8620 (John Deere)	1.0inch(d)*1.0inch	Carburized/As quenched	0.8mm-1.8mm
1018/8620/5120 (Amstedrail)	1.5inch(d)*0.4inch	Carburized/As quenched	0.5mm/1.0mm/1.5mm
Unknown (AST)	0.75inch(d)*0.8inch	Unknown	0.3mm-2.0mm

3. Experiment results

3.1. The Surface Roughness Study

Surface finish must be well defined for nondestructive testing. The Barkhausen noise testing uses the contact sensor to create electromagnetic field in the surface of the parts.

Different surface conditions have been achieved by carefully grinding with sand papers. 8620 steel is used for the surface finish study as *Figure 84* presented. Roughness is measured. The *Figure 85* shows the magnetic parameters change with the roughness. The average MP value is approximately 160. There is no obvious correlation between the MP and roughness. To avoid the effects of the surface condition. All the samples were prepared by grinding followed by vibration polish.

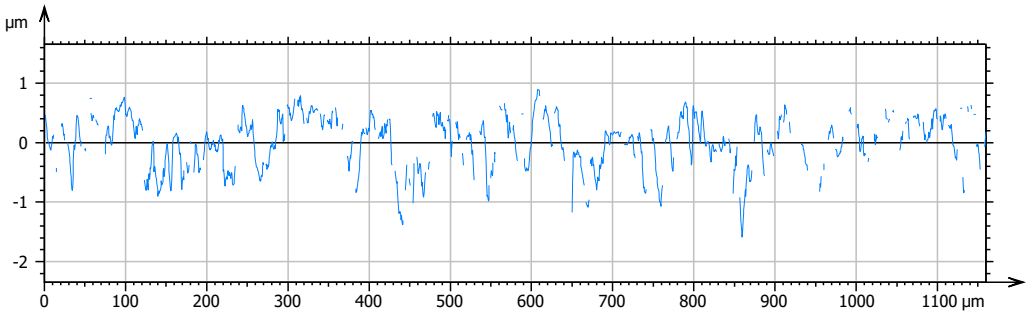

Figure 84: Surface roughness measurement with 120 grit grinding for 8620 steel

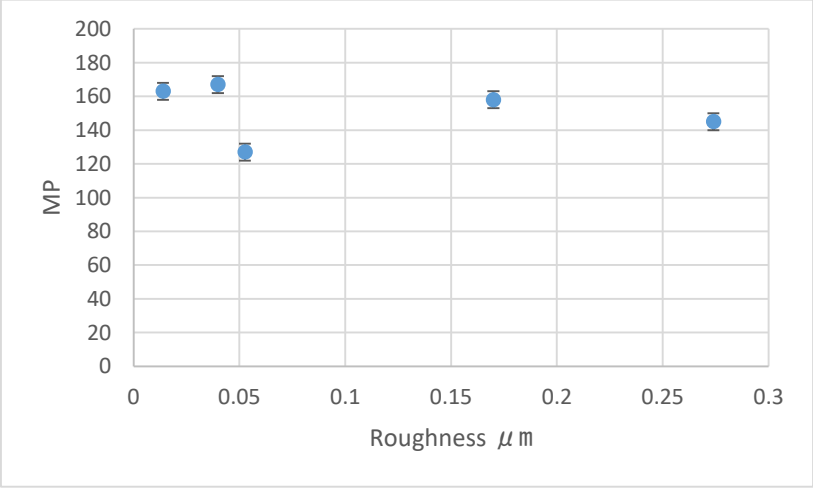

Figure 85: The MP testing on 8620 alloy with different surface roughness 5V, 50Hz

The surface residual stress was measured by X-Ray diffraction. Rougher surface has larger residual stress as presented in Figure 86. The grinding with 600 grit sand paper has the smallest stress. Though the vibration polishing gives smoothest surface finish, the residual stress does not decrease

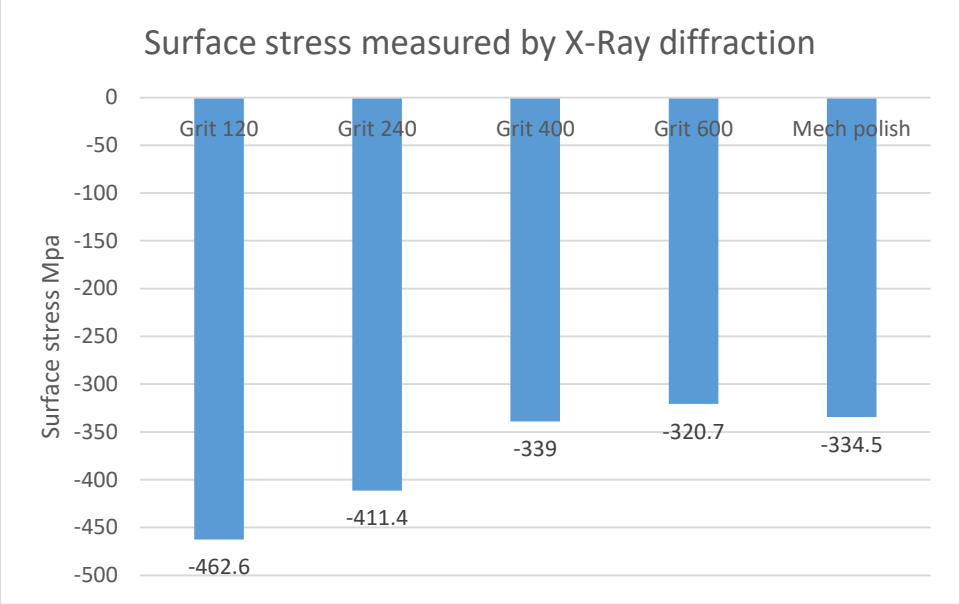

Figure 86: The residual stress measured with X-Ray Diffraction on 8620 alloy with different surface finish

3.2. Surface microstructure study

To determine the phases of the surface of 8620 sample, XRD testing was conducted as *Figure 87* presents. The blue circle shows the retained austenite existing in surface area for both samples. As calculated results, the sample with 0.5 mm case depth has 15% retained austenite, while the sample with 0.7mm case depth has 30%. To better evaluate the hardness with permeability method, the retained austenite factor must be evaluated.

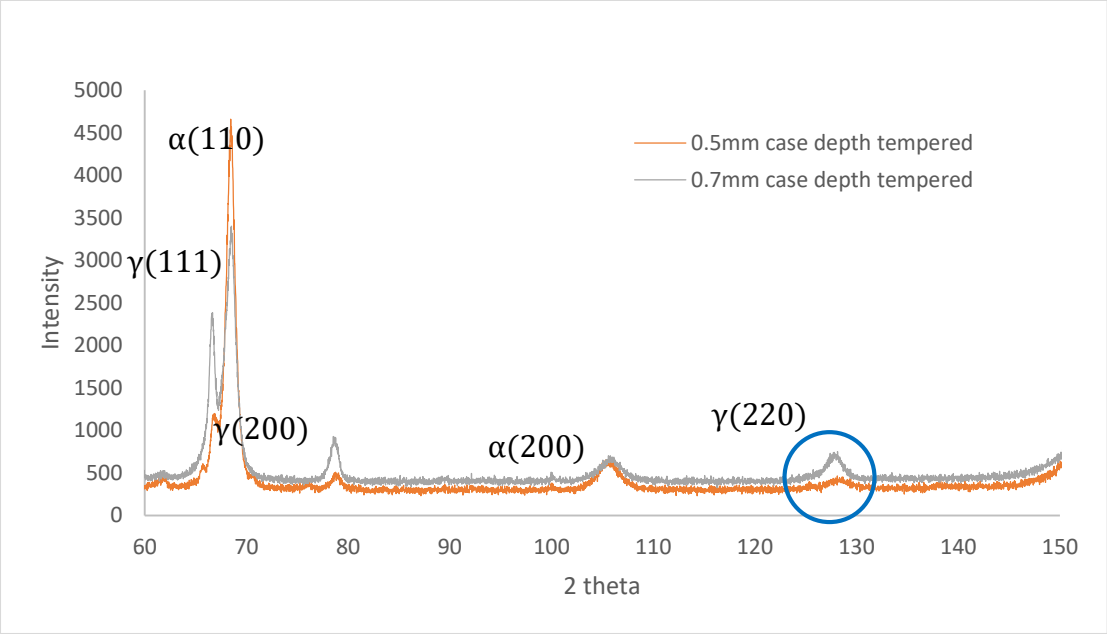

Figure 87: The XRD testing for 8620 samples

Microstructures for both samples are presented in *Figure 88*. For both samples there is tempered Martensite microstructure. There is more retained austenite in (b) than (a). Further quantity analysis will be conducted to determine the retained austenite factor.

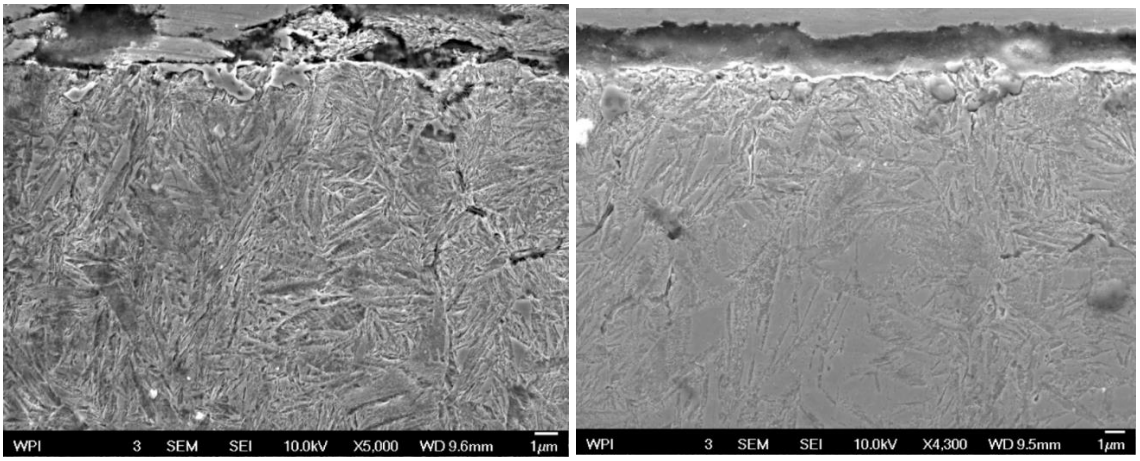

（a） Case depth=0.5 mm (b)Case depth=0.7 mm

Figure 88: The microstructure for 8620 alloy

3.3. Surface residual stress study

Stress were measured and analyzed by X-ray Diffraction as *Figure 88* and *Figure 89* presents. PANalytical X-Ray diffraction machine was used. The Stress Plus software by the PANalytical was used for the surface residual stress calculation. The peak shift at high angle of the pattern is used for stress analysis.

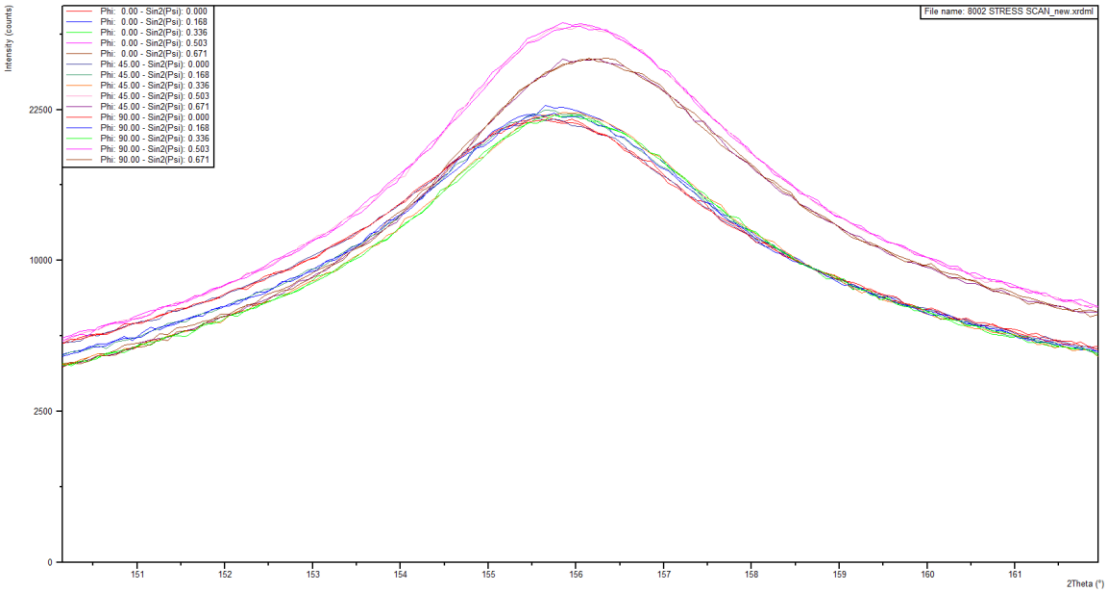

Figure 89: The original signal of XRD measurement of stress

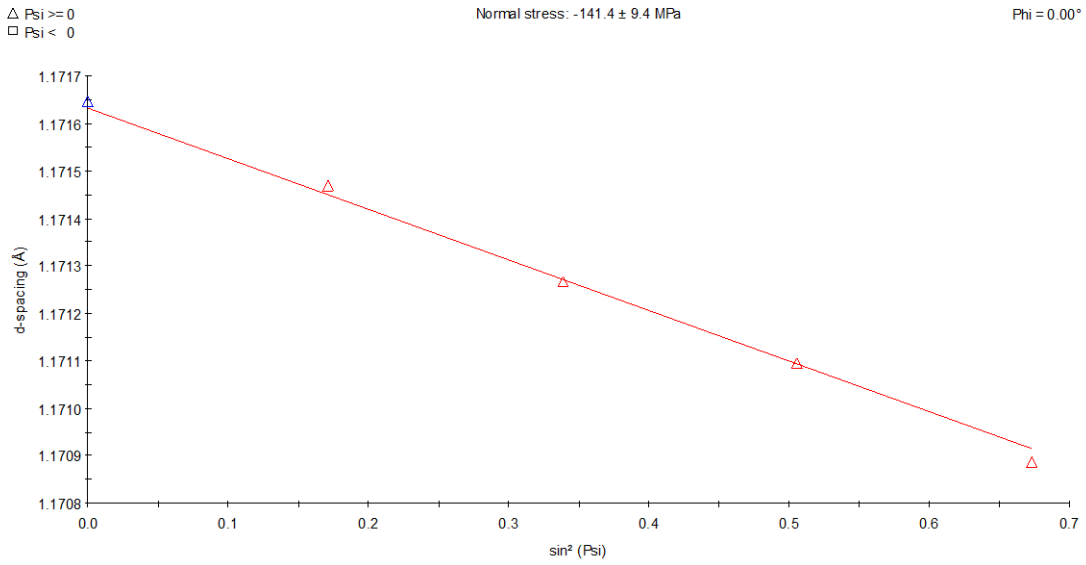

Figure 90: The analysis of surface stress of carburized 8620 steel with Panalytical stress analysis software

The bent strip test was conducted to study the effect of the stress on Magnetic Barkhausen noise. Plain steel was used for the testing with carbon concentration of 0.04% steel and 0.2 %Mn. Strip was bent and the tensile stress was measured. There will be tensile stress measured together with the plastic and elastic deformation. *Figure 91* presents the correlation between the MP and the strain. At the beginning of the bending, the MP has a value as large as 580. It decreases with the applied force. Stress played important role for Barkhausen Noise testing. The stress condition is monitored for the followed experimented.

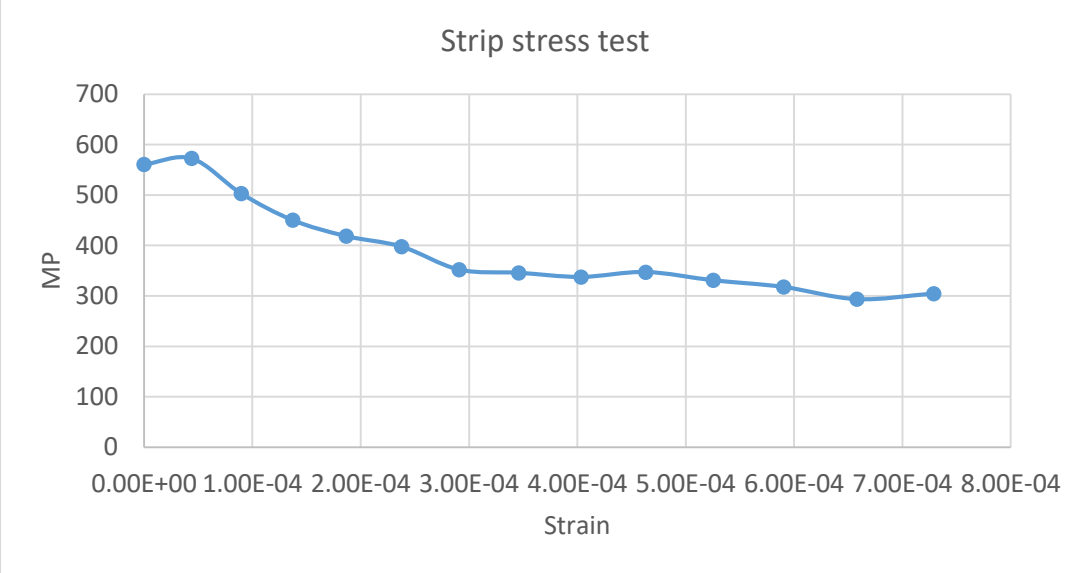

Figure 91: The stress testing for bend strip

3.4. The detection of carbides and IGO

It has been studied that the precipitation of the carbides and IGO will have strongly affect the Magnetic Barkhausen Noise [13]. *Figure 92* presents the carbon concentration profile and microhardness profile for carburized 5120 alloy. The carbon concentration profile shows that the carbon content can be as high as 1.4 wt%. It is higher than the solubility of the carbon in 5120 alloy. Fe_3C will form.

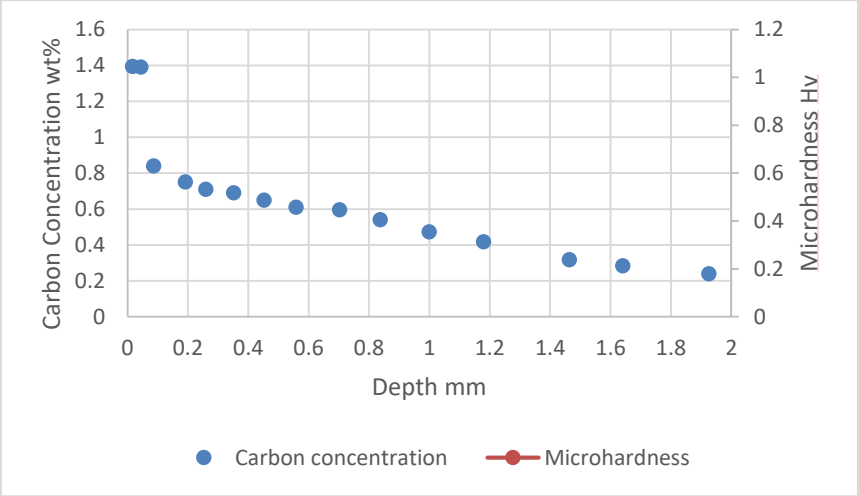

Figure 92: The carbon concentration and microhardness of carburized 5120 alloy

Figure 93 presents the formation of the IGO on the surface area. The microsturcture shows the martensitic phase with IGO at the surface. It is a case that industry will try to avoid.

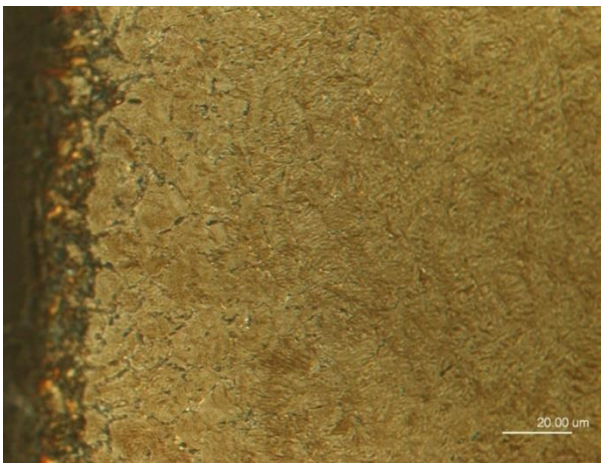

Figure 93: Microstructure of carburized 5120 Case depth=1.40 mm

Samples were measured with Barkhausen noise testing. A layer of 0.2mm was removed to get rid of the carbides/IGO rich layer. We can see the jump of the MP. The MP is as high as 519.15 for 1.40mm case depth sample, while it will drop to 36.77 after the surface removal. The Barkhausen noise is sensitive to the irregular surface with carbides and IGO.

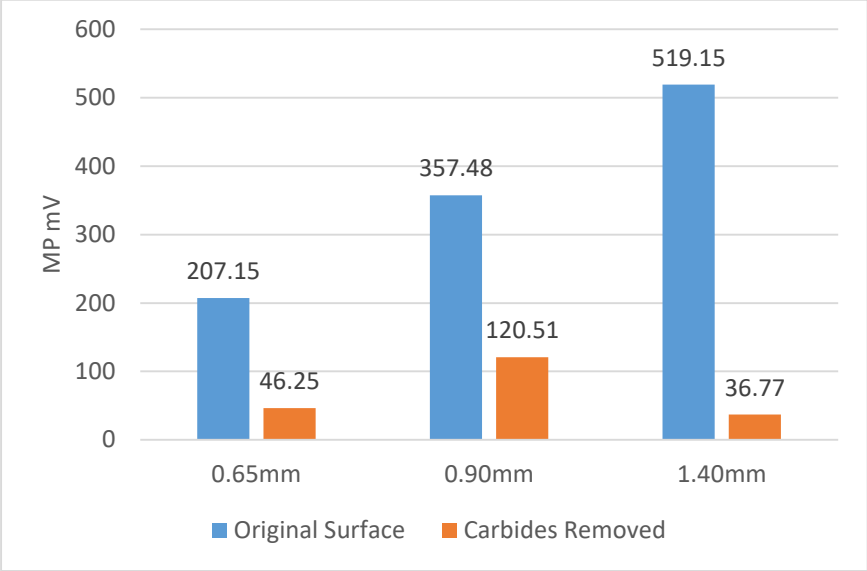

Figure 94：The Measurement of MP on the carbides/IGO rich surface for 5120 alloy

3.5. The surface hardness study: Carbon concentration

The hardness of carburized steel is determined by the surface carbon concentration and the tempering condition. The microstructure at the surface area is consist of Martensite and retained austenite. To study the measurement of MBN on the hardness, the effects of carbon concentration, tempering condition, grain size are studied.

The carburized 8620 and 1018 alloy were used for the study. A certain layer was removed for each sample to create different surface hardness due to the changing of the carbon concentration as *Figure 95* presents. After the grinding, MP will be measured as well as the hardness. The thickness of the sample is accurately measured.

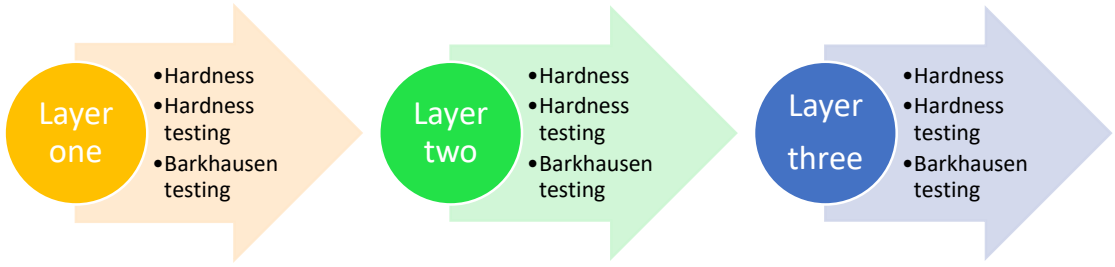

Figure 95: The removal of carburized layer for surface carbon

Figure 96 and *Figure 97* presents the microhardness profile and carbon concentration profile after the removal of the layer. It is carburized 8620 alloy with case depth of 0.5mm. The surface hardness and surface carbon concentration can be calculated.

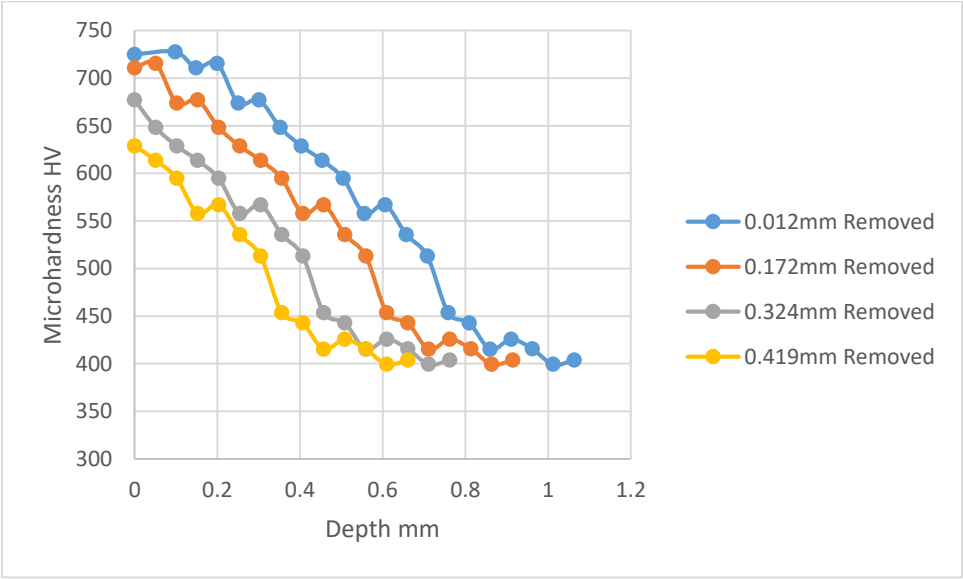

Figure 96: The hardness profile for surface removed 8620 alloy

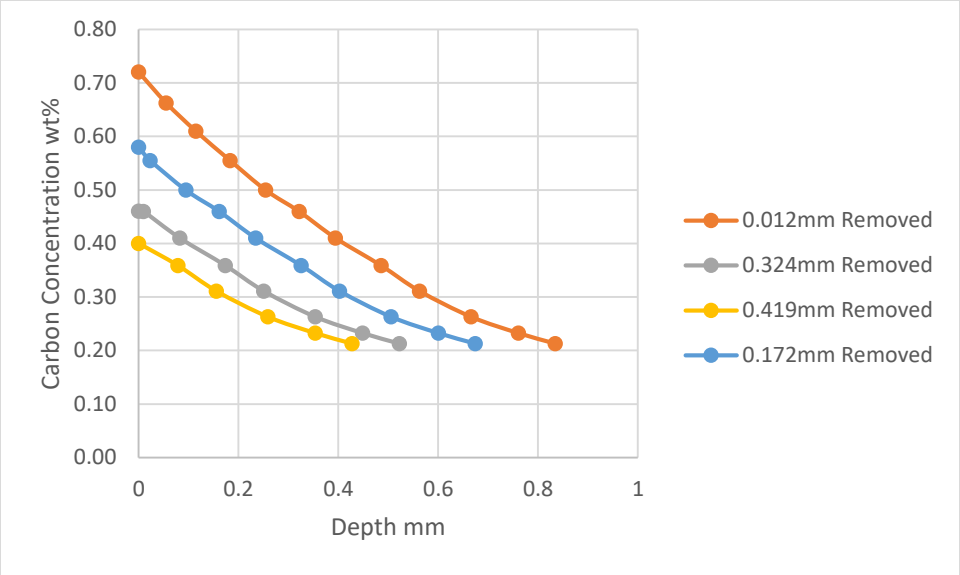

Figure 97: The concentration profile for surface removed 8620 alloy

The MP is measured for each sample. It is then correlated with the hardness. *Figure 98* and *Figure 99* present the MP measurements on the removed surface. For both sample, a linear correlation can be found for both. MP is sensitive to the surface carbon concentration change. In industry, there might be requirement to remove a certain layer off the part to avoid IGO which will also change the carbon concentration which is also related to the hardness. The MBN can be effective tool in this case.

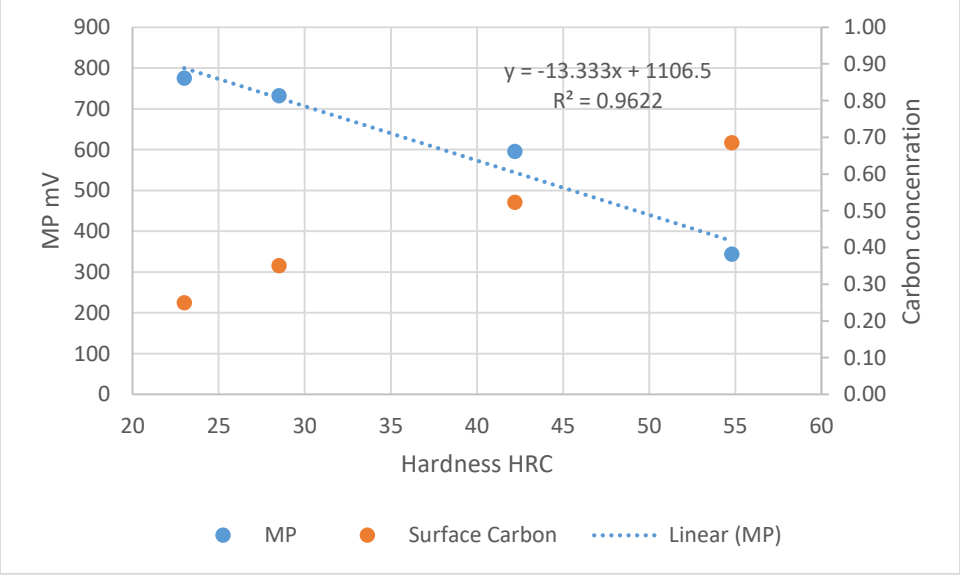

Figure 98: The MP testing on carburized 1018 alloy with surface removal

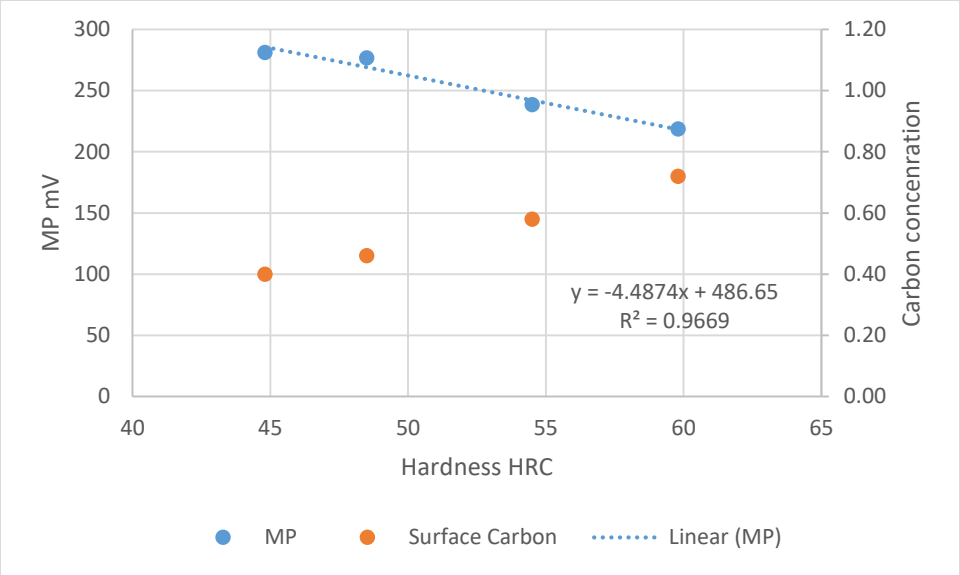

Figure 99: The MP testing on carburized 8620 alloy with surface removal

3.6. Grain size study

The grain size will affect the distribution of the magnetic domains. When the sample is placed in magnetic field, grain boundaries will interact with the domain wall motion and generate noise. J. Anglada-Rivera et, al. has studied the effect of the grain size. Pearlite microstructure alloy was studied.

Samples preparation process is presented in Figure 100. Samples were heated in the furnace and held for 1h at selected temperatures. After the Austenitizing heat treatment, the samples were quenched in oil. It will lead to samples with different grains.

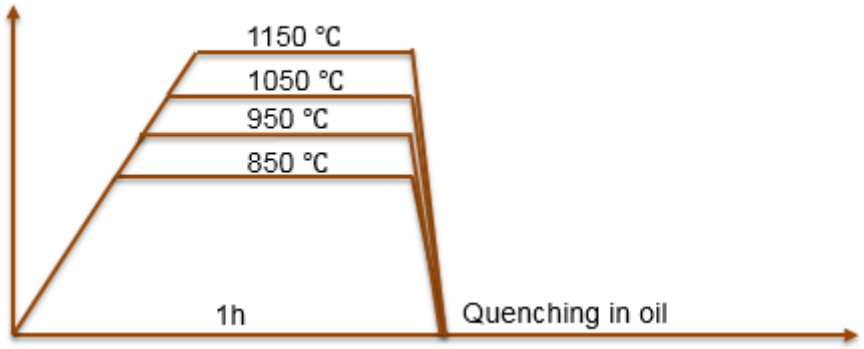

Figure 100: The heat treatment of 4140 alloys

The grain size of the 4140 samples are seen in Figure 101. It is 9µm for as-quenched from 850 compare to 65µm, quenched from 1150℃. The stress distribution for the samples are presented in Figure 102. Higher quenching temperature will lead to a smaller residual stress.

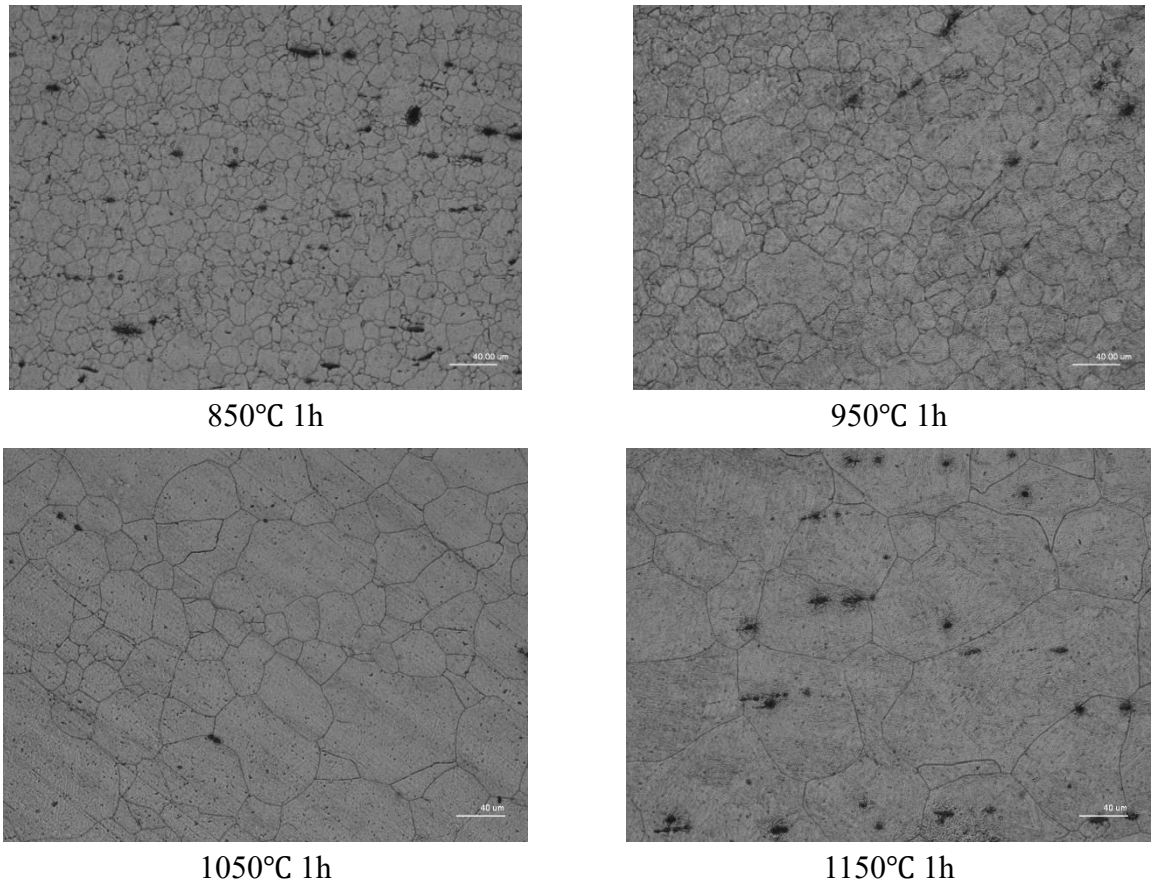

Figure 101: The microstructure for grain size study on as quenched 4140 alloy

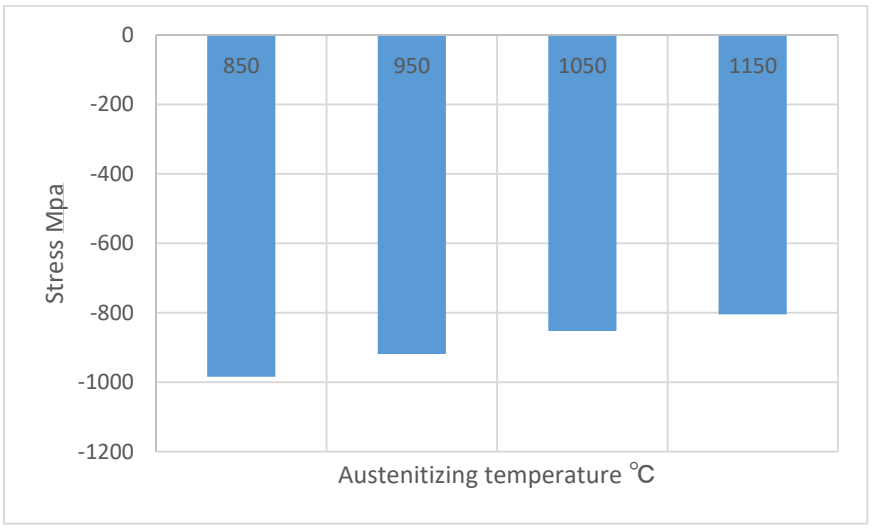

Figure 102: The residual stress measured by X-Ray Diffraction with different grain size

The Barkhausen Noise testing results are presented in Figure 103. The MP for 850℃ and 950℃ quenching is around 80 which is much smaller than quenched from 1050℃. The figure presents that the grain size does affect the MP. For the design of the standard sample, the grain size shall be well considered.

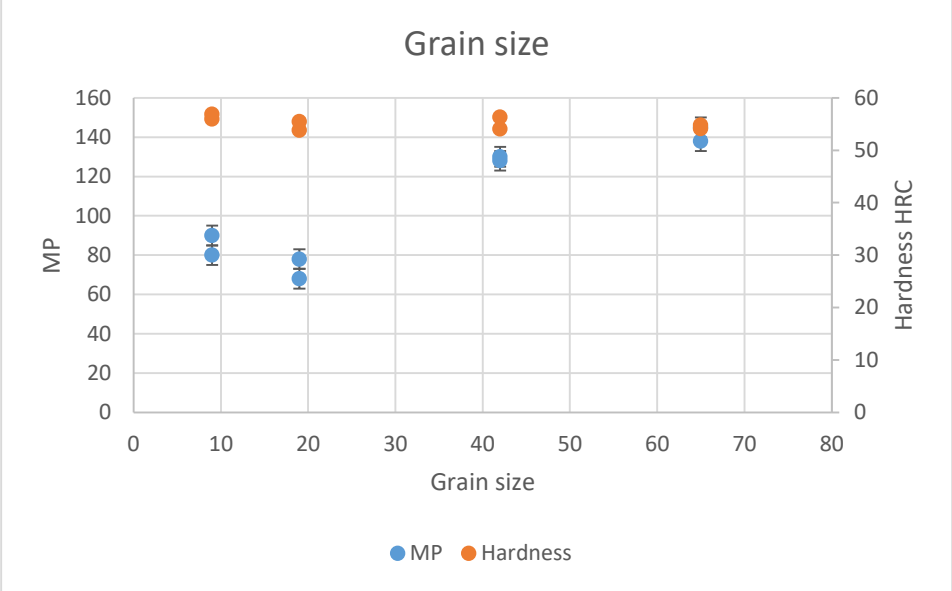

Figure 103: The MP testing on the 4140 alloy with different grain size 5V, 50Hz

3.7. Tempering effects study

J.Kameda and R. Ranjan have studied the correlation between the temperature and the MB. In his study, he tried to study the microstructure effects on the noise [4].

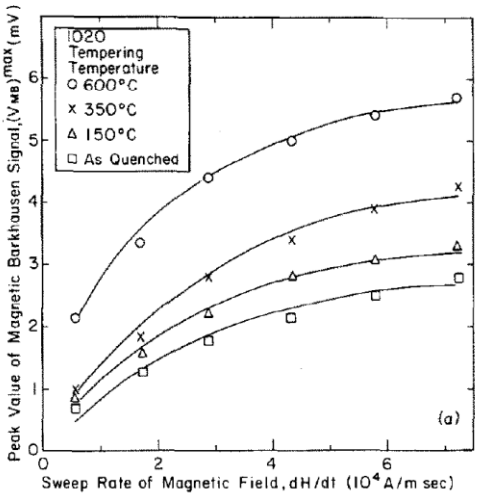

Figure 104: Relationship of MB and the tempering condition

Tempering effects are also studied. 4140 samples are used. They were quenched from 850℃ and tempered at 200℃, 300℃, 400℃ and 500℃ for 2h as Figure 105 presented. During tempering process, the case depth will not change, but residual stress and hardness will decrease. The precipitation of the carbides will increase the pinning sites, but at the same time, the residual stress will be released.

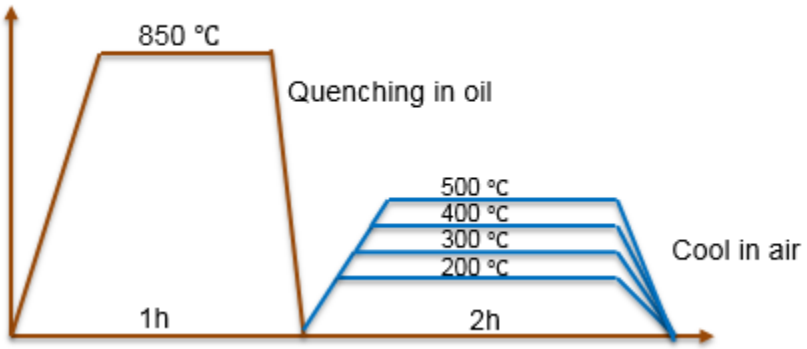

Figure 105: The temping process for the 4140 alloy

The residual stress after tempering process is presented in Figure 106 and the hardness data is in Figure 107.

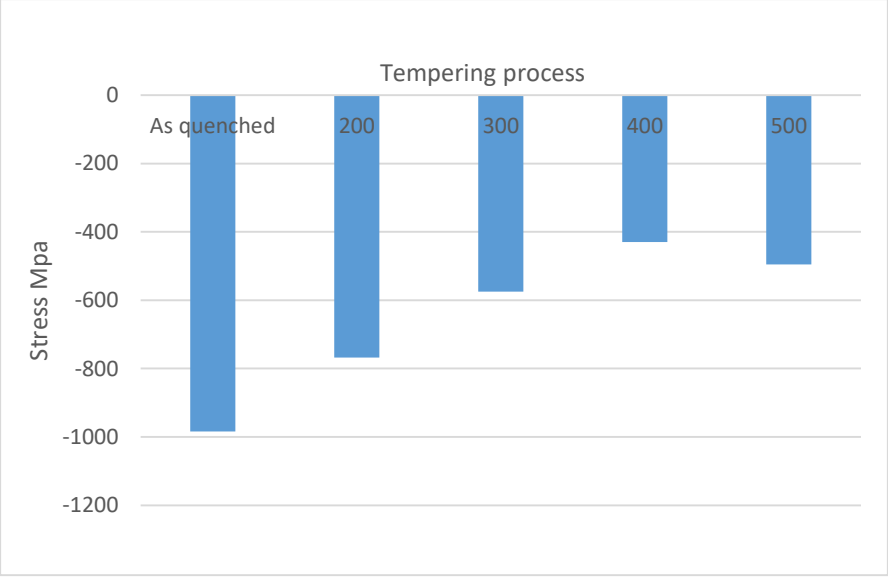

Figure 106: The residual stress for 4140 alloy with different tempering condition

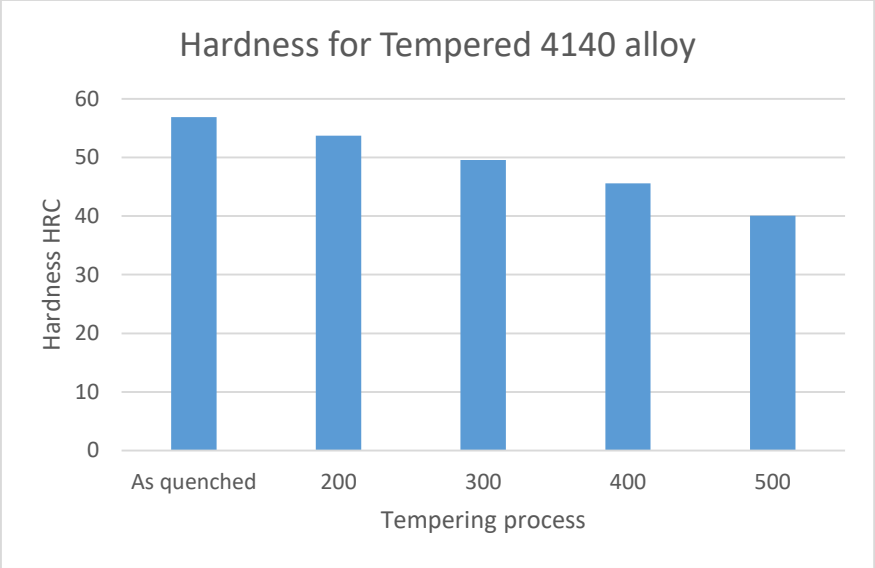

Figure 107: The hardness for tempered 4140 alloy with different tempering temperature

Figure 108 presents the effects of the tempering temperature on MP. For the 200℃ tempering, the MP is lower than the as quenched sample. The 300℃, 400℃, 500℃ tempering process will lead to a MP of 140. Though the hardness has decreased from 49 to 40HRC, the MP does not change much. The precipitated carbides growth during the process but there were not much new pinning sites created.

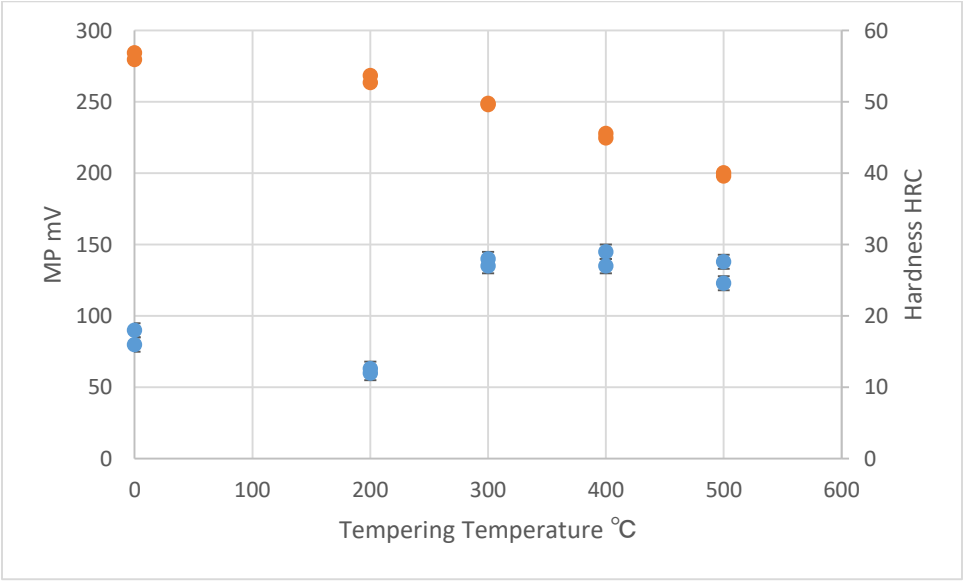

Figure 108: The MP testing on 4140 alloy with different tempering Temperature 5V, 50Hz

Tempered 4140 steel rods was also used for the testing. Diameter of the rod is 0.5 inch. They were quenched from 850℃ then tempered.

Table 16: Tempering condition for 4140

Temperature			**Time**		
250℃	1h	3h	7h	10h	
350℃	1h	3h	7h	10h	15h
450℃	1h	3h	7h	10h	
550℃	1h	3h	7h	10h	15h
650℃	1h	3h	7h	10h	

The rods are measured with MP which is presented in *Figure 109*. For tempering temperature lower than 450℃, the hardness is higher than 35HRC. It is hardly to correlate the hardness with MP. For tempering temperature that is higher than 550℃, there is linear correlation between the MP with hardness.

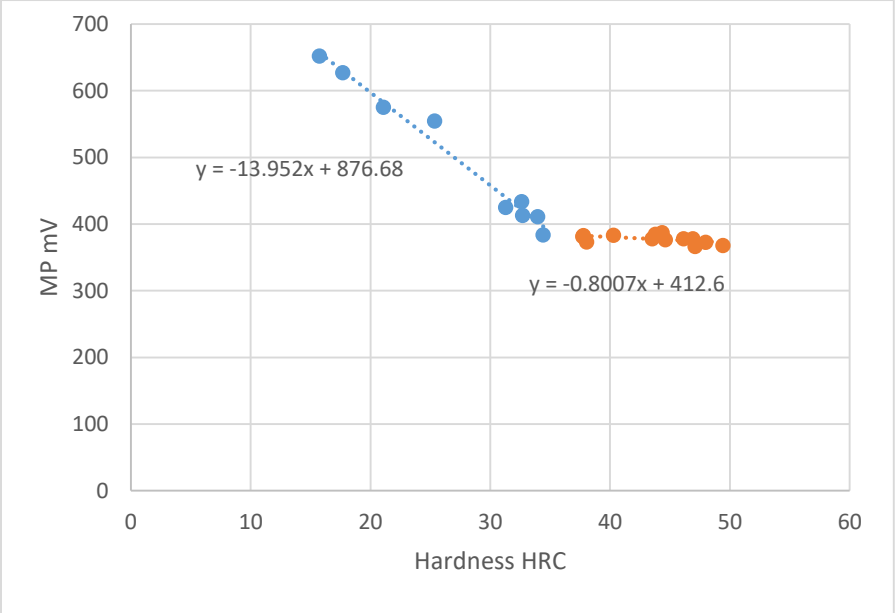

Figure 109: The MBN measurement on the hardness of tempered 4140 rods

3.8. Case depth study

Carburized steel has a higher carbon concentration at surface area and lead to a higher hardness. Typical concentration profile is presented in *Figure 110*. Compare to induction hardened steel. It has no obvious interface between the hard case and soft core. Case depth measurement is not easy to achieve with NDT method such as ultrasonic and eddy current due to the gradient change in hardness.

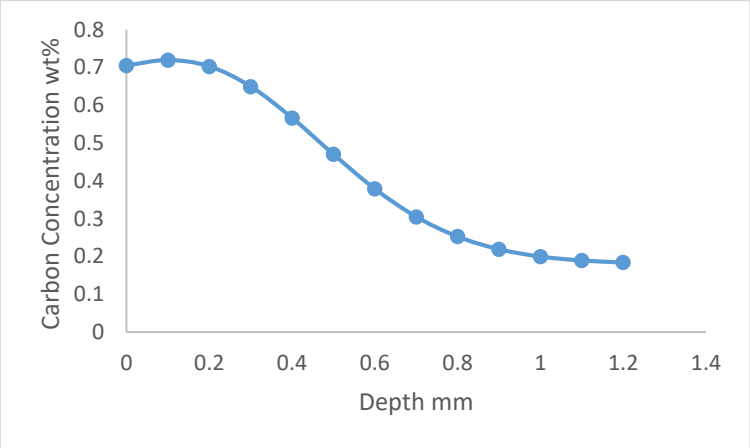

Figure 110: The carbon concentration profile

The case depth has been studied with the Magnetizing Voltage Sweep (MVS) method. The testing method was initially proposed by Suvi Santa-aho[7]. As *Figure 111* presents, two frequencies were used for the testing. Each frequency will lead to a measurement depth and obtain the information corresponding to the depth. At each frequency, magnetizing voltage changes from 0 to 16 vpp and a profile as a function of magnetizing voltage was measured. There is a max slope that can be used to correlation the properties of the steel at certain depth. In the figure, 8Hz and 125Hz was used for measurement.

Samples are from John Deere. There are three group of samples with case depth of 0.8 1.2 and 1.8mm. The *Figure 111* presents the maximum slope ratio for 20Hz and 250Hz. The large case depth will lead to a larger slope ratio. In this way the case depth can be evaluated as *Figure 112* presented.

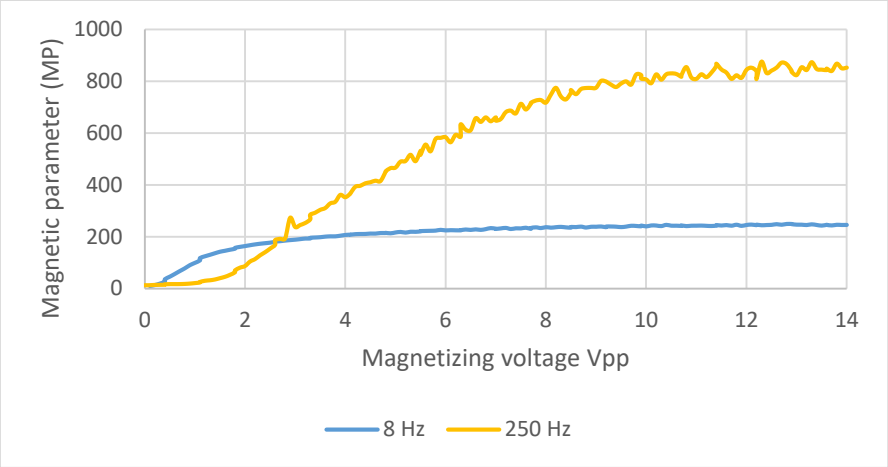

Figure 111: The original MVS data measured with Rollscan 300 unit at 8Hz and 250Hz

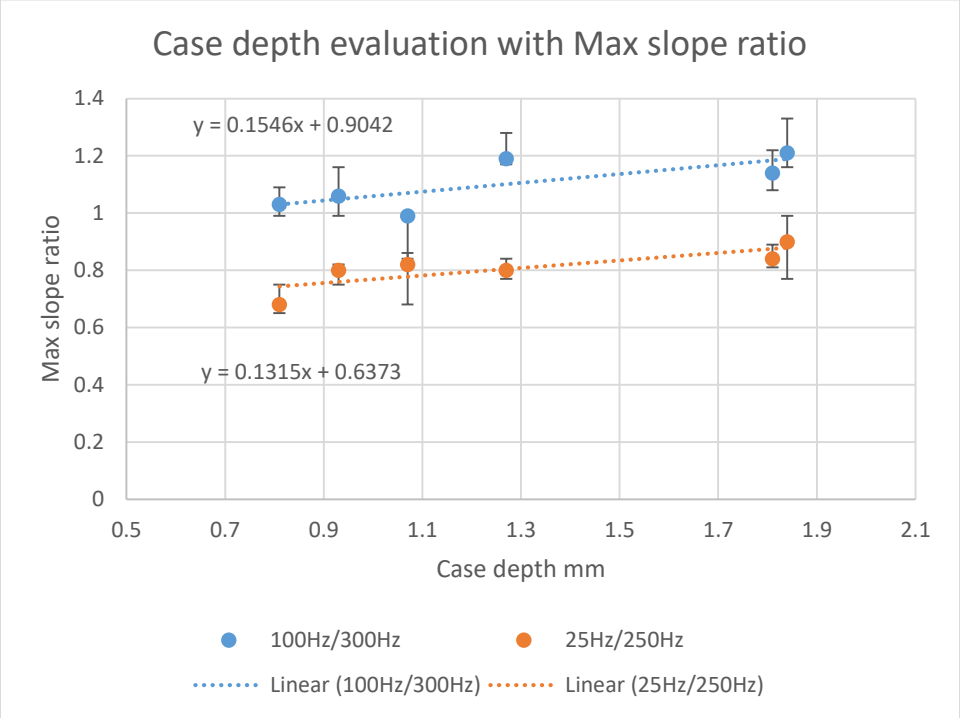

Figure 112: The case depth measurement with max slope ratio

The measurement has been applied on the carburized 1018 alloy and 5120 alloy. Due to the formation of the carbides on the surface. Samples were ground to remove the carbides. 100Hz and 25Hz frequency combination is used for the testing. 10k-70kHz band pass is used. *Figure 113* and presents the change of the MVS maximum slope ratio with case depth. Similarly, *Figure 114* presents the correlation between the MVS maximum slope ratio with case depth of carburized 5120 alloy.

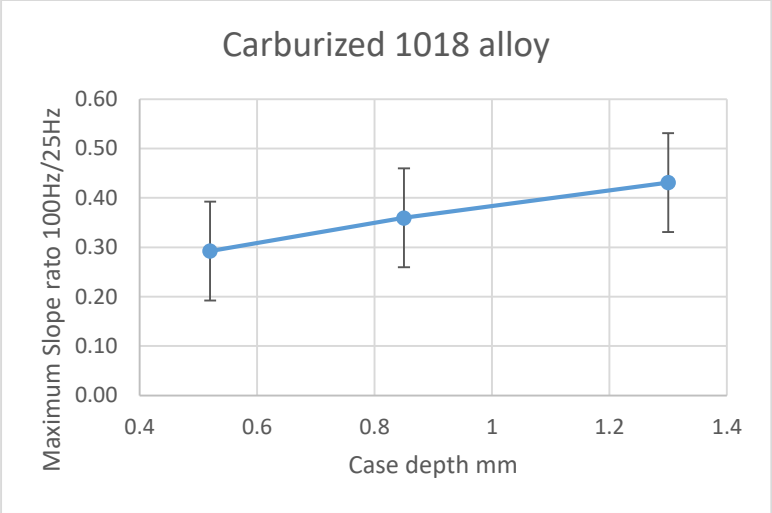

Figure 113: The MVS measurement on carburized 1018 alloy

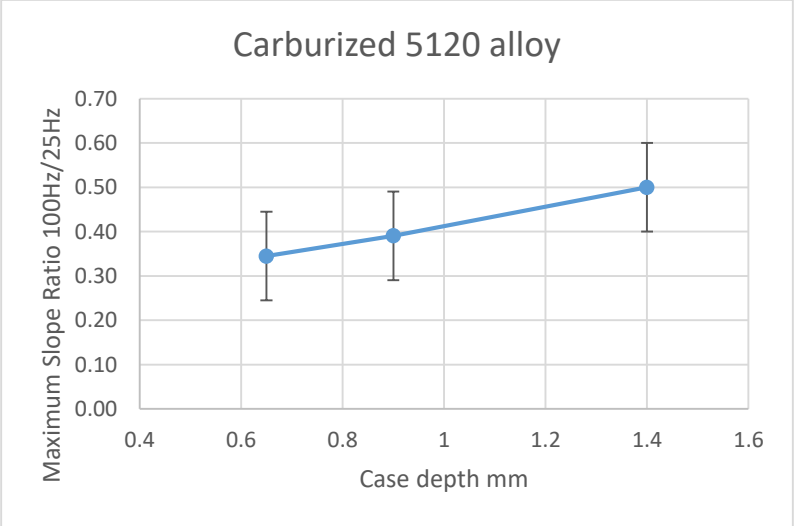

Figure 114: The MVS measurement on carburized 5120 alloy

4. Conclusion

- Barkhausen Noise is sensitive to the microstructure and stress of the steel.
- The magnetic parameter can be used for as-quenched hardness measurement of carburized steel.
- The magnetic parameter can also evaluate the hardness after tempering process of carburized steel.
- MVS method shows potential capability for case depth measurement.

Reference

[1] Sorsa, Aki, et al. "Utilization of frequency-domain information of Barkhausen noise signal in quantitative prediction of material properties." AIP Conference Proceedings. Vol. 1581. 2014.

[2] Vaidyanathan, S., et al. "Evaluation of induction hardened case depth through microstructural characterisation using magnetic Barkhausen emission technique." Materials Science and Technology 16.2 (2000): 202-208.

[3] Rollscan 300 Operation instructions Version 1.6b. Nov 2011 by Stresstech

[4] Stresscan 500C Operating Instructions V. 1.0b, Dec 2002 by Stresstech

[5] Kameda, J., and R. Ranjan. "Nondestructive evaluation of steels using acoustic and magnetic Barkhausen signals—I. Effect of carbide precipitation and hardness." Acta Metallurgica 35.7 (1987): 1515-1526.

[6] Sorsa, Aki, et al. "Quantitative prediction of residual stress and hardness in case-hardened steel based on the Barkhausen noise measurement." Ndt & E International 46 (2012): 100-106.

[7] Parakka, Anthony P., et al. "Barkhausen effect in steels and its dependence on surface condition." Journal of applied physics 81.8 (1997): 5085-5086.

[8] Santa-aho, Suvi, et al. "Utilization of Barkhausen noise magnetizing sweeps for case-depth detection from hardened steel." Ndt & E International 52 (2012): 95-102.

[9] Moorthy, V., B. A. Shaw, and S. Day. "Evaluation of applied and residual stresses in case-carburised En36 steel subjected to bending using the magnetic Barkhausen emission technique." Acta Materialia 52.7 (2004): 1927-1936.

[10] Dubois, M., and M. Fiset. "Evaluation of case depth on steels by Barkhausen noise measurement." Materials science and technology 11.3 (1995): 264-267.

[11] Vaidyanathan, S., et al. "Evaluation of induction hardened case depth through microstructural characterisation using magnetic Barkhausen emission technique." Materials Science and Technology 16.2 (2000): 202-208.

[12] Moorthy, V., et al. "Magnetic Barkhausen emission technique for evaluation of residual stress alteration by grinding in case-carburised En36 steel." Acta Materialia 53.19 (2005): 4997-5006.

[13] Blaow, M., J. T. Evans, and B. A. Shaw. "Effect of hardness and composition gradients on Barkhausen emission in case hardened steel." Journal of magnetism and magnetic materials 303.1 (2006): 153-159.

[14] Moorthy, V., B. A. Shaw, and J. T. Evans. "Evaluation of tempering induced changes in the hardness profile of case-carburised EN36 steel using magnetic Barkhausen noise analysis." Ndt & E International 36.1 (2003): 43-49.

[15] Wilson, John W., et al. "Magneto-acoustic emission and magnetic Barkhausen emission for case depth measurement in En36 gear steel." IEEE Transactions on Magnetics 45.1 (2009): 177-183.

[16] De Campos, M. F., et al. "Magnetic Barkhausen noise in quenched carburized steels." Journal of Physics: Conference Series. Vol. 303. No. 1. IOP Publishing, 2011.

[17] Anglada-Rivera, J., L. R. Padovese, and J. Capo-Sanchez. "Magnetic Barkhausen noise and hysteresis loop in commercial carbon steel: influence of applied tensile stress and grain size." Journal of magnetism and magnetic materials 231.2 (2001): 299-306.

[18] Kobayashi, Satoru, Hiroko Takahashi, and Yasuhiro Kamada. "Evaluation of case depth in induction-hardened steels: Magnetic hysteresis measurements and hardness-depth profiling by differential permeability analysis." Journal of Magnetism and Magnetic Materials 343 (2013): 112-118.

[19] Saquet, O., J. Chicois, and A. Vincent. "Barkhausen noise from plain carbon steels: analysis of the influence of microstructure." Materials Science and Engineering: A 269.1 (1999): 73-82.

[20] Moorthy, V., et al. "Microstructural characterization of quenched and tempered 0.2% carbon steel using magnetic Barkhausen noise analysis." Journal of magnetism and magnetic materials 171.1 (1997): 179-189.

[21] Moorthy, V., et al. "On the influence of tempered microstructures on magnetic Barkhausen emission in ferritic steels." Philosophical Magazine A 77.6 (1998): 1499-1514.

[22] Jiles, D. C., and L. Suominen. "Effects of surface stress on barkhausen effect emissions: Model predictions and comparison with x-ray diffraction studies." IEEE transactions on magnetics 30.6 (1994): 4924-4926.

[23] Gauthier, J., T. W. Krause, and D. L. Atherton. "Measurement of residual stress in steel using the magnetic Barkhausen noise technique." NDT & E International 31.1 (1998): 23-31.

[24] Perez-Benitez, Jose Alberto, et al. "Investigation of the magnetic Barkhausen noise using elementary signals parameters in 1000 commercial steel." Journal of magnetism and magnetic materials 263.1 (2003): 72-77.

[25] Sakamoto, H., M. Okada, and M. Homma. "Theoretical analysis of Barkhausen noise in carbon steels." IEEE transactions on magnetics 23.5 (1987): 2236-2238.

[26] Hwang, D. G., and H. C. Kim. "The influence of plastic deformation on Barkhausen effects and magnetic properties in mild steel." Journal of Physics D: Applied Physics 21.12 (1988): 1807.

[27] Wang, Ping, et al. "Stress measurement using magnetic barkhausen noise and metal magnetic memory testing." Measurement Science and Technology 21.5 (2010): 055703.

Chapter Four: Research Conclusions

The thesis has optimized the modeling for both CarbTool© and CarbonitrideTool©.

Regarding to the low pressure carburizing process, the existing model doesn't simulate the AISI 9310 and AISI 5120 accurately. Experiments are designed to study the surface microstructure after boost step. It is found that the graphite and carbides appear at surface which changed the diffusion mechanism. It has also been studied by a few scholars that the carbon deposit will form after about 5min during the low pressure carburizing process. The boundary needs to be optimized to better modeling the processes.

In the modified model, the carbon potential similar with the boundary condition with the gas carburizing modeling is used. It has been tested from the literature that the surface carbon concentration becomes constant after a long while low pressure carburizing. It makes the carbon potential applicable for the simulation. The mass transfer coefficient is calculated corresponding to the carbon potential. It has proved the updated model can meet the experimental result better.

The carboniriding simulation is also studied. Both carbon and nitrogen profiles were well studied by previous researchers. In this thesis, the hardness profile is predicted. Carbonitriding process strengthens the parts by diffuse both carbon and nitrogen atoms into the surface. They are both Austenite stabilizer leading to high fraction of retained Austenimte which is soft compare to the Martensite microstructure.

The Martensite start temperature is studied which is a function of the composition of the alloy elements. The traditional empirical equation for Martensite start temperature is modified by considering the concentration of the nitrogen. Nitrogen play as important role as carbon for Austenite faction. The Martensite start temperature is predicted with the new model and used for the retained Austenite fraction prediction. Once the microstructure is predicted, mixture rule can be used for the prediction of the hardness profile.

The carburizing samples are also tempered in this thesis. The hardness profile after tempering process is also need by the industry because it is necessary step for manufacturing. Hollomon Jaffe equation is used for the hardness. It is discussed that the Hollomon Jaffe parameter is a function of carbon concentration. It cannot be used directly for the hardness profile prediction of tempered carburized samples. The Hollomon Jaffe parameter needs to be determined corresponding to different carbon concentration.

A matrix of tempering experiments were designed and conducted for different tempering temperature and tempering time combinations. AISI 8620 and AISI9310 are used for the research. The hardness profiles are measured and used for the calculation of the Hollomon Jaffe parameter mathematically. With the calculated parameter, the hardness profile can be predicted with the input of tempering time, temperature and the carbon concentration profile. AISI9310 and AISI 8620 have presented different trend for the Hollomon Jaffe parameter against the carbon concentration. It is caused by the large fraction of the retained Austenite which is also discussed in the thesis.

The properties of the hardened case by carburizing process are critical for industry. The current methods for the measurement of the case depth and surface hardness are destructive with high cost of time and money. Industry is seeking nondestructive method for surface hardness and case depth evaluation. Magnetic Barkhausen Noise(MBN) is chosen for the testing.

A variety of samples are prepared for the measurements. The hardness is studied by correlating the MBN with the samples has different carbon centration. The hardness is also studied by measuring tempered the samples. MBN has been proved to be promising way for the hardness evaluation because it is sensitive to the microstructure. The case depth is also studied by Magnetizing Voltage Sweep method. The testing results present the linear correlation between the MVS measurement with the case depth. Further studied is still need to improve the accuracy and repeatability.